

Final Report on OETR Nova Scotia Margin Project: Forward Dynamical Modelling of: 1) Margin Development during Rifting, and; 2) Salt Tectonics

Part 1 of 3 (Part 2 is Appendix 1A and Part 3 is Appendix 1B which describe Scientific Objectives and Progress)

Project number 400-150-10-23

Project start date: 1 January 2010

Period covered by report: 1 January – 30 July 2010

Christopher Beaumont, Professor and Canada Research Chair in Geodynamics

Oceanography Department

Dalhousie University, Halifax, NS B3H 4J1

chris.beaumont@dal.ca

Tel: 902-494-3779

Fax: 902-494-3877

Submission date: 30 July 2010

2. Summary

This project is designed to investigate some basic processes associated with: 1) the rifting of the lithosphere, and; 2) the salt tectonics of the Nova Scotia margin using forward two-dimensional (cross sectional) finite element models. The background to this project is the existing expertise that the Dalhousie Geodynamics Group has developed in separate forward numerical modeling studies of both of these processes (see list of publications, Appendix 2). Its anticipated significance is to gain insight into the thermo-mechanics of these processes and to understand and place improved constraints on the rift mechanisms, the early development of the margin, and the subsequent salt tectonics. The research is primarily of a basic scientific nature but has implications for hydrocarbon exploration of the Nova Scotian margin and should therefore be of interest to the energy industry.

3. Table of Contents

1. Title Page
2. Summary
3. Table of Contents
4. Introduction
5. Discussion of Objectives, Methodology and Results (see appendices)
6. Dissemination and Technology Transfer
7. Conclusions and Recommendations
8. Publications
9. Expenditure of OETR Funds
10. Employment Summary
11. Bibliography/References (see appendices)
12. Appendices

4. Introduction

The research comprises two projects which are listed below together with their scientific objectives. For completeness these objectives are also listed in Appendix 1 which describes progress on the project

Project 1: Forward Dynamical Modelling of Lithospheric Extension and Rifting Linked to the Development of the Nova Scotian Margin

Despite the existence of three well-studied crustal scale transects of the Nova Scotian margin (papers by Loudon, Funck, Wu, Dehler), and similar transects from Morocco, we have only a rudimentary understanding of the way the final crustal structure, as observed today, is linked to the Triassic-Jurassic lithospheric extension and rifting between Nova Scotia and Morocco. In particular, the form of the syn-rift and early post-rift sedimentary basins can only be determined approximately from either the large-scale crustal structure or interpretation of the ION/GXT NovaSpan seismic reflection images of the deep sedimentary structures. What is required is a more fundamental understanding of the rift process and how it imparts geometries to the sedimentary basins. While this remains a long term goal, progress has been made in the geodynamical forward modelling of depth-dependent lithospheric extension and rifting with the purpose of relating observed crustal structure to the properties of the lithosphere responsible for particular styles. This approach seeks an explanation of the observed discrepancies by comparison with the Uniform Extension (McKenzie 1978) model. So far it has been shown to provide an explanation for the differences between narrow, Type I margins (e.g. Iberia-Newfoundland) and ultra-wide Type II margins (e.g. South Atlantic) based on the coupling/decoupling of upper and lower lithosphere. It also allows the characteristics of the associated sedimentary basins to be predicted...for example sag basins in Type II margins (Huisman and Beaumont, 2008) but not Type I (Huisman and Beaumont, in prep.)

We propose to investigate the development of the Nova Scotian margin using the same approach.

- 1) List the margin characteristics as determined by crustal and basin-scale seismic, subsidence and potential field studies of the conjugate Nova Scotian and Moroccan margins.
- 2) Use dynamical models with a range of lithospheric properties to determine their depth-dependent stretching properties.
- 3) Use those models that match the observations to predict the character of the sedimentary basins. This proposed research will also take into account: i) single and double-phase rifting and ii) sedimentation as the models evolve, in particular deposition of evaporites and the linked problem of the salt tectonics. This approach is designed for magma-poor rifted margins and is therefore considered suitable for much of the Nova Scotia margin. We will also consider the role of moderate levels of magmatism for the southwest part of the margin in assisting rifting and breakup and on its potential to modify the observed geometry. The Nova Scotian margin is not an end member and has characteristics that are intermediate to the Types I and II noted above. The challenge is to determine the lithospheric properties that impart these characteristics.

The intent of the research is to understand: 1) how the geometrical characteristics of the Nova Scotian margin developed, 2) the reasons for the change in characteristics with position along the margin, 3) the relationship of the geometrical style to the properties of the lithosphere from a general perspective and in relationship to inheritance from the Acadian and Alleghanian orogenies.

In addition, the geodynamical models predict surface heat flow as a function of position and time. The predicted heat flux can be used in conjunction with thermal subsidence basin modelling to test the range of levels of sediment thermal maturation and its development through time.

Project 2: Salt Tectonics of the Scotian Basin, offshore Nova Scotia

In recent research (Albertz et al., in press) we have been able to identify and explain three styles, A-C, of salt (strictly evaporite) tectonics of the Nova Scotian margin and show how they operate using 2D mechanical numerical models. The models include the autochthonous salt basins, tectonic, thermal and isostatic subsidence of the rifted margin, and loading by prograding and aggrading compacting sediments. The results provide particular insight into the effect of the position of the autochthonous salt basins on the margin and the timing and style of sedimentation in creating the three salt tectonic structural styles.

Structural style A, an open-ended roho system with a synkinematic wedge, is reproduced by models with early post-rift deltaic progradation and seaward spreading/gliding of sediments above a salt detachment. Structural style B, a roho system with landward regional normal faults and allochthonous salt sheets climbing seaward over Late Cretaceous and Paleogene strata, is shown to be a consequence of early aggradation followed by progradation. Structural style C is characterized by salt diapirs and intervening minibasins and is reproduced by models with Rayleigh-Taylor (buoyancy) instabilities requiring compaction driven density inversions, weak sediments, and initial perturbations of the overburden/salt interface. These results are also consistent with the observed timing and patterns of sedimentation on the margin. We have also investigated models with more complex autochthonous salt basin geometries and shown that significant basement topography beneath the salt causes additional salt diapirism during sediment progradation (Albertz and Beaumont, sub.).

The Albertz et al. (in press.) and Albertz and Beaumont (in press) numerical modelling assumes frictional-plastic overburden with specified pore fluid pressures deposited on linear viscous salt. These are approximations that are justifiable for first-order calculations but will certainly fail to predict the full range of observed salt tectonic structures, particularly those that involve dynamical development of fluid overpressures leading to gravitational gliding or spreading instabilities of the salt and its overburden.

We propose research that uses both the basic mechanical modelling and more advanced thermal-mechanical coupled calculations to forward model the effects of temperature, coupled basement-salt tectonics, and more realistic sedimentation regimes. The numerical model experiments will be designed to be representative of typical rifted margins, such that results will be of general interest, and tailored to specific Scotian Basin examples.

Specific sub-projects that will be undertaken using these approaches include the following.

- 1) The effect of temperature dependent salt viscosity on salt tectonics and the effect of high salt thermal conductivity on temperatures and thermal maturation of adjacent sediments.
- 2) The interaction between syn-rift extension and crustal faulting on the associated tectonics of overlying salt. This sub-project couples the two parts of the proposal by including salt and clastic sediment deposition in the upper-mantle scale extension and rifting models. The salt will be subject to deformation driven by both the tectonics of the underlying crust and gravitational forces.

5. Discussion of Objectives, Methodology and Results

See Appendices 1A and 1B.

6. Dissemination and Technology Transfer

Work on the project started as of 1 January 2010. To date, there has been no dissemination of the results, except at OETR meetings, and no technology transfer. Steven Ings attended an RPS meeting in Paris on salt tectonics. Steven Ings and Chris Beaumont attended the RPS meeting on Plate Tectonics in Halifax. Steven Ings and Chris Beaumont attended the Nova Scotia Energy Research and Development Forum 2010. Steven Ings, Rajesh Goteti and Chris Beaumont attended the RPS PFA integration meeting in Halifax. We have not attended other conferences or events during the reporting period.

7. Conclusions and Recommendations

See Appendices 1A and 1B.

8. Publications

No papers have been submitted for publication during the reporting period. See Appendix 1 for progress report.

9. Funding

No other sources of cash and in-kind funding have been secured for this project.

10. Expenditures of OETR Funds

To be completed by Dalhousie University Financial Services.

11. Employment Summary

Project 1: Forward Dynamical Modelling of Lithospheric Extension and Rifting Linked to the Development of the Nova Scotian Margin

This project is being undertaken by a small team, Steven Ings (Research Associate), Rajesh Goteti (Postdoctoral Fellow), Christopher Beaumont (Professor) using the 2D geodynamical thermal-mechanical, plane strain finite element software (Sopale) developed at Dalhousie University. This software is capable of modelling the stretching and rifting of lithosphere at the upper-mantle scale. Douglas Guphill (Research Programmer) has assisted with modifications to the finite element software.

Project 2: Salt Tectonics of the Scotian Basin, offshore Nova Scotia

The project is being undertaken by a small team, Steven Ings (Research Associate), Rajesh Goteti (Postdoctoral Fellow), and Christopher Beaumont (Professor) using the 2D thermal-mechanical plane strain finite element software (Sopale) developed at Dalhousie University. The thermal-mechanical software is capable of modelling coupled thermal-mechanical problems. Douglas Guphill (Research Programmer) has assisted with modifications to the finite element software.

Name	Position	Student	Full/Part Time	Scientific Contributions	Work Months Associated with Project
Steven Ings	Res. Assoc.	No	80%FT	Contributions to Projects 1&2	80% x 7months
Rajesh Goteti	Postdoc.	No	80%FT	Contributions to Projects 1&2	80% x 7months
Douglas Guphill	Res. Programmer		25%FT	Software development	25% x 7months
Chris Beaumont	Prof.	No	FT	P.I.	

12. Next Steps

The next steps will follow those described in the proposal (Schedule A) for Q3-4 2010, provided the amendment to the contribution agreement is signed and implemented. In addition, given suitable additional amendments to the contribution agreement, we will investigate the thermal effects of emplacement of an intrusive magmatic body into the margin during rifting, as requested and agreed with RPS.

Research Targets/Deliverables – Year 2

Q3-Q4, 2010

Refinement of the models and first-order prediction of the sedimentary basin subsidence in terms of syn- and post-rift evolution as a function of dip and strike position across and along the margin.

Investigation of the variation in margin characteristics with position along the margin. Does this variation represent major changes in the style and mechanism of rifting or can the variability be explained by more minor variability?

Compile interim results for inclusion in the 'Basin Atlas'. These results will likely be preliminary in nature, perhaps indicating the range of viable options for rifting configurations, plus a list of those that can be rejected.

Q1-Q2, 2011

Assess progress and redefine research targets if necessary

Write up results of Project 1 Q1-Q4, 2010 as manuscript to be submitted for publication if the results are sufficient.

Q1-Q3, 2011

Assess the implications of the results from the PFA seismic refraction profile with regard to the lithospheric extension modelling.

Refinement of model results to better determine the lithospheric properties of the Nova Scotian margin as compared with narrow (Newfoundland-Iberia) and ultra-wide (South Atlantic) end-members. In addition to insight into the structural evolution during rifting, the models will provide additional constraints on surface heat flow as a function of time and position along the margin. These models will be run with and without simple clastic sediment progradation to determine the effect of basin formation and sediment filling on the style of rifted continental margin that develops.

Q2-Q4, 2011

Include syn-rift evaporite sedimentation and syn- and post-rift clastic sedimentation as the models evolve, thereby providing an investigation of salt tectonics in the context of a large scale thermo-mechanical rift model (using the dual-scale 'nested' modelling approach).

Q2-Q4, 2011

Write up results of Project 1 Q1-Q4, 2011 as manuscript(s) to be submitted for publication.

Project 2 Salt Tectonics

Sub-project 1- Year 2

Q3-Q4, 2010 Investigate consequences of thermal dependence of salt viscosity, variability of thermal properties of the sediments and variations in basal heat flux (from models of Project 1) on the salt tectonic evolution of the models and in regard to temperature of the sediments.

Q4 Compile interim results for inclusion in the 'Basin Atlas'

Q1-Q2, 2011 Assess progress and redefine research targets if necessary.

Write up results of Project 2 Q1-Q4, 2010 as manuscript(s) to be submitted for publication if the results are sufficient.

Q1-Q2, 2011 Refine models with thermal dependence of salt viscosity including a continued investigation of the effects of thermal properties of the salt and sediments, and variations in basal heat flux (again linking with Project 1 results) in the Albertz et al. (sub.) models. This will include preliminary results of the effect of salt tectonics on sediment maturation in the different structural styles investigated by Albertz et al. (sub.).

Q1-Q3, 2011 Investigation of more realistic sedimentation models that better match the sedimentation rates and distribution (including known sedimentation hiatus) of the Nova Scotian margin. In particular, this will be investigated in models of Structural style B (Sable Sub-basin roho system) and C (minibasins/diapirs).

Q3-Q4, 2011 Develop models with layered evaporite sequences. Drilling results often indicate layered evaporites in autochthonous salt and nearly pure halite in allochthonous salt. The relationship between evaporite layering and deformation rate and style will be investigated to determine potential differences in autochthonous and allochthonous salt tectonics including circumstances that may lead to the preferential evacuation of halite prone units into allochthonous salt bodies.

Prepare manuscript for publication.

Sub-project 2 – Year 2

Q3-Q4, 2010 Investigate generic models showing how syn-rift lithospheric tectonics may interact with and drive syn- and post-rift salt tectonics

Q4 Compile interim results for inclusion in the 'Basin Atlas'

Q1-Q2, 2011 Assess progress and redefine research targets if necessary.
Continue development of models with salt tectonics aided by rift-related tectonics using the nested modelling approach.

Q3-Q4, 2011 Incorporate more detailed sedimentation models and thermal salt properties investigated in sub-project 1 into the nested models of coupled salt and rift tectonics.
Prepare manuscript for publication.

Final Report on OETR Nova Scotia Margin Project: Forward Dynamical Modelling of: 1) Margin Development during Rifting, and; 2) Salt Tectonics

Steven Ings, Rajesh Goteti, Christopher Beaumont and Douglas Guphill

Oceanography Department, Dalhousie University, Halifax, NS, B3H 1R3

Project number 400-150-10-23

Project start date: 1 January 2010

Period covered by report: 1 January – 30 July 2010

Appendices 1A and 1B. Scientific Objectives, Methodology and Results

The research comprises two projects. For completeness the scientific objectives are also listed in Appendix 1 which describes progress on the project. Appendix 1 is located at the end of the report.

Appendix 2. Recent publications of the Dalhousie Geodynamics Group concerning, lithospheric rifting, formation of sedimentary basins and salt tectonics

Publications from 2008 to 2010

Names of students are boldface.

19) Albertz, M., Beaumont, C., Shimeld, J.W., Ings, S.J., and **Gradmann, S.**, (in press). An investigation of salt tectonic structural styles in the Scotian Basin, offshore Atlantic Canada: Part 1, Comparison of observations with geometrically simple numerical models (in press, *Tectonics*).

Abstract

Three primary salt tectonic structural styles (A, B, C) of the Scotian Basin, offshore Atlantic Canada, are compared with plane strain finite element models in order to investigate their origin. Here, we focus on model salt basins with initial rectangular cross-sectional geometries and follow their evolution in the context of tectonic and thermal subsidence and under various sedimentation regimes. Structural style A, an open-ended roho system with a synkinematic wedge of Jurassic sediments, is reproduced by models including post-rift deltaic progradation and seaward spreading/gliding of synkinematic sediments above a salt detachment. Structural style B, a roho system with landward regional listric normal faults and allochthonous salt sheets with canopies climbing over Late Cretaceous and Paleogene strata in the seaward region, is shown to be a consequence of early sediment aggradation followed by progradation. Structural

style C is characterized by salt diapirs and intervening minibasins and is reproduced by models with Rayleigh-Taylor instabilities requiring compaction driven density inversions, weak sediment ($\phi \sim 5^\circ$) and finite perturbations of the overburden/salt interface. Model results are consistent with the evolving sedimentation regimes. Remaining unexplained salt structures may arise from complex initial geometries of the salt basins.

18) Albertz, M., and Beaumont, C., (in press). An investigation of salt tectonic structural styles in the Scotian Basin, offshore Atlantic Canada: Part 2, Comparison of observations with geometrically complex numerical models (in press, *Tectonics*).

Abstract

Having established the first-order controls of the three primary salt tectonic structural styles of the Scotian Basin in Paper 1 of this contribution, in Paper 2 we investigate and show that many unexplained structures can be attributed to more complex initial geometries of the autochthonous salt basins than the simple rectangular shapes used in Paper 1. Basement highs modify and reduce the efficiency of salt evacuation during sediment aggradation followed by progradation. Low angle taper (ca. 3°) of the basin edge slows Poiseuille flow and allows for trapping of salt beneath distal salt sheets. Seaward basement step ups do not necessarily hinder salt flow and basement step downs can localize diapirs. Mid-basin salt sheets can emerge when basement blocks as high as the salt is thick divide a basin into two subbasins. Deep salt basins that form above basement lows are efficiently evacuated. Weak overburden sediments augment the formation of salt sheets.

17) **Gradmann, S.**, Beaumont, C., and Albertz, M., 2009. Factors controlling the evolution of the Perdido Fold Belt, northwestern Gulf of Mexico, determined from numerical models, *Tectonics*, 28, TC2002, doi:10.1029/2008TC002326.

Abstract.

The Perdido Fold Belt (PFB) is a prominent salt-cored deep-water structure in the northwestern Gulf of Mexico. It is characterized by symmetric, kink-banded folds of a ca. 4.5km thick pre-kinematic layer and its vicinity to the extensive Sigsbee Salt Canopy. We use 2D finite element numerical models to study the evolution of the PFB as a gravity-driven fold belt both in a local context and in the context of the larger-scale passive margin, influenced by adjacent allochthonous salt structures. We show that parameters such as overburden strength, salt geometry or salt viscosity determine timing, extent and location of the modeled fold belt. Simplified models of the Gulf of Mexico show that toe-of-slope folding is a viable mechanism to develop diapirs in the deep salt basin, and to delay folding of the distal overburden. In this scenario, the PFB likely represents the terminal folding of a much larger, diachronously formed fold belt system.

16) Ings, S.J., and Beaumont, C., 2010. Shortening viscous pressure ridges: a solution to the enigma of initiating salt 'withdrawal' minibasins. *Geology*, 38, 339-342, doi: 10.1130/G30520.1.

Abstract

Salt ‘withdrawal’ sedimentary minibasins are common features of rifted continental margin salt tectonic provinces and important sources of hydrocarbons. They are typically subcircular, 10-30 km in diameter, and contain up to 10 km of sediment above an evaporite layer that has been expelled into diapir structures that surround the minibasin. Although commonly invoked, the early development of these minibasins cannot be attributed to buoyant Rayleigh-Taylor (R-T) instabilities because the average density of the sediment overburden is in most circumstances initially less than that of the salt. We analyze an alternative mechanism involving early sedimentation onto the salt layer, the lateral flow and shortening of sediment and salt to form dynamically induced viscous pressure ridges (the key process), and positive feedback that inflates and grows the pressure ridges by the loading of sediment ponded between them. We show using lubrication theory and numerical models that this mechanism solves the enigma and grows minibasins until the compacting sediment is sufficiently thick and dense for R-T instabilities to take over.

15) Buiter, S.J.H., Huismans, R.S., and Beaumont, C., 2008. Dissipation analysis as a guide to mode selection during crustal extension and implications for the styles of sedimentary basins, *Jour. Geophysical Research*, 113, B06406, doi:10.1029/2007JB005272.

Abstract

We analyze the initial modes of continental extension with the aim of providing an improved understanding of the dynamic development of sedimentary basins. We first examine simple two-layer crustal-scale models which consist of a frictional-plastic upper crust bonded to a linear viscous lower crust of equal thickness. The mode of deformation is predicted by using an analytical analysis of the rate of internal dissipation of energy and the gravitational rate of work. It is assumed that models deform in the mode in which the total rate of work is minimized. For strain-softening models we predict the following modes of crustal extension: (1) pure shear, (2) multiple conjugate or parallel shear zones, (3) two shear zones, which form either one symmetric basin or two asymmetric basins, and (4) a single shear zone forming an asymmetric basin. The transitions between these modes are shown to depend on the trade off between “gains” that reduce the rate of energy dissipation and “penalties” that increase it. A single asymmetric basin is preferred for a strong brittle layer which has a high amount of strain softening (high plastic gain), a weak viscous layer and slow extension (low viscous penalty). A decrease in the plastic gain and/or an increase in the viscous penalty leads to modes with more shear zones in the upper crust. The pure shear mode is found for low strain softening, a high viscosity, and/or fast extension. Results of finite element calculations of equivalent simple two-layer models agree with the analytical mode predictions.

14) Huismans, R. S., and Beaumont, C., 2008. Complex rifted continental margins explained by dynamical models of depth-dependent lithospheric extension, *Geology*, 36, 163-166.

Subsidence of rifted continental margins is explained by the isostatic response to lithospheric stretching, which leads to syn-rift tectonic subsidence followed by lithospheric cooling and long-

term post-rift thermal subsidence. Despite the success of the Uniform Extension model (lithospheric stretching is uniform with depth), observations from some margins, including central South Atlantic, Exmouth Plateau, and central and north Atlantic, are not consistent with its predictions. For these distinctive margins, wide regions of extremely attenuated crust but relatively thin overlying syn-rift sediments with upper layers that were deposited in shallow seas, are more compatible with the Depth-Dependent Extension model (lithospheric stretching varies with depth). Although the kinematics of depth-dependent stretching are understood, the conditions favouring this style and the consequences for a complete rift zone in space and time require investigation. We show that dynamical models which lead to depth dependent extension explain characteristic features of these distinctive margins. A template developed from the dynamical model results which divides margins into Proximal, Sag and Distal (P, S, D) zones is broadly compatible with observations from approximately conjugate South Atlantic margins. Key to reproducing the observed characteristics are decoupling between upper and lower parts of the lithosphere during stretching, contrasting wide and narrow extensional styles above and below the decoupling level, and progressive focusing of crustal extension toward the rift axis. This behaviour explains the formation of the associated array of sedimentary basins, and in particular the origin and context of so-called 'sag' basins, and why these basins are prone to shallow water evaporite deposition during the late syn-rift. Evaporite-bearing South Atlantic margins of this type (e.g. Angolan and Brazilian margins), have recently been sites of new giant hydrocarbon discoveries. Conceptual and quantitative insight based on the model proposed here can help evaluate the overall hydrocarbon potential of these basins.

13) **Simon, K.**, Huismans, R.S., and Beaumont, C., 2009. Dynamical modelling of lithospheric extension and small-scale convection: implications for magmatism during the formation of volcanic rifted margins, *Geophysical Jour. International*, 176, 327-350, doi: 10.1111/j.1365-246X.2008.03891.x

SUMMARY

Enhanced melt productivity as a consequence of buoyant upwelling and small-scale convection of the mantle during rifting may play an important role in determining the fundamental structure of igneous crust produced during and following continental breakup. This paper investigates the relationship between rift-related decompression melting and the influence of small-scale mantle convection and rift geometry on the subsequent production and distribution of melt-related crust. Extension of the lithosphere is modelled numerically using a two dimensional plane-strain finite element method for viscous-plastic creeping flows. The evolving temperature and pressure fields within the model are coupled to an algorithm that predicts the amount and timing of decompression melting of upwelling mantle. Predicted melt fractions are converted to equivalent thicknesses of igneous crust, and the predicted crustal thicknesses for a series of models are compared to the observed crustal structure of rifted margins inferred from seismic data. Models characterized by small-scale mantle convection can to first order reproduce the general architecture of most volcanic rifted margins, that is, a relatively narrow band of thick (12-13 km) igneous crust (inferred to occur along strike of the margin), juxtaposed with thinner oceanic crust farther offshore. The variability in thickness (4-7 km) predicted for the later-stage thinner igneous crust is however difficult to reconcile with global observations of oceanic crustal thickness (7 ± 1 km). Also, the peak 13 km thickness of igneous crust predicted for models with

convectively enhanced upwelling fails to match the great thicknesses (> 20 km) of igneous crust observed at many volcanic margins. Composite models that include both small-scale convection and a small increase to mantle potential temperature predict large pulses in initial magmatism and generation of 17-21 km thick crust, followed by unstable production of thinner igneous crust. The results indicate that models with small-scale convection and no temperature anomaly may play a role in explaining the formation of volcanic margins with only moderately thick (11-15 km) igneous crust. Further, convection coupled with small increases to mantle temperature may be important during the initial phase of very thick igneous crust generation at some volcanic margins. Predicted distributions of igneous crust are moderately sensitive to asymmetric rifting of the lithosphere. Prior to breakup, igneous crust accretion is asymmetric; subsequent to breakup, symmetry in the thermal structure of the upwelling sublithospheric mantle is the dominant control on the final distribution of igneous crust.

12) Braun, J., Thieulot, C., Fullsack, P., DeKool, M., Beaumont, C., and Huisman, R.S., 2008. DOUAR: a new three-dimensional creeping flow model for the solution of geological problems, *Physics of the Earth and Planetary Interiors*, 171, 76-91.

11) Albertz, M., Beaumont, C., and Ings, S.J., (in press). Geodynamical modeling of sedimentation-induced overpressure, gravitational spreading and deformation of passive margin mobile shale basins. *American Assoc. Petroleum Geologists*, Hedberg Volume on shale tectonics, (accepted, November 2007, to be published in 2010).

ABSTRACT

We investigate differential loading and pore fluid pressure required for failure and subsequent prolonged, gravitational spreading of passive margin shale basins using 2D analytical limit analysis and plane strain finite element modeling. The limit analysis, supported by the models, indicates that narrow margins (slope regions that are ca. 50 to 100 km wide) require pore fluid pressures that are 80-94 % of the overburden weight for failure to occur, whereas for wider margins (ca. 400 km wide) like the Niger Delta, the corresponding values are 95-99 %, these ranges depending on the intrinsic strength of sediments. In the large deformation models gravitational spreading in response to sedimentation induced overpressure caused by delta progradation is investigated. Shale is modeled as a viscoplastic Bingham fluid that is frictional-plastic below yield and has a yield criterion that depends on the effective pressure (mean stress minus pore fluid pressure). The velocity of the post-yield flow of the shale is limited by the viscosity of the Bingham fluid, chosen for this study to be 10^{18} Pa.s. Pore fluid pressure is predicted parametrically to be proportional to the local sedimentation rate during progradation, where the proportionality constant, k_c , depends inversely on the hydraulic conductivity. Varying the sediment progradation rate, the depth of onset of excess pore pressure, and k_c , produces model deformation patterns consistent with seaward directed squeeze-type flow of overpressured shale (Poiseuille flow) or wholesale seaward motion of the shale and overburden (Couette flow), depending on the overall mobility of the model.

Publications from before 2008

10) Morency, C., Huismans, R.S., Beaumont, C., and Fullsack, P., 2007. A numerical model for coupled fluid flow and matrix deformation with applications to disequilibrium compaction and delta stability, *Jour. Geophysical Research*, 112, B10407, doi:10.1029/2006JB004701.

Abstract.

A model is developed which couples fully-saturated porous compaction to the viscous-plastic deformation of the skeleton matrix. The Darcy fluid flow during compaction is described by an advection-diffusion equation for the excess pressure with two source/sink terms that depend on the mechanical compressibility and viscous compaction of the pore space, the latter representing the effect of pressure solution. The incompressible deformation of the composite medium is described by a force balance equation and its rheology can be viscous, plastic or viscoplastic (Bingham material). For the plastic and viscoplastic cases, the coupling between the compacting and plastically deforming parts of the system is through the Drucker-Prager frictional-plastic yield criterion modified by Terzaghi's principle, so that the yield strength depends on the effective dynamical pressure. The coupled system is solved using a 2-D finite element method. Two problems are solved to demonstrate the behavior of our theory. The first considers compaction of a uniform sediment layer. The numerical results agree with the predictions of the non-dimensional control parameters and previously published results. The second problem concerns 2-D kinematic progradation of deltaic sediments. Substratum and delta sediments have the same compaction properties and a Bingham rheology during deviatoric deformation, such that the delta undergoes linear post-yield viscous flow. For certain depositional regimes overpressure is generated. When pore pressures approach critical values, yielding occurs and the delta front fails and becomes unstable, spreading gravitationally under its own weight. The flow velocity is limited to geological rates by the Bingham viscosity. For the range of parameter values considered, pressure solution is the most effective mechanism for generating near-lithostatic fluid pressures that lead to initial failure, and it appears that mechanical compaction hardly contributes to the fluid overpressure at this stage.

9) Huismans, R.S., and Beaumont, C., 2007. Roles of lithospheric strain softening and heterogeneity in determining the geometry of rifts and continental margins, in: eds, G. Karner, G. D. Manatschal, and L.M., Pinheiro, *Imaging, Mapping and Modelling Continental Lithosphere Extension and Breakup*, Geological Soc., London, Spec. Publ., 282, 107-134.

Abstract

Plane strain thermo-mechanical finite-element model experiments are used to investigate the effects of frictional-plastic strain softening and inherited weakness on the style of lithospheric extension. The model results are compared with the Newfoundland-Iberia conjugate rifted margins with the goal of understanding the lithospheric properties that controlled their evolution during rifting. Our proposition is that coupling between the plastic-viscous layering, acting together with frictional-plastic strain softening localized on inherited weak heterogeneities, can explain the initial wide rift and distributed rift basins that are later abandoned in favour of a narrow rift in which mantle lithosphere is exhumed to the surface. The models comprise uniform composition viscous and plastic layers in which focused deformation is nucleated on either a single weak 'seed' or a statistical white noise distribution of inherited

strain. Strain softening of frictional–plastic layers acts as a positive feedback mechanism that creates localized shear zones from the inherited weak heterogeneities. The sensitivity of deformation to the choice of softening parameters and the type of inherited noise is examined in cases where the deeper part of the crust is either weak or strong. Lithosphere-scale models with a single weak seed exhibit a range of asymmetric and symmetric rifting modes that are mostly determined by the feedback between two primary controls, coupling between the plastic and viscous layers and strain softening. Decreasing and increasing the rifting velocity can change the mode, and asymmetry is strongest in models with low rifting velocities and a strong lower crust. Analysis of equivalent simple-bonded plastic–viscous two-layer models using the minimum rate of dissipation principle demonstrates that the mode selected depends on the division of the dissipation between the layers. Criteria developed on minimizing the total dissipation show how mode selection changes with increasing viscosity, or rifting velocity, from the: asymmetric plug or half-graben (AP) mode; through the symmetric plug or graben (PS) mode, to the distributed pure shear (PS) mode. Numerical models confirm these results. Models with statistical white-noise-inherited strain have similar modes to those with a single seed. In addition, modes with multiple sets of shear zones develop in the plastic layer for a range of intermediate parameter combinations. We believe that distributed noise in combination with a weak lower crust and slow extension can produce model results in accord with general features of the Newfoundland–Iberia conjugate margins; an initially distributed wide rift mode, followed by a late-stage narrow rift with a significant component of mantle exhumation.

8) Huisman, R.S., and Beaumont, C., 2005. Effect of lithospheric stratification on extensional styles and rift basin geometry, in: ed., Post, P., *Petroleum Systems of Divergent Continental Margin Basins, 25th Annual GCSSEPM Foundation Bob F. Perkins Research Conference proceedings*, (On CD Rom ISSN: 1544-2462.)

7) Gemmer, L., Beaumont, C., and Ings, S.J., 2005. Dynamic modelling of passive margin salt tectonics- effects of water loading, sediment properties, and sedimentation patterns, *Basin Research*, 17, 383-402.

ABSTRACT

We investigate the evolution of passive continental margin sedimentary basins that contain salt through two-dimensional (2D) analytical failure analysis and plane-strain finite-element modelling. We expand an earlier analytical failure analysis of a sedimentary basin/salt system at a passive continental margin to include the effects of submarine water loading and pore fluid pressure. Seaward thinning sediments above a weak salt layer produce a pressure gradient that induces Poiseuille flow in the viscous salt. We determine the circumstances under which failure at the head and toe of the frictional-plastic sediment wedge occurs, resulting in translation of the wedge, landward extension and seaward contraction, accompanied by Couette flow in the underlying salt. The effects of water: (i) increase solid and fluid pressures in the sediments; (ii) reduce the head to toe differential pressure in the salt and (iii) act as a buttress to oppose failure and translation of the sediment wedge. The magnitude of the translation velocity upon failure is reduced by the effects of water. The subsequent deformation is investigated using a 2D finite-element model that includes the effects of the submarine setting and hydrostatic pore pressures.

The model quantitatively simulates a 2D approximation of the evolution of natural sedimentary basins on continental margins that are formed above salt. Sediment progradation above a viscous salt layer results in formation of landward extensional basins and listric normal growth faults as well as seaward contraction. At a later stage, an allochthonous salt nappe overthrusts the autochthonous limit of the salt. The nature and distribution of major structures depends on the sediment properties and the sedimentation pattern. Strain weakening of sediment favours landward listric growth faults with formation of asymmetric extensional depocentres. Episodes of low sediment influx, with partial infill of depocentres, produce local pressure gradients in the salt that result in diapirism. Diapirs grow passively during sediment aggradation.

- 6) Huismans, R., Buiter, S.J.H., and Beaumont, C., 2005. The effect of plastic-viscous layering and strain softening on mode selection during lithospheric extension, *Jour. Geophysical Research* 110, B02406, doi:10.1029/2004JB003114.

Factors controlling the selection of deformation modes during continental extension are investigated using analytical and numerical methods. We view the lithosphere as a laminate and examine a simple system with a uniform plastic layer overlying a uniform linear viscous layer. The rate of energy dissipation is analyzed for pure shear (PS), symmetric plug (SP), and asymmetric plug (AP) extension modes, and the analysis reveals that the primary control is the relative rate of dissipation in the two layers. A basic difference is that the plastic layer yield strength is independent of the strain rate, whereas the viscous stress depends on strain rate; therefore dissipation scales linearly and quadratically with extension velocity for these respective layers. When other parameters, e.g., extension velocity, and properties are held constant, minimum dissipation predicts that the modes AP, SP, and PS will be selected in this order with increasing viscosity of the lower layer. Transition viscosities between modes, hT1 and hT2 are 4×10^{21} Pa s and 8×10^{22} Pa s, respectively, for our parameters values. Numerical models confirm the analysis results, inferred mode controls, and order of mode selection when strain softening of the plastic layer occurs during extension. Implications for lithosphere that acts as a bonded plastic/viscous laminate include the following (1) asymmetric extension (AP mode) is preferred when the extension rate and/or effective viscosity is low or the viscous region temperature is high, (2) symmetric (SP mode) extension is preferred for intermediate combinations of parameters, and (3) overall pure shear (PS mode) may occur for opposite end-member parameter combinations.

Citation: Huismans, R. S., S. J. H. Buiter, and C. Beaumont (2005), Effect of plastic-viscous layering and strain softening on mode selection during lithospheric extension, *J. Geophys. Res.*, 110, B02406, doi:10.1029/2004JB003114.

- 5) Gemmer, L., **Ings, S.J.**, Medvedev, S., and Beaumont, C., 2004. Salt tectonics driven by differential loading: stability analysis and finite element experiments, *Basin Research*, 16, 199-208.

ABSTRACT

At many continental margins, differential sediment loading on an underlying salt layer drives salt deformation and has a significant impact on the structural evolution of the basin. We use 2-D

finite element modelling to investigate systems in which a linear viscous salt layer underlies a frictional plastic overburden of laterally varying thickness. In these systems, differential pressure induces the flow of viscous salt, and the overburden experiences updip deviatoric tension and downdip compression. A thin-sheet analytical stability criterion for the system is derived and used to predict conditions under which the sedimentary overburden will be unstable and fail, and to estimate the initial velocities of the system. The analytical predictions are in acceptable agreement with initial velocity patterns of the numerical models. In addition to initial stability analyses, the numerical model is used to investigate the subsequent finite deformation. As the systems evolve, overburden extension and salt diapirism occur in the landward section and contractional structures develop in the seaward section. The system evolution depends on the relative widths of the salt basin and the length scale of the overburden thickness variation. In narrow salt basins, overburden deformation is localised and characterised by high strain rates, which cause the system to reach a gravitational equilibrium and salt movement to cease earlier than for wide salt basins. Sedimentation enhances salt evacuation by maintaining a differential pressure in the salt. Continued sedimentary filling of landward extensional basins suppresses landward salt diapirism. Sediment progradation leads to seaward propagation of the landward extensional structures and depocentres. At slow sediment progradation rates, the viscous flow can be faster than the sediment progradation, leading to efficient salt evacuation and salt weld formation beneath the landward section. Fast sediment progradation suppresses the viscous flow, leaving salt pillows beneath the prograding wedge.

- 4) **Ings, S.**, Beaumont, C., and Gemmer, L., 2004. Numerical modeling of salt tectonics on passive continental margins: preliminary assessment of the effects of sediment loading, buoyancy, margin tilt, and isostasy, *24th Annual GCSSEPM Bob F. Perkins Research Conference proceedings*, 36-68. (On CD Rom ISSN: 1544-2462.)

Salt tectonics in passive continental margin settings is investigated using a 2D vertical cross-sectional finite element numerical model of frictional-plastic sedimentary overburden overlying a linear viscous salt layer. We present preliminary results concerning the effects of sediment progradation over the salt, buoyancy driven flow owing to density contrast between the sediment and salt, regional tilt of the salt layer, and local isostatic adjustment of the system. Sediment progradation causes a differential load on the underlying salt, which may lead to instability of the system with landward extension accommodated by seaward distal contraction. Slow progradation ($V_{sp} = 0.5$ cm/yr) of aggrading sediments gives a diachronous evolution comprising four main phases: 1) initiation of salt channel flow and the formation of minibasins and associated diapirs; 2) onset of listric normal growth faulting and extension of the sedimentary overburden; 3) large scale evacuation of the salt, formation of pre-rafts and rafts, and inversion of the minibasins; 4) formation of a contractional allochthonous salt nappe that overthrusts the depositional limit of the salt.

Buoyancy effects are investigated using models with density contrasts between overburden and sediment of 0, 100 and 400 kg/m³. Although the lateral flow driven by differential loading dominates in all cases, the form of the minibasins, the overall salt evacuation, and style of

diapirism are sensitive to buoyancy forces, with the large density contrast producing the most developed diapiric and minibasin structures.

A regional basinward tilt of 0.2° (of the type that may be produced by thermal contraction of the rifted margin) enhances and accelerates the overall seaward flow of the unstable slope region of the model leading to much earlier overthrusting of the distal depositional limit of the salt. The added downslope gravitational component also modifies the style of the minibasins by enhancing the horizontal channel flow by comparison with the vertical buoyancy driven flow. This reduces the apparent efficiency of diapirism.

Local isostatic adjustment, owing to overburden and water loading, introduces a landward tilt of the system, thereby requiring salt to flow updip against gravity during evacuation. Isostasy also changes the overburden geometry and, therefore, modifies the stability and flow velocity of the extending overburden through the increased strength of the isostatically thickened proximal overburden, and through the modified differential pressure acting on the salt under these circumstances. The seaward flow of the unstable slope region is slower for the same overburden progradation velocity, more salt remains beneath the shelf as rollers and pillows during evacuation, counter-regional faults are more pronounced, and the allochthonous salt nappe progressively climbs above the isostatically adjusting sediments as it overthrusts.

- 3) Huisman, R.S., and Beaumont, C., 2003. Symmetric and asymmetric lithospheric extension: relative effects of frictional-plastic and viscous strain softening, *Jour. Geophysical Research*, 108, 2496, doi: 10.1029/2002JB002026.

Strain-dependent rheologies may play a critical role in the deformation of the lithosphere and particularly in the development of focused shear zones. We investigate the effects of strain softening on lithospheric extension using plane strain thermomechanical finite element model experiments. Parametric softening is specified as a linear decrease of the effective internal angle of friction, the effective viscosity, or both in the model rheologies. The sensitivity of deformation to the choice of softening parameters is investigated in cases where the crust is either strongly or weakly coupled to the mantle lithosphere. Results are classified according to the symmetry (S) or asymmetry (A) of the deformation of the upper and lower lithosphere during rifting. Strain softening is required for rifting asymmetry but is not always sufficient. A range of model tectonic styles occurs including pure and simple shear modes with focused shear zones. Mode selection is mostly determined by the feedback between two primary controls, the “dominant” rheology and the parametric strain-softening mechanisms listed above. Softening of the dominant rheology promotes asymmetric extension of that part of the lithosphere controlled by the dominant rheology. Model results are consistent with the proposed primary controls and the factors that contribute to these controls. In particular, decreasing and increasing the rifting velocity can change the mode by changing the dominant rheology. Asymmetry is strongest in coupled models which include a decrease in the internal angle of friction and have low rifting velocities.

2) Huismans, R.S., and Beaumont, C., 2002. Asymmetric lithospheric extension: the role of frictional-plastic strain softening inferred from numerical experiments, *Geology*, 30, 211-214.

ABSTRACT

Plane-strain thermomechanical finite element model experiments of lithospheric extension are used to investigate the effects of strain softening in the frictional plastic regime on the asymmetry of extension. Strain softening is considered in cases where the crust is either strongly or weakly coupled to the mantle, and as the extension velocity varies from 0.3 to 30 cm/yr. In the absence of strain softening, extension is symmetric (SS mode). When strain softening takes the form of a reduction in the internal angle of friction with increasing strain, lithospheric extension may be asymmetric at a lithospheric scale (AA mode), or exhibit crustal asymmetry concomitant with mantle symmetry (AS mode). The different styles depend on the relative control of the system by the frictional plastic and ductile layers, which promote asymmetry and symmetry, respectively. High extension velocities and weak ductile crust-mantle coupling tend to suppress the fundamental asymmetry induced by frictional strain softening. This is because they, respectively, increase the effective strength of the lower lithosphere and decrease the control by frictional plasticity.

Short Course Notes

Adam, J., Beaumont, C., Huismans, R., Ings, S., and Stockmal, G., 2005. Advances in Geodynamical Modelling... *Notes for Short Course SC-4, GAC Annual General Meeting, Halifax*. 394pp.

Other Publications.

1) **Ings, S.J.**, and Shimeld, J.W., 2006. A new conceptual model for the structural evolution of a regional salt detachment on the northeast Scotian margin, offshore eastern Canada, *Am. Assoc. Petrol. Geol. Bull.*, 90, 1407-1423, 2006.

ABSTRACT In this study we examine, using seismic data in conjunction with numerical modeling, a regional-scale salt detachment and associated syn-kinematic sediments from the Scotian, offshore eastern Canada. This portion of the Scotian Margin is characterized by an up to 4.5 km thick and ~175 km long syn-kinematic wedge of Jurassic sediments with internal sigmoidal, landward dipping reflectors. The syn-kinematic wedge is laterally extensive, encompassing an area of ~30,000 km², and soles into an interpreted salt detachment. The Jurassic syn-kinematic wedge is interpreted to have formed as an open-ended allochthonous salt nappe was loaded by prograding sediments during the Jurassic. This loading squeezed the salt seaward and caused the overlying sediments to undergo extension and gravity spreading/gliding, detaching on the salt sheet. The open-ended nappe model provides a mechanism for producing a large amount of extension with very little compensating contraction. Numerical model results indicate that high rates of extension, detaching on even a thin salt layer, can result in similar sigmoidal, landward dipping strata. Based on the numerical modeling and seismic interpretation results, we propose a new conceptual model for the Jurassic-Paleogene structural evolution of the

study area; this model may also have implications for other passive margin salt basins with regional salt detachments.

Theses

Ings, S.J. 2006. Passive continental margin salt tectonics: Numerical modelling, analytical stability analysis, and applications to the Scotian Margin, offshore eastern Canada. Ph.D. Thesis, 352 pp. Dalhousie University, Halifax, Nova Scotia, Canada.

Simon, K, M., 2007. Dynamical modelling of lithospheric extension and small-scale convection: implications for magmatism during the formation of volcanic rifted margins, M.Sc. Thesis, Dalhousie University, Halifax, Nova Scotia Canada, completed March 2007.

Appendix 1A (Part 2)

Discussion of Objectives, Methodology and Results for Project 1: Forward Dynamical Modelling of Lithospheric Extension and Rifting Linked to the Development of the Nova Scotian Margin

1. Summary

Despite the existence of two well-studied crustal scale transects of the Nova Scotian margin (Funck et al., 2004; Wu et al., 2006), and similar transects from Morocco conjugate margin (Contrucci et al., 2004; Klingelhöfer et al., 2009), we have only a rudimentary understanding of the way the final crustal structure, as observed today, is linked to the Triassic-Jurassic lithospheric extension and rifting between Nova Scotia and Morocco. In particular, the form of the syn-rift and early post-rift sedimentary basins can only be determined approximately from either the large-scale crustal structure or interpretation of the ION/GXT NovaSpan seismic reflection images of the deep sedimentary structures. What is required is a more fundamental understanding of the rift process and how it imparts geometries to the sedimentary basins. While this remains a long term goal, progress has been made in the geodynamical forward modelling of depth-dependent lithospheric extension and rifting with the purpose of relating observed crustal structure to the properties of the lithosphere responsible for particular styles. This approach seeks an explanation of the observed discrepancies by comparison with the Uniform Extension (McKenzie, 1978) model. So far, depth-dependent extension has been shown to provide an explanation for the differences between narrow, Type I margins (e.g. Newfoundland-Iberia) and ultra-wide Type II margins (e.g. South Atlantic) based on the coupling/decoupling of upper and lower lithosphere. This approach also allows the characteristics of the associated sedimentary basins to be predicted; for example ‘sag basins’ in Type II margins (Huisman and Beaumont, 2008) but not Type I (Huisman and Beaumont, *submitted*).

2. Scientific Objectives

We propose to investigate the development of the Nova Scotian margin using the following approach:

1. List the margin characteristics as determined by crustal and basin-scale seismic, subsidence and potential field studies of the conjugate Nova Scotian and Moroccan margins,
2. Use geodynamical forward models with a range of lithospheric properties to determine their depth-dependent stretching properties.
3. Use those models that match the observations to predict the character of the sedimentary basins.

This proposed research will also take into account: i) single and double-phase rifting and ii) sedimentation as the models evolve, in particular deposition of evaporites and the linked problem of the salt tectonics. This approach is designed for magma-poor rifted margins and is therefore

considered suitable for much of the Nova Scotia margin. We will also consider the role of moderate levels of magmatism for the southwest part of the margin in assisting rifting and breakup and on its potential to modify the observed geometry. The Nova Scotian margin is not an end member and has some characteristics that are intermediate to the Types I and II noted above. The challenge is to determine the lithospheric properties that impart these characteristics.

The intent of the research is to understand:

1. How the geometrical characteristics of the Nova Scotian margin developed,
2. The reasons for the change in characteristics with position along the margin,
3. The relationship of the geometrical style to the properties of the lithosphere from a general perspective and in relationship to inheritance from the Acadian and Alleghanian orogenies.

In addition, the geodynamical models predict surface heat flow as a function of position and time. The predicted heat flux can be used in conjunction with thermal subsidence basin modelling to test the range of levels of sediment thermal maturation and its development through time.

The project will utilize the 2D geodynamical thermal-mechanical, plane strain finite element software (Sopale) developed at Dalhousie University. This software is capable of modelling the stretching and rifting of lithosphere in models at the upper-mantle scale and has been used to investigate and develop the links between lithospheric compositional and rheological properties and its style of depth-dependent extension (see Huismans and Beaumont papers in bibliography).

We will also be able to draw on Ritske Huismans' (University of Bergen, Norway) modelling experience. The research will be integrated with the Plate Tectonic component of the overall project.

2.1 Research Targets/Deliverables for Q1-Q2 2010

Investigate the mechanisms causing the large-scale rifting characteristics of the Nova Scotia margin. This will include an evaluation of the existing data constraints and possible alternative interpretations followed by a series of 'what if' questions which will be tested using generic forward modelling.

If successful, this will establish a general template in which the NS margin can be compared /contrasted with (narrow) Newfoundland-Iberia and (ultra-wide) South Atlantic margins. The variation along strike between a possible amagmatic to a magmatic margin will also be assessed.

Progress on the evaluation of mechanisms and characteristics will be reported at the end of Q1 and Q2.

3. Description of Progress

Progress has been made in developing a basic understanding of the crustal architecture of the Nova Scotian Margin and how this compares with other better-studied margins.

3.1 Nova Scotia Rifted Margin

The Nova Scotia rifted margin has been studied using two published seismic refraction lines, the recently acquired GeoPro 2009 line, and a line from the SW part of the margin, courtesy of S. Dehler (*pers. comm.*); locations are shown in Figure A1. The GeoPro2009 line (Fig. A2A) is located on the northeast end of Banquereau Bank and approximately parallels SMART Line 2. Line 2 is situated on the southwest end of Banquereau Bank and was interpreted by Funck et al. (2004) who produced a detailed velocity model (Fig. A2B).

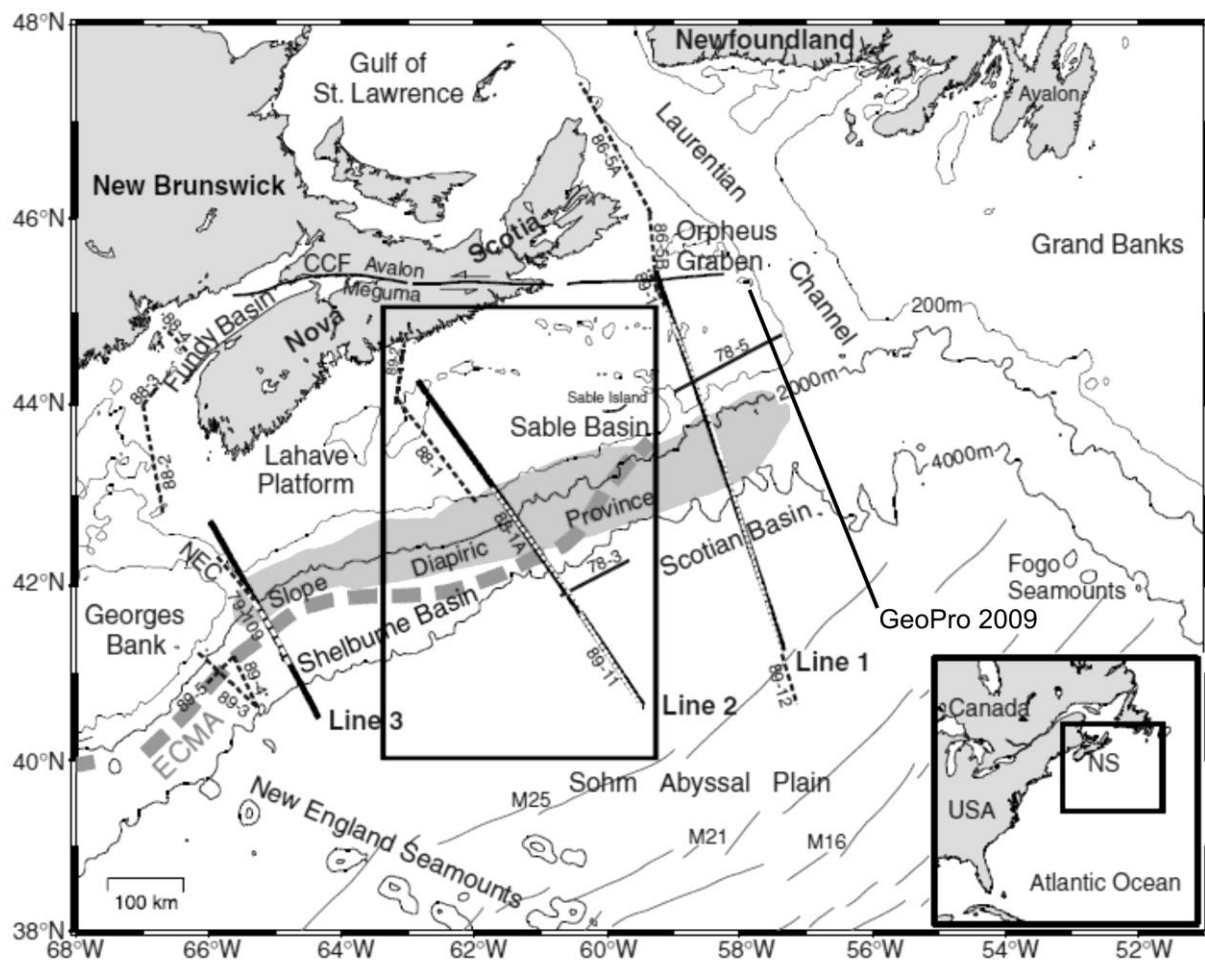
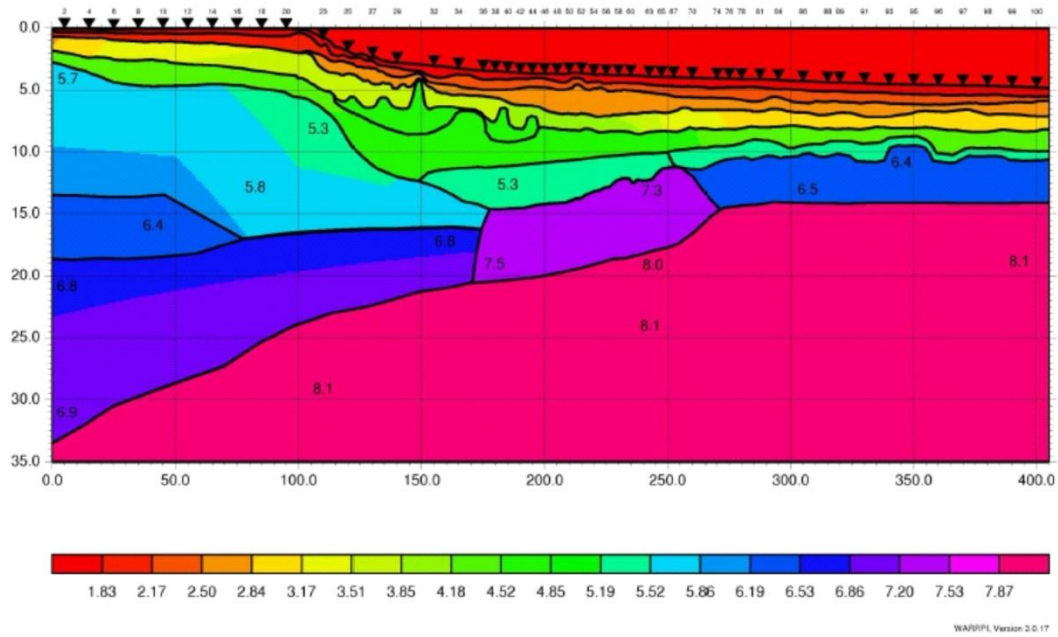


Figure A1. Location of seismic refraction lines on the Scotian Margin (from Wu et al., 2006). Line 1 was interpreted by Funck et al., 2004; line 2 was interpreted by Wu et al. (2006). Line 3 is shown in Figure A2C (Dehler, *pers comm*). The GeoPro 2009 line location is approximate.

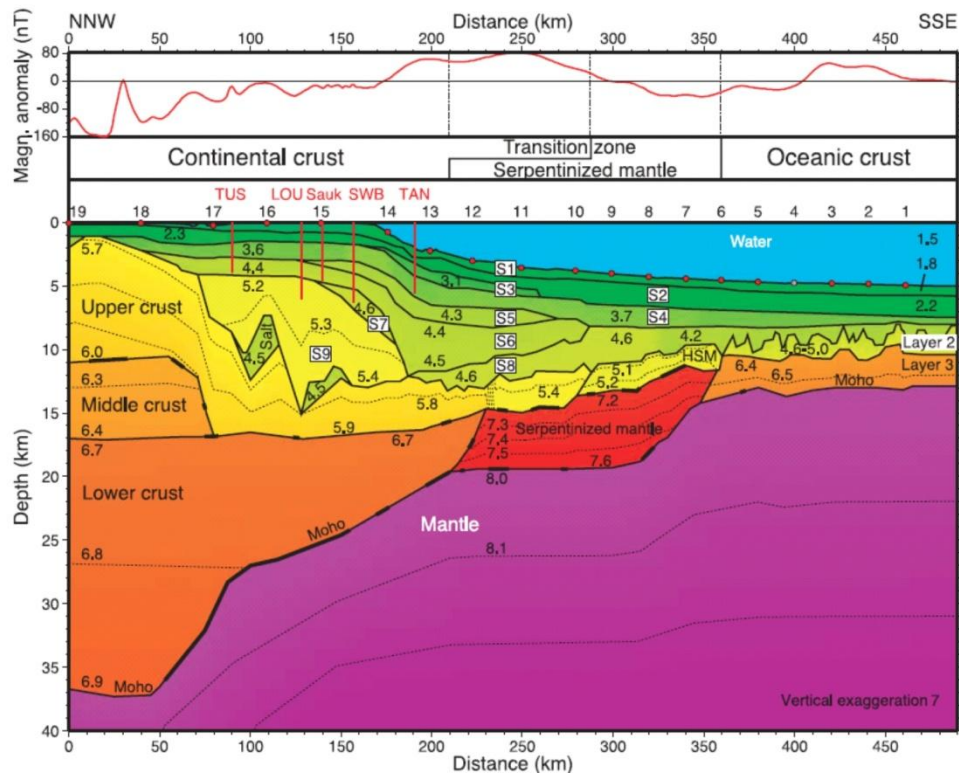
A

GeoPro 2009



B

Line 1



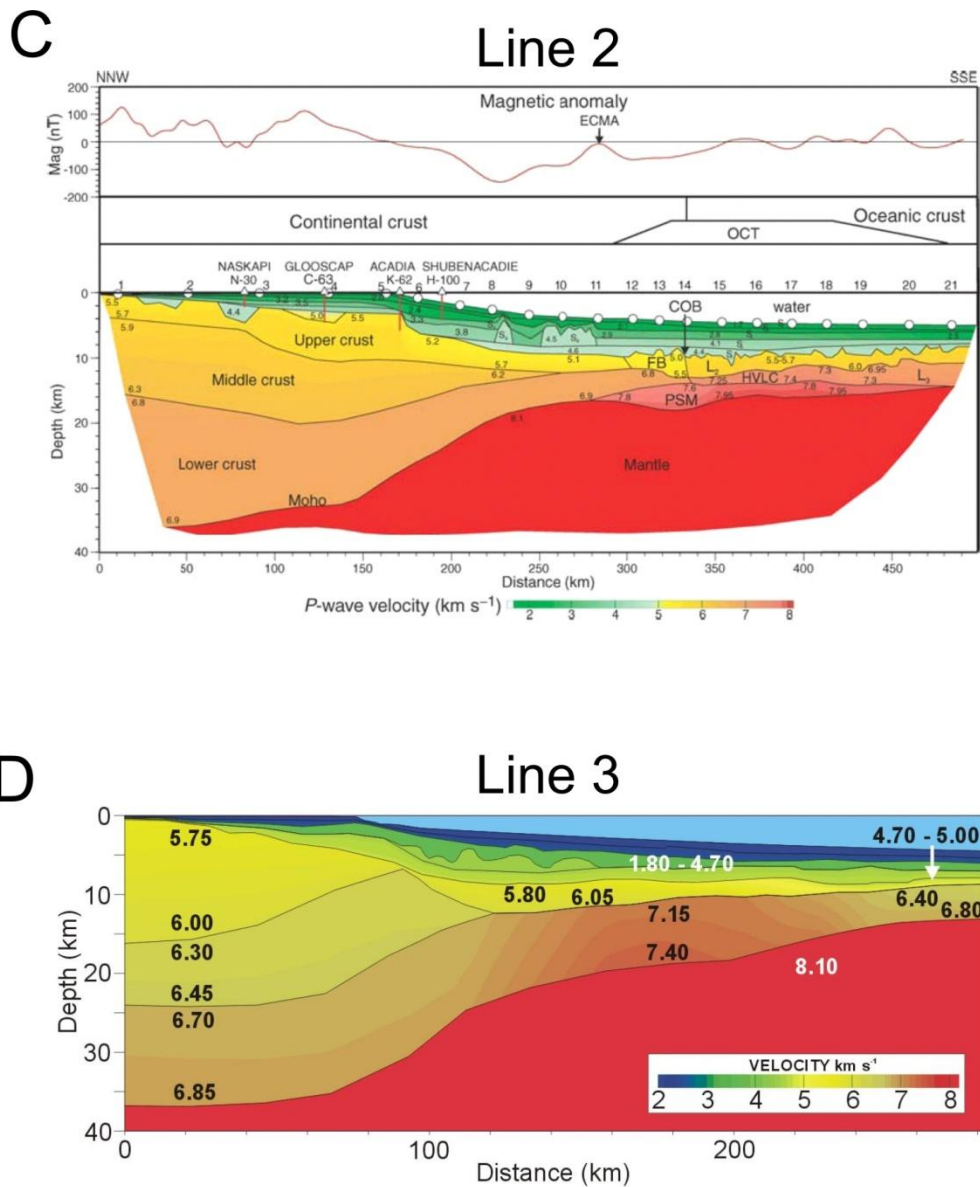


Figure A2. Velocity models of seismic refraction lines from the Scotian Margin. A) GeoPro 2009, showing broad zone of extended crust, and an anomalous high velocity transitional crust interpreted to be serpentinized mantle, and thin oceanic crust. B) Line 1, interpreted by Funck et al., 2004, showing a similar broad zone of crustal extension, limited extent of middle crust, serpentinized mantle block, and deep sedimentary basin. C) Line 2, interpreted by Wu et al., 2006, showing wider zone of extension with middle crust extending significantly further than in line 1, thinner partially serpentinized mantle (PSM), and a relatively shallow sedimentary basin. D) Line 3, from the southwest part of the margin, which shows a narrow zone of crustal thinning, landward dipping ‘middle crust’, interpreted magmatic underplate with high seismic velocity overlain by a wedge of material with velocities consistent with the upper crust, and normally thick oceanic crust (Dehler *pers comm*).

Line 2 (Fig. A2C) is located ~200 km southwest of Sable Island; a velocity model of this line was presented by Wu et al. (2006). Both lines are oriented approximately perpendicular to the Nova Scotia coastline (i.e., they are dip lines). Line 3 (Fig. A2D) is located on the southwest end of the margin, and is the shortest of the four available lines.

3.1.1 Magma-poor northern Nova Scotian Margin

The seismic interpretations show that the northern Nova Scotia margin is characterized by a zone of crustal thinning 200-320 km wide in GeoPro 2009 and lines 1 and 2 (Fig. A2). The undeformed continental crust is ~37 km thick in line 1 and ~36 km in line 2. In each line the crust has been divided into three layers (upper, middle, and lower) based on seismic velocity.

In line 1 the upper crust is ~10 km thick beneath the continental shelf and thins to ~3 km thick beneath the outer slope over a distance of ~230 km. Immediately seaward of the highly thinned upper crust is a relatively low velocity domain interpreted to be highly serpentinized mantle; this domain is ~50 km wide (HSM in Fig. A2B). The thickness of the lower crust varies from ~20 to ~5 km over a distance of ~180 km. The middle crust thins from ~6.5 to 0 km over a narrow zone ~25 km wide. Beyond $x = 80$ km in line 1 (Fig. A2B), the middle crust is absent and upper crust directly overlies lower crust. In addition to thinned crust, the velocity model of line 1 includes a body of anomalously high P-wave seismic velocity, interpreted to be serpentinized mantle, ~130 km wide and a maximum of ~6 km thick. Oceanic crust is located seaward of the serpentinized mantle and is thinner than normal. The sedimentary basin imaged in line 1 is up to ~14 km thick beneath the shelf. Significant sediment thicknesses occur well outboard of the shelf break; ~5 km of sediment overlies the continent-ocean boundary ($x = 360$ in Fig. A2B).

The GeoPro2009 line has a similar character to SMART line 1. The landward end of the line does not extend far enough northwest to determine undeformed crustal thickness. The width and style of the crustal stretching is similar, as is the existence of a high velocity transitional crustal body, interpreted to be serpentinized mantle. Oceanic crust is thinner than normal. The primary difference between GeoPro 2009 and line 1 is the thickness and distribution of interpreted continental crust above the high velocity body.

Line 2 is similar to line 1 with respect to crustal thickness and the width of the zone of crustal thinning. However, there are several differences. The upper crust thins from ~4 to ~2 km over a distance of ~285 km (Fig. A2B). The middle crust thins from ~12 to 0 km over a distance of ~245 km. Below this, the lower crust thins from ~18 to ~2 km over a distance of ~300 km. Owing to the limited extent of middle crustal thinning, the upper crust directly overlies lower crust within a ~60 km wide zone beneath the outer slope (Fig. A2B). An anomalously high velocity region interpreted to be 'partially serpentinized mantle' (Wu et al., 2006) is located between $x = 275 - 480$ km in Fig. A2B ('PSM') and is a maximum of ~4 km thick. Only the landward 50 km of the PSM domain is situated beneath thinned crust of continental origin; the remainder is overlain by oceanic crust. Oceanic crust is also thin along this line. The maximum sediment thickness in line 2 is ~6 km.

To a first approximation GeoPro 2009, lines 1 and line 2 have similar characteristics, which we list below. There are, however, four differences that are noteworthy:

1. The lateral extent of the middle crust,
2. The total width of the crustal thinning zone that defines the margin,
3. The location and extent of serpentinized mantle material,
4. The thickness of the overlying sedimentary basin.

Figure A3 shows how the northern Nova Scotia margin (GeoPro 2009 and Lines 1 and 2) and its Morocco conjugate compares with example cross sections from the North Atlantic Newfoundland – Iberia conjugate margins and the central South Atlantic Brazil – Angola conjugate margin. The Newfoundland – Iberia margins are characterized by relatively narrow zones of crustal thinning, e.g., ~175 km wide on the Newfoundland side (Fig. A3A; crust shown in orange), and serpentinized mantle material exposed on the Iberia side (light blue). Both margins have relatively thin sediment cover and the syn-rift sediments are locally confined to crustal half grabens (green). The Newfoundland – Iberia conjugates are Type I margins (Huisman and Beaumont, *submitted*).

The Brazil – Angola conjugate margins, shown in Figure A3C, are significantly wider than the Newfoundland- Iberia margins. On the Angola side, the crust (orange) thins from ~30 to ~5 km over a zone ~60 km wide. Seaward of this, the nearly-uniform thickness crust extends seaward an additional ~200 km giving a total margin width of ~260 km. A significant difference between this system and the Type I Newfoundland – Iberia system is the thickness and distribution of syn-rift sediments. Early syn-rift sediments (green) fill basement lows and are covered by a laterally-extensive layer of thick (up to 4 km) late syn-rift sediments (yellow). This style of basin with thick, laterally extensive, and relatively undeformed sediments is generally referred to as a ‘sag basin’. Above the syn-rift fill, post-rift salt (magenta) and other sediments (grey) define a ~6 km thick post-rift sedimentary basin. The Brazil – Angola conjugates are Type II margins (Huisman and Beaumont, 2008, *submitted*).

The northern Nova Scotia – Morocco conjugate system is shown in Figure A3B at the same scale as the Newfoundland – Iberia margins and the Brazil – Angola margins. In Figure A3B the crust is separated into upper (orange), middle (red), and lower (sand-colour) units. Serpentinized mantle is shown in medium-blue and ‘highly serpentinized mantle’ (Funck et al., 2004) is shown in pink. Oceanic crust is shown in light-blue and sediments are shown in grey. No detailed information is available to determine if significant syn-rift sediments exist on the Scotian Margin. The serpentinized mantle on the Nova Scotian margin is an interpretation based on seismic velocities and velocity gradients (Funck et al., 2004), whereas continental mantle is known to be exposed at the seabed on the Newfoundland and Iberian margins.

As discussed earlier, the most striking feature of the northern Nova Scotia margin is its lateral scale; the zone of crustal thinning is significantly wider than that of the Newfoundland – Iberia margin and is at least as wide as the ‘ultra wide’ Angolan margin. The Nova Scotia – Morocco margin has characteristics of both Type I (Fig. A3A) and Type II (Fig. A3C) margins. The total margin width and the geometry of the thinned crust is compatible with Type II margins, while the existence of interpreted serpentinized mantle is more compatible with Type I margins. The presence of a deep sedimentary basin (>15 km) separates it from the other margins shown in

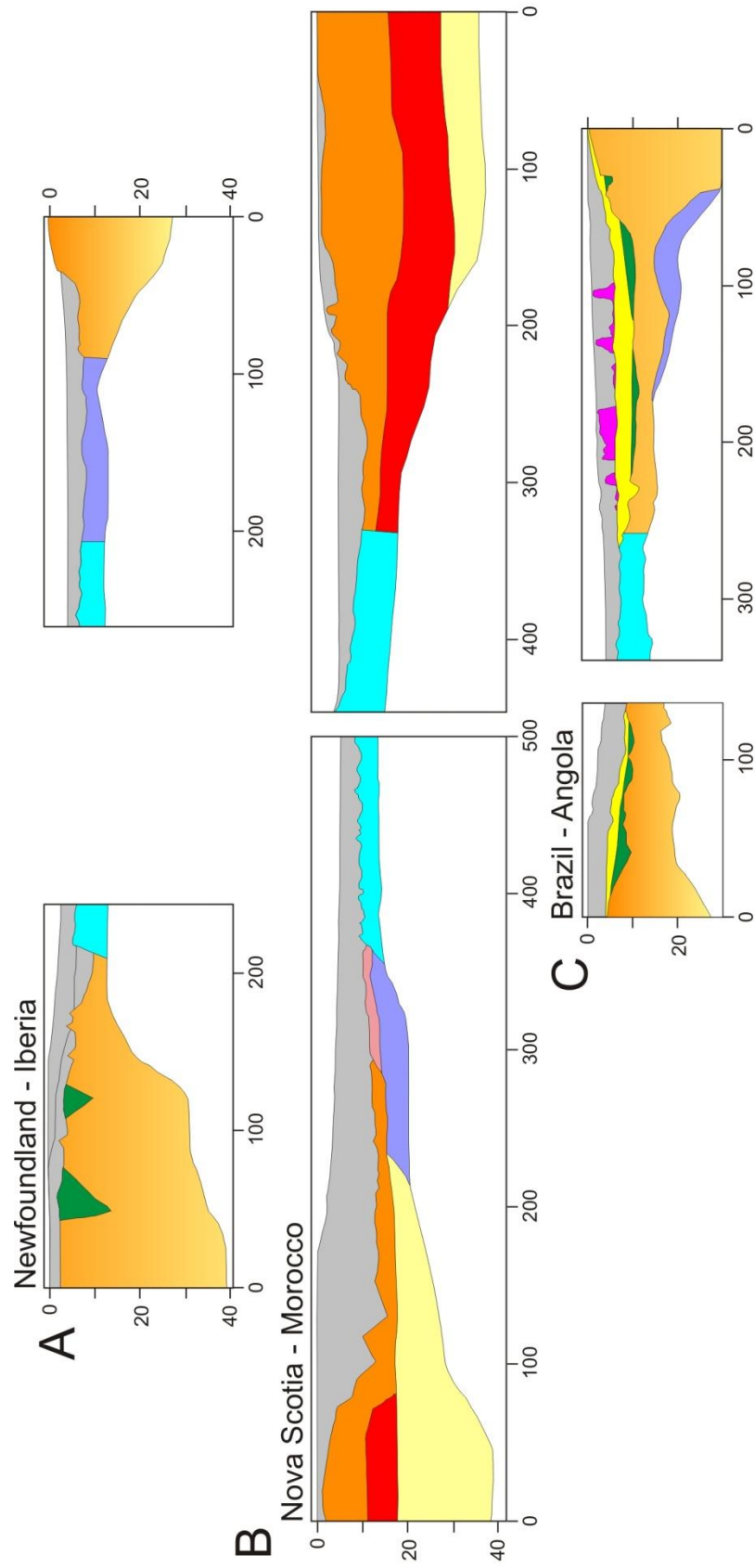


Figure A3. Crustal cross sections from the A) Newfoundland - Iberia margins (modified after Huismans and Beaumont, 2007; original data from Keen and de Voogd, 1989; Keen et al., 1987; Dean et al., 2000), B) Nova Scotia - Morocco margins (modified after Funck et al., 2004; Contrucci et al., 2004) and C) the Brazil Camamu - Angola margins (modified after Huismans and Beaumont, 2008; original data from Moulin et al., 2005; Rosendahl et al., 2005). (A, C) Crust is shown in orange shades and B) orange (upper crust), red (middle crust), and sand colour (lower crust). Early syn-rift sediments (green), late syn-rift sediments (yellow), serpentinized mantle (light blue), highly serpentinized mantle (pink), oceanic crust (cyan), post-rift sediments (grey) and salt (magenta) are also shown. All sections are shown at the same scale. Vertical exaggeration is 2.8.

Figure A3. The Nova Scotian and Moroccan margins each contain significant salt deposits not shown in Figure A3B.

The magma-poor northern Nova Scotia margin therefore has the following general characteristics:

1. A tapered zone of crustal thinning that is 200 to 300 km wide;
2. Mantle material that becomes exposed or underplates thin crust during rifting, thereby having the potential to be serpentinized to varying degrees;
3. Highly thinned crust overlaps the partially serpentinized mantle;
4. The upper crust is faulted and has syn-rift sedimentary basins;
5. Oceanic crust is thinner than 'normal' oceanic crust.

3.1.1 Magma rich southern Nova Scotian Margin

Line 3 has an entirely different nature. The zone of continental crust thinning, ~100 km wide and is significantly narrower than in the northern lines (i.e., GeoPro2009, Line1 and Line 2). In addition, line 3 shows a pronounced landward dipping middle crust and a region at ~80 km where the upper crust appears to have been removed, perhaps broken, with sediments directly overlying middle crust (Fig. A2D). There is a high velocity transitional crust in line 3, which is interpreted as a magmatic underplate. This magma-rich part of the margin therefore has the following set of characteristics:

1. Narrow region (~100km wide) in which the continental crust thins;
2. Thick magmatic underplate separating thinned continental and oceanic crust;
3. Seaward dipping reflectors (SDR's) above the seaward end of the high velocity body;
4. Normally-thick oceanic crust;
5. Thin sedimentary basin;
6. Wedge of low velocity material above underplated region.

Based on these characteristics, the southwest Nova Scotia margin can be interpreted as the northern extension of the magma-rich margin domain that characterises the US east coast, and that a transition from this style to a magma-poor rift style occurs somewhere between lines 2 and 3. Figure A4 shows the location of various crustal transects from the US east coast and SMART line 3 from the southwest Nova Scotia margin. Figure A5 shows four crustal transects, at the same scale, through the magma-rich domain, and illustrates that the character of SMART line 3 is consistent with magma-rich margins to the south. These transects are similar in terms of the total width of stretched continental crust, thickness of oceanic crust, the presence of an interpreted magmatic underplate, and seaward dipping reflectors (not shown in Fig. A5). This contrasts with the style of margin shown in Figure A2A-C and Figure A3B-C which have significantly wider stretching profiles, faulted upper crust with syn-rift basins on the shelf, thin oceanic crust, no seaward dipping reflectors, and interpreted zone of serpentinized mantle.

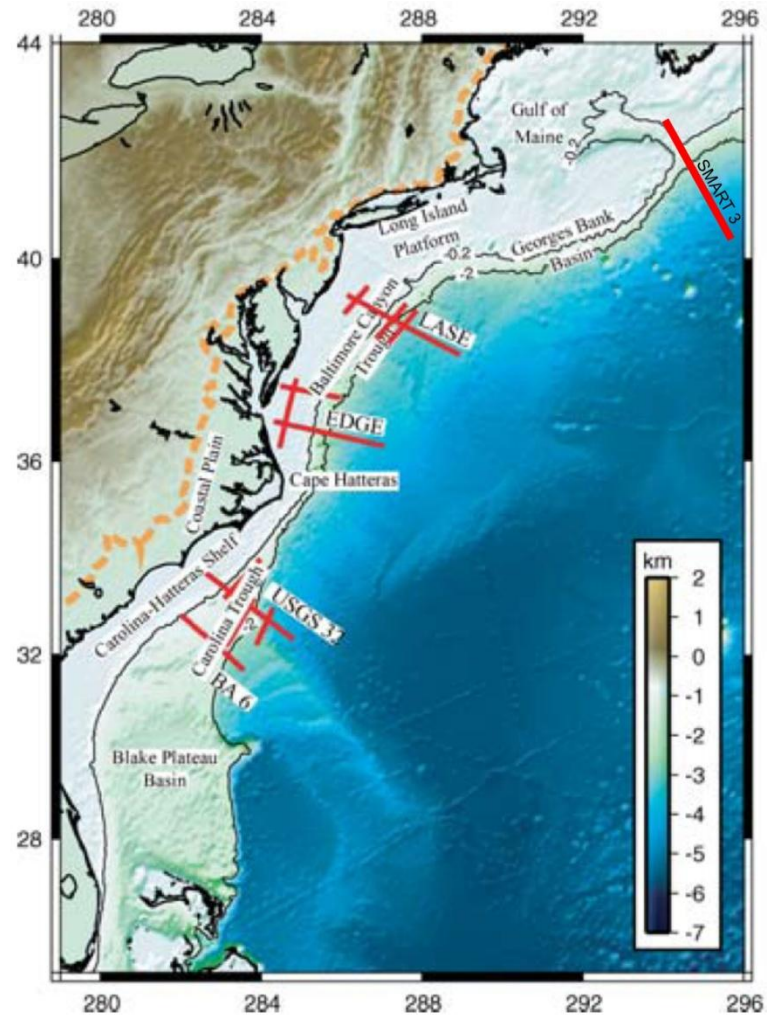


Figure A4. Location of crustal transects through magma-rich east coast margins (modified from Wyer and Watts, 2006).

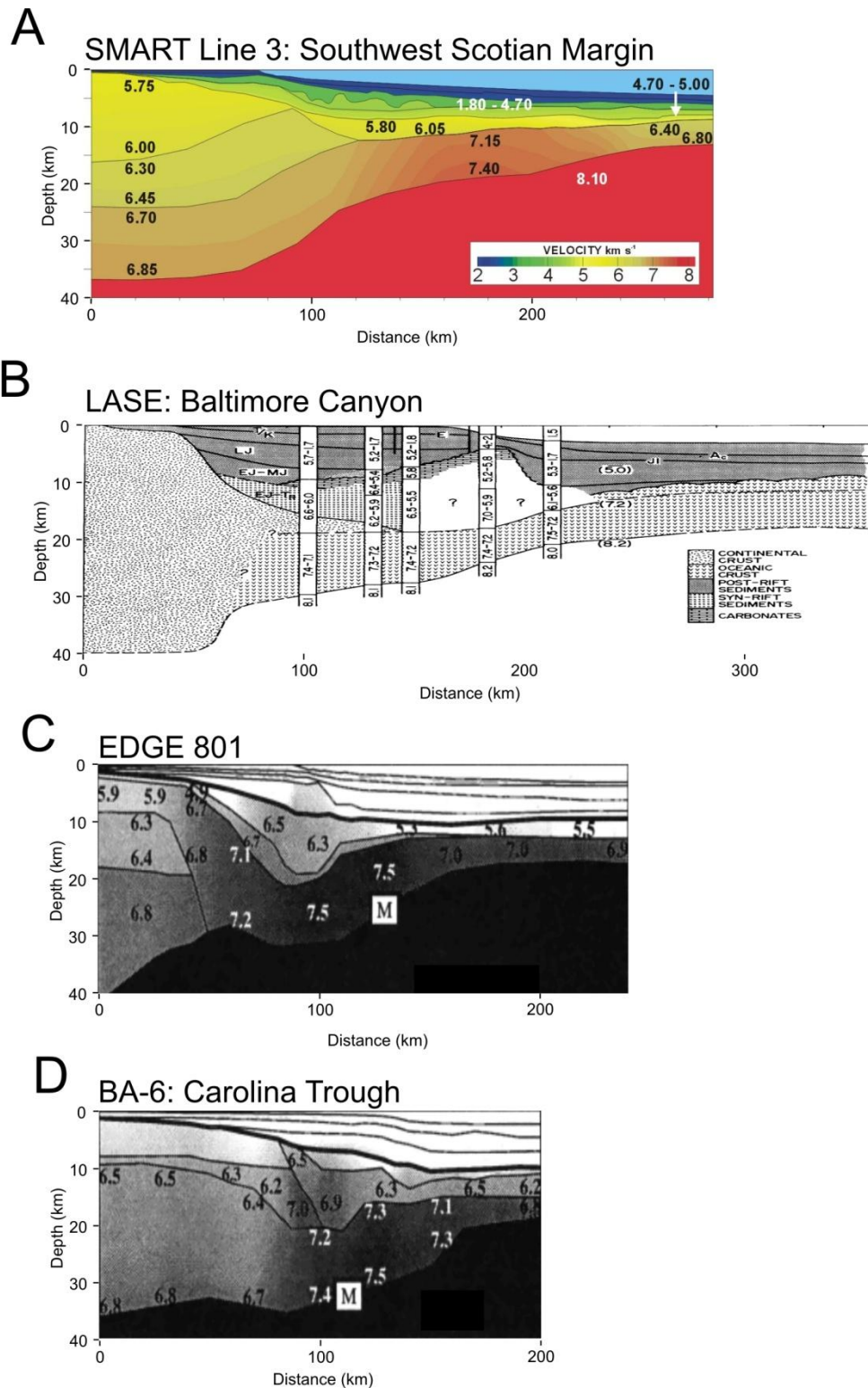


Figure A5. Crustal transects through magma-rich East coast margins. A) SMART Line 3 from the southwest Nova Scotia Margin (Dehler, *pers. comm.*), B) LASE line through the Baltimore Canyon (LASE Study Group, 1986), C) EDGE-801 (Holbrook et al., 1994, and D) Line BA-6 through the Carolina Trough (Kelemen and Holbrook, 1995). All lines at the same approximate scale and have a vertical exaggeration of ~ 3 . Line locations shown in Figure A4.

3.2 Numerical Modelling of Continental Rifting

Numerical models are useful aids in understanding the processes involved in continental rifting and yield insight into the reason a particular style of rifting occurs in some cases and not in others. The design of the numerical models is purposely simple; the goal of the numerical models or ‘experiments’ is to develop a basic understanding of the underlying physics and thereby processes.

We use an Arbitrary-Lagrangian-Eulerian (ALE) finite element model, Nested Sopale, developed at Dalhousie University (Fullsack, 1995), for the calculations. The model solves 2D thermo-mechanically coupled, incompressible viscous-plastic creeping (Stokes) flows of a layered crust, lithosphere, and asthenosphere with brittle (frictional-plastic) and thermally-activated power-law viscous rheologies. The rheologies used in the models shown are based on ‘wet’ quartzite (Gleason and Tullis, 1995) (upper crust), ‘dry’ Maryland diabase (Mackwell et al., 1998) (lower crust) and ‘wet’ Olivine (Karato and Wu, 1993) (lithosphere and sublithospheric mantle). The model uses laboratory derived parameters for these rheologies to calculate the effective viscosity, η , using the following power-law expression for dislocation creep when the state of stress is below plastic yield:

$$\eta = f A^{-1/n} (\dot{I}_2')^{(1-n)/2n} \exp\left[\frac{Q + Vp}{nRT}\right]$$

where A is the pre-exponential scaling factor, \dot{I}_2' is the second invariant of the deviatoric strain rate tensor ($\frac{1}{2} \dot{\epsilon}_{ij}' \dot{\epsilon}_{ij}'$), n is the power law exponent, f is a scaling factor representing viscous weakening or strengthening, Q is the activation energy, V is the activation volume, which makes the viscosity dependent on pressure, p , T is the absolute temperature, R is the universal gas constant, and $\dot{\epsilon}_{ij}'$ is the strain rate tensor.

When materials deform by brittle failure, the plastic yield obeys the Druker-Prager yield criterion:

$$\sigma_y = (J_2')^{1/2} = C \cos \phi_{eff} + p \sin \phi_{eff}$$

where $J_2' = \frac{1}{2} \sigma_{ij}' \sigma_{ij}'$ is the second invariant of the deviatoric stress, C is the cohesion, ϕ_{eff} is the effective internal angle of friction, and σ_{ij}' is the deviatoric stress tensor. Strain softening is included by decreasing $\phi_{eff}(\epsilon)$ from 15°-2° over a strain interval of 0.5-1.5 (all materials).

In addition to the mechanical calculation, the models include a thermal calculation using the following energy balance equation:

$$\rho c_p \left(\frac{\partial T_K}{\partial t} + v_i \frac{\partial T_K}{\partial x_i} \right) = k \frac{\partial}{\partial x_i} \frac{\partial T_K}{\partial x_i} + A$$

where c_p is specific heat, T_K is the absolute temperature, t is time, k is thermal conductivity, and A is volumetric radioactive heat production. The mechanical and thermal systems are coupled through the temperature dependent viscosity and density. The initial temperature field is laterally uniform and the system is assumed to be in thermal steady state in the initial configuration. The model has a constant heat flux across the base ($q = 19.4 \text{ mW/m}^2$) and is insulated ($q = 0$) along the sides (i.e., no heat flux). The tectonics is driven by side boundary conditions where horizontal velocities are applied to the lithosphere at a rate of $V/2$ on each side. All models in this report use $V = 1 \text{ cm/yr}$.

3.2.1 Model 1

The evolution of a simple numerical model (design shown in Figure A6), is shown in Figure A7.

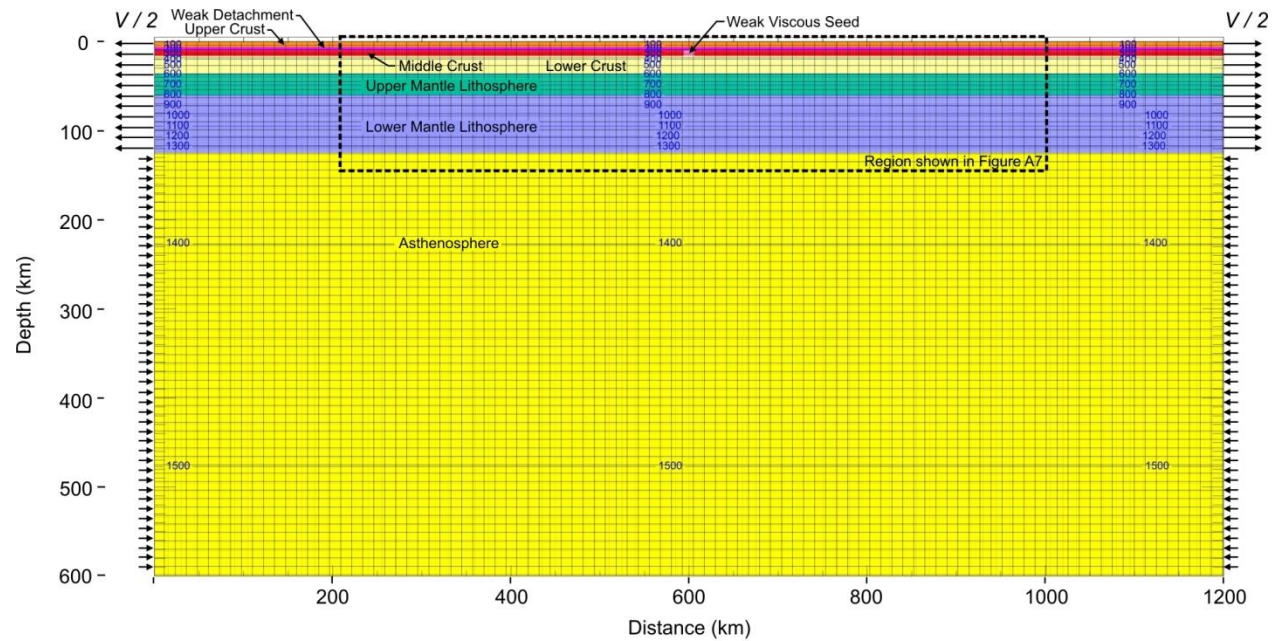


Figure A6. Model setup showing upper crust (orange), upper crust detachment (magenta), middle crust (red), lower crust (sand colour), upper mantle lithosphere (green), lower mantle lithosphere (light blue), and the asthenosphere (yellow). The crust and lithosphere are subjected to velocities at the side boundaries as shown by the arrows. The upper crust has a wet quartz rheology ($f = 0.02$) and the ‘detachment’ layer at the base of the upper crust (magenta) is frictional plastic ($\phi = 2^\circ$). The strong middle crust is dry Maryland diabase ($f = 0.02$), the weak lower crust is dry Maryland diabase ($f = 0.005$), the mantle lithosphere (upper and lower) has a wet olivine rheology ($f = 5$) and the sub-lithospheric mantle has a wet olivine rheology ($f = 1$). The reference density of the crust is 2860 kg/m^3 , and 3300 kg/m^3 for the mantle lithosphere and asthenosphere. The weak seed (pink) is located at the mid-crust level.

In this model the upper and lower crust are weak relative to the strong middle crust. As a result the middle crust ‘snaps’ early with conjugate normal faults soling in the weak seed (Fig. A7B). As extension continues, the weaker upper and lower crust flows and eventually laminate together forming a zone where the middle crust is absent (Fig. A7C). The upper mantle lithosphere is in the brittle part of the failure envelope and also breaks early (Fig. A7C). After continued extension, the lower mantle lithosphere thins significantly and breaks completely, while the low strength upper and lower crust continues to stretch and thin over the zone of rifting (Fig. A7D, E). The crust finally breaks at ~ 18 Ma and oceanic crust is introduced (Fig. A7E; light blue). Subsequent to this, the margins drift apart and no further crustal or continental mantle lithosphere deformation occurs.

Model 1 produces a pair of narrow conjugate margins with several distinctive features:

1. Margins characterised by a narrow crustal thinning profile, <100 km wide;
2. A landward dipping middle crust with a completely exhumed portion above which the upper crust is absent;
3. A domain seaward of this where upper and lower crust are laminated together with no middle crust present;
4. Sidewall convection of the lower lithosphere and asthenosphere once rifting occurs.

The overall style of deformation shown by Model 1 arises from a combination of the strength contrast between the strong middle crust and the encasing upper and lower crust, and the position of the weak seed at the mid-crust level. Model 1 is compatible with line 3 in terms of both the style of continental crust deformation and the width of the resulting margin. It does not, however, contain any magmatic underplating. A comparison of Model 1 and Line 3 at the same scale is shown in Figure A8.

It is not claimed that Model 1 is unique. Models with different lithospheric properties may produce equally acceptable or better results. Model 1 is shown here as a preliminary result to illustrate the methodology by which numerical experiments are used to investigate combinations of model properties that give results that match the characteristics of a given margin cross section. It is possible that models with a simpler setup may produce similar results.

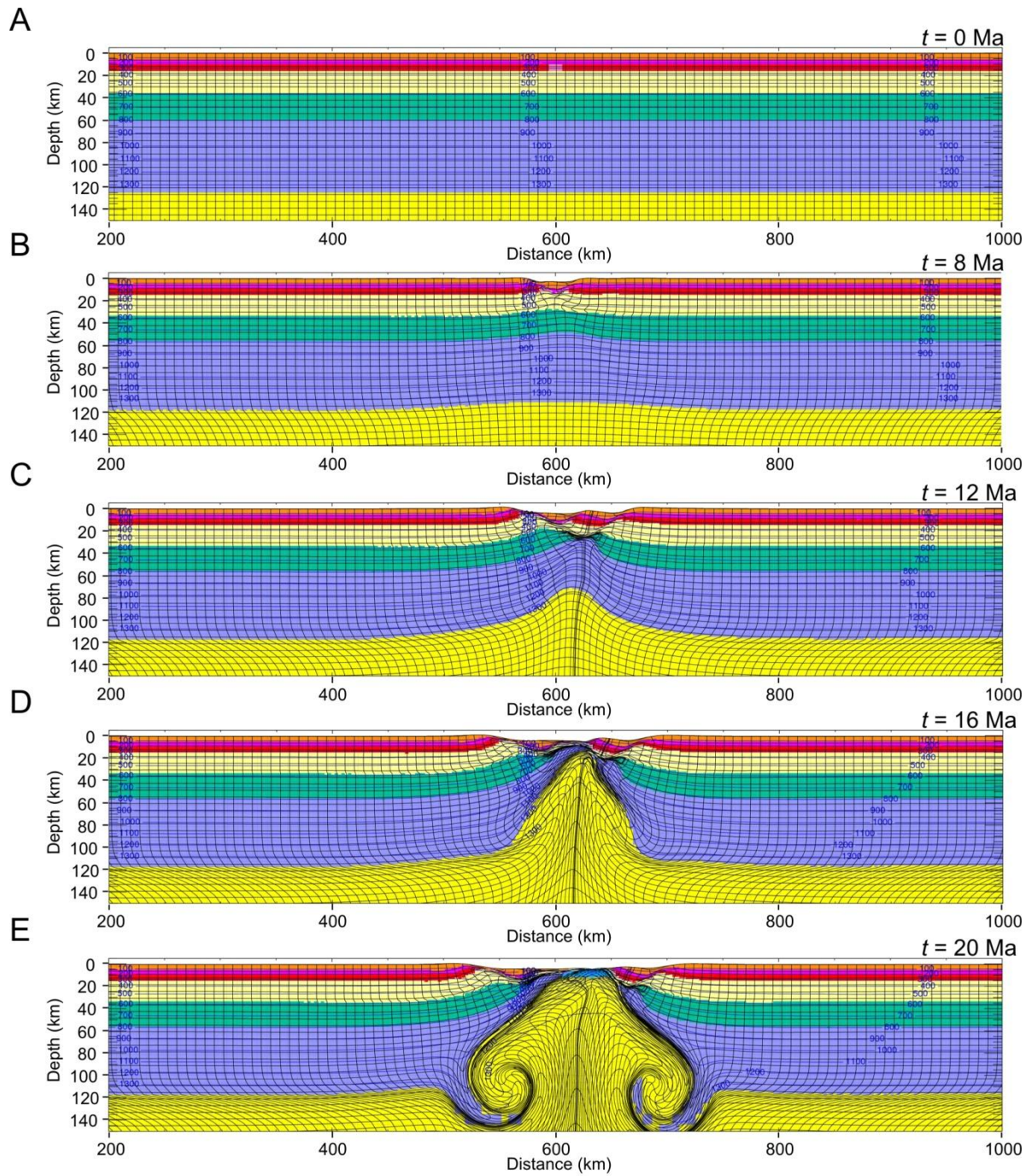


Figure A7. Evolution of Model 1 showing a narrow mode of rifting.

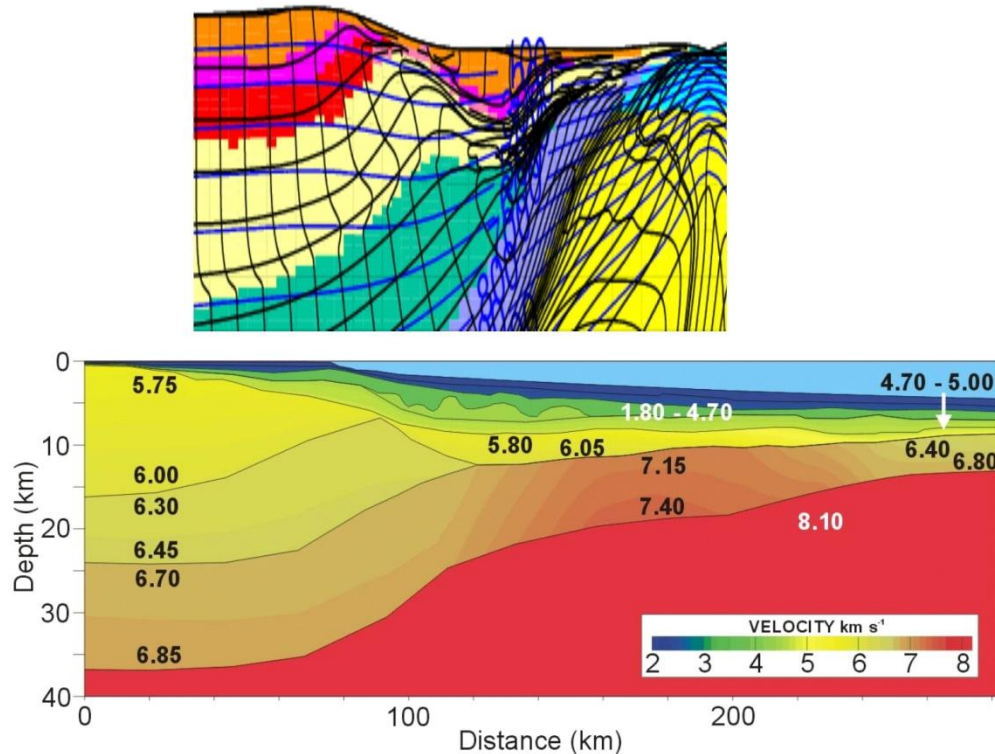


Figure A8. Comparison of A) Model 1 with B) Line 3 at the same scale. The vertical exaggeration is ~ 3 . The model produces a narrow zone of extended crust with landward dipping middle crust, and a zone where the middle crust is not present where upper crust overlies directly lower crust.

3.2.1 Model 2

Model 1 produces a style of rifting compatible with the magma-rich narrow margin characteristic of the southwest Nova Scotia margin (line 3). An alternative model design is required to produce wide margins typical of the northern Nova Scotia margin (GeoPro 2009, lines 1 and 2).

The design of Model 2 is shown in Figure A9. This model is different from Model 1 in that it uses a ‘nested’ modelling approach where a high resolution, small scale (SS) embedded model (Fig. A9B) sits within a lower resolution, large scale (LS) model (Fig. A9A). Each model is an independent finite-element solution and the two are linked through the boundary conditions of the small scale model which are derived from the LS solution for each timestep. In addition, in each model time step a decimated version of the higher resolution embedded model result replaces its equivalent part of the large scale model. This technique maximizes the utility of the embedded calculation and reduces drift between the large and small scale models. The primary motivation for using this approach is that a significantly higher resolution can be attained in the region of the embedded model. This allows a more accurate calculation and an improved image of crustal deformation and syn-rift sedimentation and deformation.

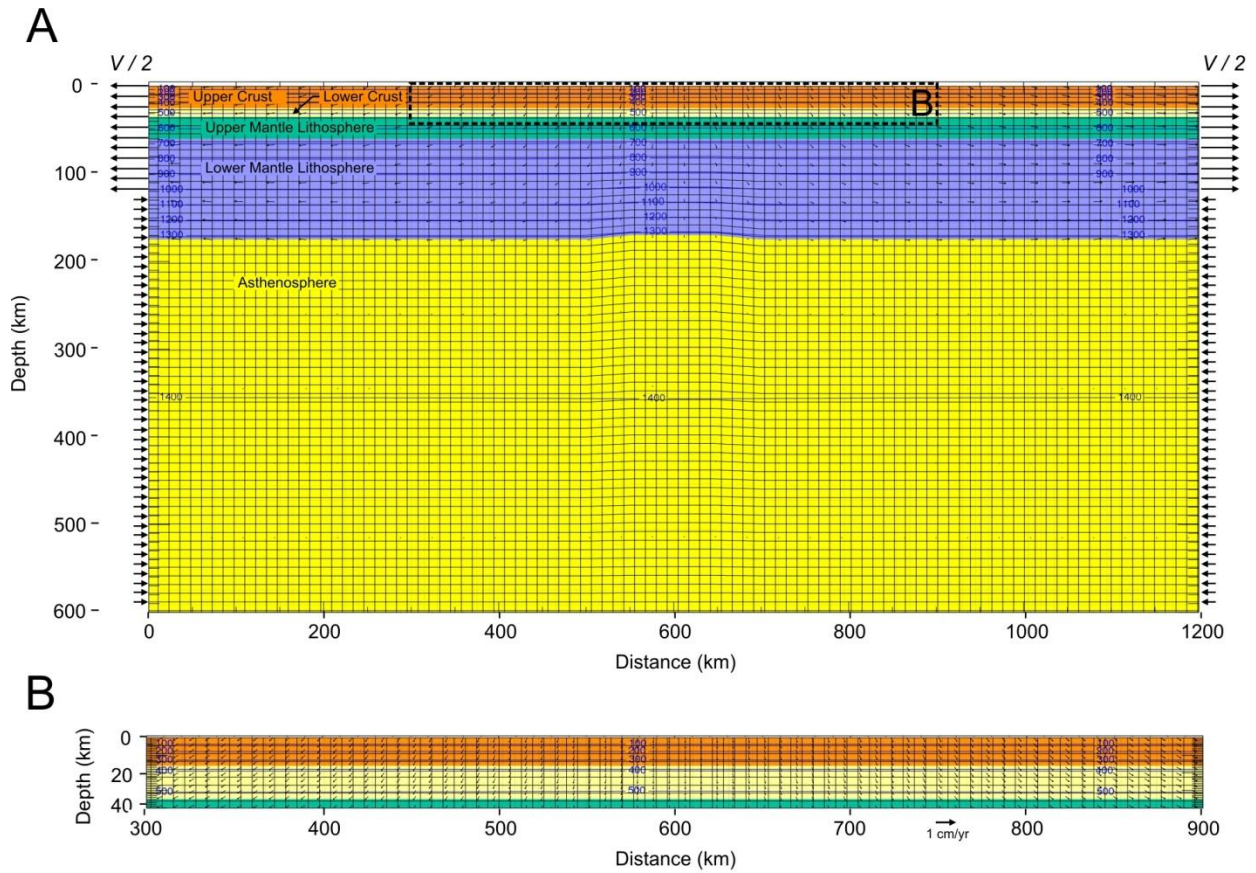


Figure A9. A) Large scale model setup showing upper crust (orange), lower crust (sand colour), upper mantle lithosphere (green), lower mantle lithosphere (light blue), and the asthenosphere (yellow). The lithosphere is subjected to velocities at the side boundaries as shown by the arrows. The upper and lower crust have a wet quartz rheology ($f = 0.014$ for upper crust, $f = 0.04$ for the lower crust). The mantle lithosphere (upper and lower) has a wet olivine rheology ($f = 2$) and the sub-lithospheric mantle has a wet olivine rheology ($f = 1$). The reference density of the crust is 2860 kg/m^3 , and 3250 kg/m^3 for the mantle lithosphere, and 3300 kg/m^3 for the asthenosphere. This model has no weak seed, but instead has a central 100 km wide zone where the mantle lithosphere is 5 km thinner than in adjacent regions. B) Small scale embedded model setup. Location of embedded domain in the large scale model is shown in A. The resolution of the embedded small scale model is 4 times greater than the large scale model.

The rheological stratification in Model 2 contrasts that of Model 1 in that the crust is composed of two layers, both of which are wet quartz controlled and tuned to be weak. The upper crust (orange) is Gleason and Tullis (1995) wet quartzite with an effective viscosity scaling parameter, f , of 0.014 (i.e., $1/70$). The lower crust (sand colour) has the same basic rheology but has $f = 0.04$ ($=1/25$). The choice of parameters for the effective viscosity of wet quartz controlled rheologies arises from the wide range of laboratory measured viscosities, as shown in Figure A10. The Gleason and Tullis (1995) wet quartzite flow (GT) predicts relatively high effective viscosities and it is also valid to consider lower values which we do by scaling GT flow law by f .

For this illustrative example, we choose f values that are on the low end of measured viscosities, but are not completely unreasonable. The dashed lines in Figure A10 show the effective viscosity for a range of f .

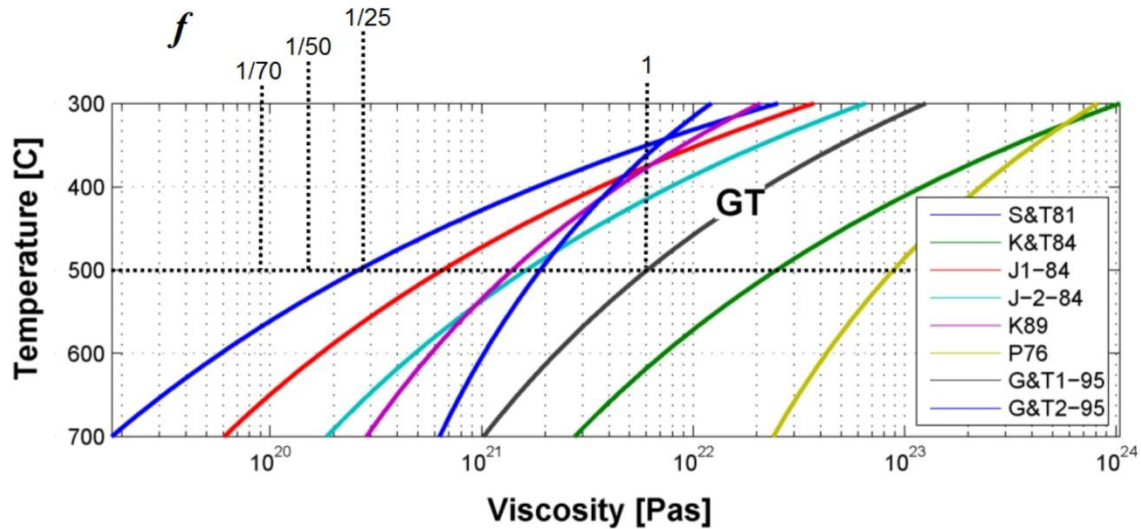


Figure A10. Variable effective viscosity of wet quartz controlled rheologies (modified from Huismans and Beaumont, submitted).

The evolution of Model 2 is shown in Figure A11. This is the embedded SS, high-resolution result. After 20 Ma of extension, the upper mantle lithosphere (green) has necked and lower mantle lithosphere underlies the crust. However, at this stage crustal thinning is relatively minor. Thus, the distribution of stretching in this model is strongly depth dependent, consistent with Type II models of Huismans and Beaumont (*submitted*).

This occurs because the crust is weak and thins slowly over a wide zone. Although the lower crust has a larger f , it flows more efficiently than the upper crust because it is hotter (note the relationship between effective viscosity and temperature shown in Figure A10). This contrasts Model 1 where the model rifts the crust and mantle lithosphere completely in 20 Ma, producing oceanic crust, with the same applied boundary velocities (i.e., 1 cm/yr full rate). After 30 Ma, the zone of crustal thinning is ~250 wide and deformation is symmetric relative to Model 1. After 40 Ma, the crust is very thin above the nascent ridge and each conjugate margin is ~200 km wide (i.e., measured from the centre of the ridge to the location of fully-thick continental crust). At this stage several basins bounded by conjugate normal faults occur on each margin. By 50 Ma, each continental margin is ~300 km wide and rifting has occurred producing oceanic crust in the centre of the model (Fig. A11E).

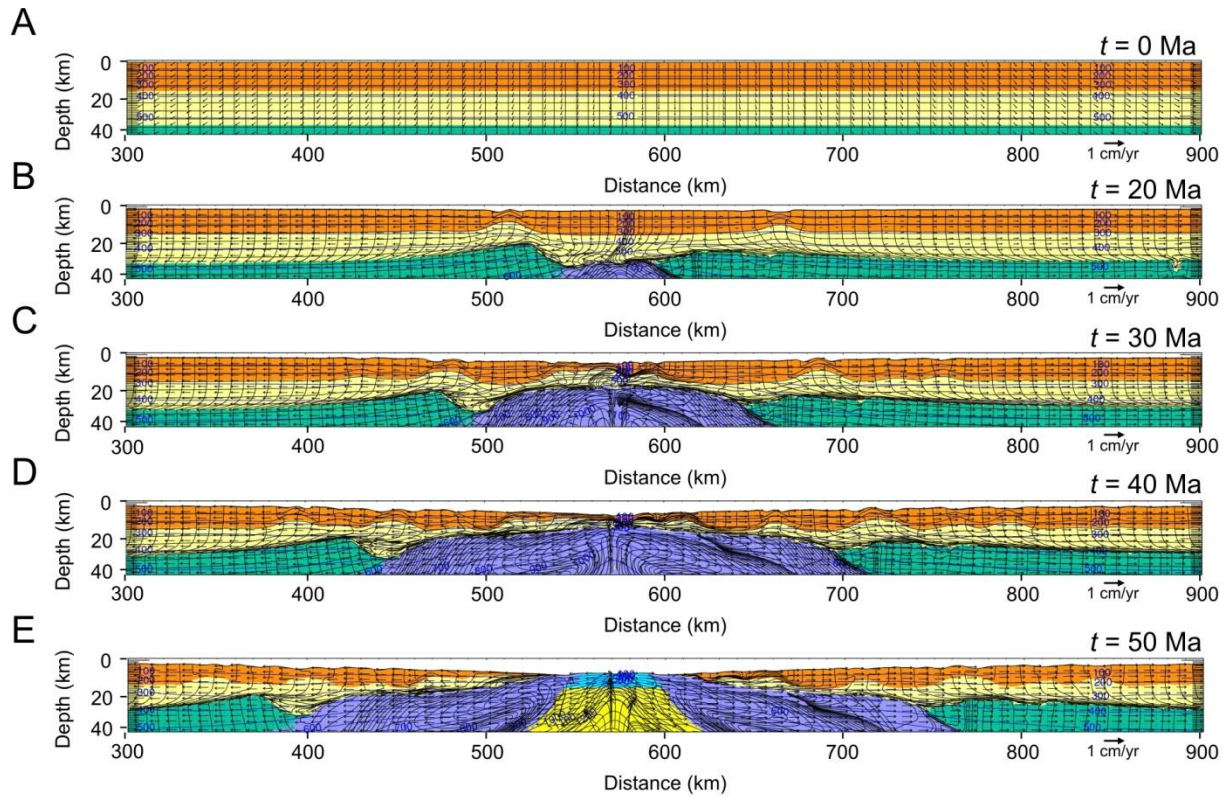


Figure A11. Evolution of Model 2 showing the formation of very wide continental margins. This contrasts with Model 1 shown in Figure A7.

3.2.3 Model 3: significant syn-rift sedimentation

The starting design of Model 3 is exactly the same as Model 2, as shown in Figure A9. However, as Model 3 evolves, syn-rift sedimentation is included such that all the available accommodation space is filled on the left margin. Restricting sedimentation to the left margin allows us to compare and contrast a starved margin with one with sediments. The sediment has the same properties as the upper crust, except that it has a density of 2300 kg/m^3 .

Early stages of Model 3 are similar to Model 2, with a pair of basins forming on either side of the model centre (Fig. A12B). However, after prolonged stretching and the creation of more accommodation space, the evolution of Model 3 diverges from Model 2. After 30 Ma (Fig. A12), a thick sequence of sediments has been deposited between 450-600 km. This causes the thinning crust to be buried an additional 12 km resulting in higher crustal temperatures beneath the sedimentary basin, and more efficient flow. Crustal flow is contemporaneous with sedimentation, as evidenced by the growth faulted basins on each end of the evolving basin (i.e., 450-500 km and 525-575 km in Fig. A12C). This style of deformation continues and the thickness of the sedimentary basin increases significantly by 40 Ma and significant growth continues to occur along faults extending through the sedimentary basin. This model does not rift completely owing to the extreme nature of sedimentation; the ridge centre is continuously covered by sediments and this discourages the formation of oceanic crust.

Model 3 evolves asymmetrically owing to the sedimentation on one of the conjugate margins. As a result of the increased flow rate of the crust, the side with sediments has a significantly wider stretching profile.

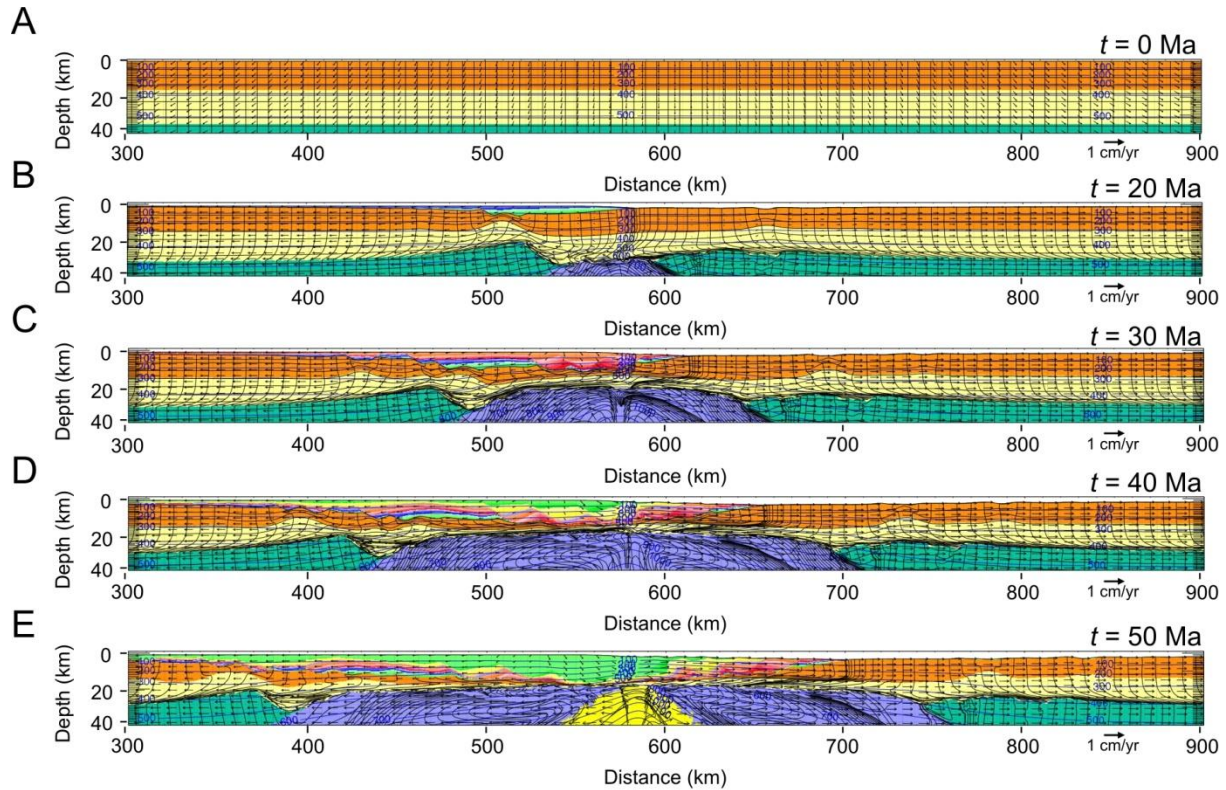


Figure A12. Evolution of Model 3 showing the formation of very wide continental margins during extensive syn-rift sedimentation.

3.2.4 Model 4: moderate syn-rift sedimentation

Model 4 has the same initial design as Model 2, but has moderate syn-rift sedimentation such that the accommodation space is only partially filled on the left side of the model, and the depocentre migrates to the left with time. As in Model 3, no sediment is deposited on the right side of the model (Fig. A13A-B).

After 30 Ma of extension (Fig. A13C), the basins on the shelf of the left margin are filled with sediments which show minor growth. At this stage the rifting is essentially symmetric and the sediments have a minimal effect on the style of rifting; this contrasts with Model 3. After 40 Ma (Fig. A13D), sedimentation has ceased over most of the model (distance > 400 km). Much of the sedimentary basin has been segmented into a series of faulted and rotated blocks. By 40 Ma, the evolving rift is somewhat asymmetric, but to a lesser degree than in Model 3. It is notable that syn-rift sedimentation reduces the amplitude of the pinch and swell (boudinage) structures that form in these models; this is best observed by comparing the left and right margins in Figure A13D. After 50 Ma, the model is close to rifting and has an ultra-wide (>300 km) margin on the left side and a sediment starved ~250 km wide margin on the right side.

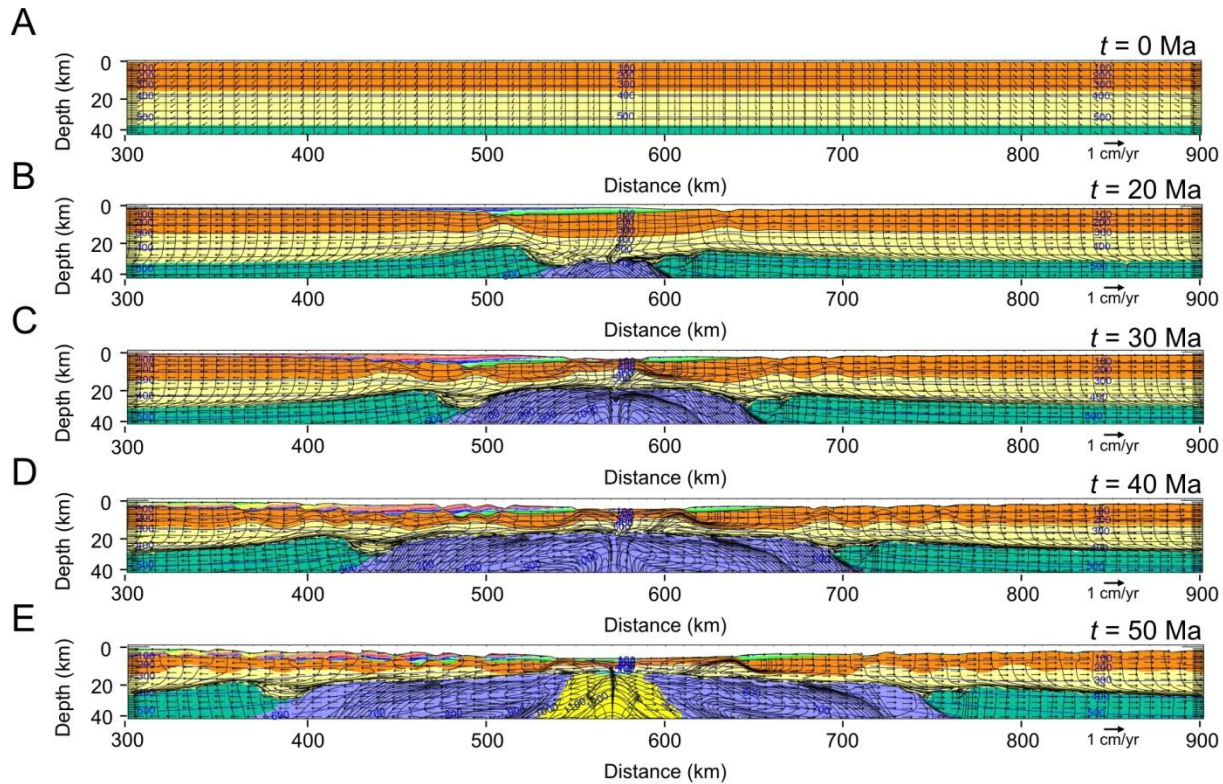


Figure A13. Evolution of Model 4 showing the formation of very wide continental margins during moderate syn-rift sedimentation.

3.3 Summary

The results presented here are preliminary and are designed to show the types of lithospheric properties that may be required in order to explain the difference in characteristics between the wide, magma-poor, region of the northern part of the Nova Scotian margin and the contrasting narrow, magma-rich region to the south, which has the same characteristics as the United States East Coast margin. We do not regard these results as robust, but there is a general indication that the crust needs to be weak in order to produce a wide margin in the models, whereas crust containing a strong mid-crustal region will break in the presence of a weak ‘seed’ leading to a narrow margin. An important but seldom considered consequence is that given a uniform rate of extension for both regions of the margin, breakup will occur much earlier at the narrow margin (~ 18 Ma Model 1) versus later (~ 45 Ma Model 2) for the wide margin. If rifting in both regions starts at the same time, the long and short syn-rift intervals may have important consequences for the evolution of the syn-rift sedimentary basins and, in particular, the deposition of evaporites and the subsequent salt tectonics. For example, evaporite deposition could be during the middle of the syn-rift period in one case and at the end of rifting in the other. In the former the salt tectonics may be partly driven by the continued extension during rifting.

4. References

- Contrucci, I., Klingelhöfer, F., Perrot, J., Bartolome, R., Gutscher, M.-A., Sahabi, M., Malod, J., and Rehault, J.-P. 2004. The crustal structure of the NW Moroccan continental margin from wide-angle and reflection seismic data. *Geophysical Journal International*: 159, 117-128, doi: 10.1111/j.1365-246X.2004.02391.x
- Dean, S. M., Minshull, T. A., Whitmarsh, R. B. & Loudon, K. E. 2000. Deep structure of the ocean-continent transition in the southern Iberia abyssal plain from seismic refraction profiles; the IAM-9 transect at 40 degrees 20'N. *Journal of Geophysical Research*: 105, 5859-5885.
- Funck, T., Jackson, H.R., Loudon, K.E., Dehler, S.A., and Wu, Y. 2004. Crustal structure of the northern Nova Scotia rifted continental margin (eastern Canada). *Journal of Geophysical Research*: 109, B09102, doi:10.1029/2004JB003008.
- Fullsack, P. 1995. An arbitrary Lagrangian-Eulerian formulation for creeping flows and applications in tectonic models. *Geophysical Journal International*: 120, 1-23.
- Gleason, G.C. and Tullis, J. 1995. A flow law for dislocation creep of quartz aggregates determined with the molten salt cell. *Tectonophysics*: 247, 1-23.
- Holbrook, W.S., Purdy, G.M., Sheridan, R.E., III, L.G., Talwani, M., Ewing, J. & Hutchinson, D. 1994. Seismic structure of the U.S. mid-Atlantic continental margin. *Journal of Geophysical Research*: 99, 17871-17891.
- Huisman, R.S. and Beaumont, C. *submitted*.
- Huisman, R.S., and Beaumont, C., 2007. Roles of lithospheric strain softening and heterogeneity in determining the geometry of rifts and continental margins, in: eds, G. Karner, G. Manatschal, and L. Pinheiro, *Imaging, Mapping and Modelling Extensional Processes*, Geological Soc. London, Spec. Publ., 282, 111-138.
- Huisman, R.S. and Beaumont, C. 2008. Complex rifted continental margins explained by dynamical models of depth-dependent lithospheric extension. *Geology*: 36, 163-166.
- Karato, S.I. and Wu, P. 1993. Rheology of the upper mantle; a synthesis. *Science*: 260, 1-23
- Keen, C. E., Stockmal, G. S., Welsink, H. J., Quinlan, G. and Mudford, B. 1987. Deep crustal structure and evolution of the rifted margin northeast of Newfoundland: results from LITHOPROBE East. *Can. Journal of Earth Sciences*: 24, 1537-1549.
- Keen, C. E. and de Voogd, B. 1989. The continent-ocean boundary at the rifted margin off eastern Canada: new results from deep seismic reflection studies. *Tectonics*: 7, 107-124.

- Kelemen, P., and Holbrook, S. 1995. Origin of thick, high-velocity igneous crust along the U.S. East Coast Margin. *Journal of Geophysical Research*: 100, 10077-10094.
- Klingelhöfer, F., Labails, C., Cosquer, E., Rouzo, S., Géli, L., Aslanian, D., Olivet, J.-L., Sahabi, M., Nouzé, H., and Unternehr, P. 2009. Crustal structure of the SW-Moroccan margin from wide-angle and reflection seismic data (the DAKHLA experiment) Part A: Wide-angle seismic models. *Tectonophysics*: 468, 63-82.
- LASE study group. 1986. The Structure of the US East Coast Passive Margin from Large Aperture Seismic Experiments (LASE). *Marine and Petroleum Geology*: 3, 234-242.
- Mackwell, S.J., Zimmerman, M.E., and Kohlstedt, D.L. 1998. High-temperature deformation of dry diabase with application to tectonics on Venus. *Journal of Geophysical Research*: 103: 975-984.
- McKenzie, D. 1978. Some remarks on the development of sedimentary basins. *Earth and Planetary Science Letters*: 40, 25-32.
- Moulin, M., Aslanian, D., Olivet, J.-L., Contrucci, I., Matias, L., Geli, L., Klingelhofer, F., Nouze, H., Rehault, J.-P., and Unternehr, P. 2005. Geological constraints on the evolution of the Angolan margin based on reflection and refraction seismic data (ZaiAngo project). *Geophysical Journal International*: 162, 793-810 doi: 10.1111/j.1365-246X.2005.02668.x.
- Rosendahl, B.R., Mohriak, W.U., Odegard, M.E., Turner, J.P., and Dickson, W.G. 2005. West African and Brazilian conjugate margins: Crustal types, architecture, and plate configurations: *in* Post, P., et al., eds., *Petroleum systems of divergent continental margin basins*: Houston, 25th Gulf Coast Section, Society Sedimentary Geology, Bob F. Perkins Research Conference, 4-7 December 2005, CD-ROM.
- Wyer, P. and Watts, A.B. Gravity anomalies and segmentation at the East Coast, USA continental margin. *Geophysical Journal International*: 166, 1015-1038.
- Wu, Y., Loudon, K.E., Funck, T., Jackson, H.R., and Dehler, S.A. 2006. Crustal structure of the central Nova Scotia margin off Eastern Canada. *Geophysical Journal International*: 166, 878-906. doi: 10.1111/j.1365-246X.2006.02991.x

Appendix 1B (Part 3)

Discussion of Objectives, Methodology and Results for Project 2: Salt Tectonics of the Scotian Basin, offshore Nova Scotia

Preliminary results from thermo-mechanical finite element models of salt systems in passive margin settings

1. Summary

In recent research (Albertz et al., in press) we have been able to identify and explain three styles, A-C, of salt (strictly evaporite) tectonics of the Nova Scotian margin and show how they operate using 2D mechanical numerical models. The models include the autochthonous salt basins, tectonic, thermal and isostatic subsidence of the rifted margin, and loading by prograding and aggrading compacting sediments. The results provide particular insight into the effect of the position of the autochthonous salt basins on the margin and the timing and style of sedimentation in creating the three salt tectonic structural styles.

Structural style A, an open-ended roho system with a synkinematic wedge, is reproduced by models with early post-rift deltaic progradation and seaward spreading/gliding of sediments above a salt detachment. Structural style B, a roho system with landward regional normal faults and allochthonous salt sheets climbing seaward over Late Cretaceous and Paleogene strata, is shown to be a consequence of early aggradation followed by progradation. Structural style C is characterized by salt diapirs and intervening minibasins and is reproduced by models with Rayleigh-Taylor (buoyancy) instabilities requiring compaction driven density inversions, weak sediments, and initial perturbations of the overburden/salt interface. These results are also consistent with the observed timing and patterns of sedimentation on the margin. We have also investigated models with more complex autochthonous salt basin geometries and shown that significant basement topography beneath the salt causes additional salt diapirism during sediment progradation (Albertz and Beaumont, in press).

The Albertz et al. (in press.) and Albertz and Beaumont (in press) numerical modelling assumes frictional-plastic overburden with specified pore fluid pressures deposited on linear viscous salt. These are approximations that are justifiable for first-order calculations but will certainly fail to predict the full range of observed salt tectonic structures, particularly those that involve dynamical development of fluid overpressures leading to gravitational gliding or spreading instabilities of the salt and its overburden.

We proposed research that uses both the basic mechanical modelling and more advanced thermal-mechanical coupled calculations to forward model the effects of temperature, coupled basement-salt tectonics, and more realistic sedimentation regimes. The numerical model experiments will be designed to be representative of typical rifted margins, such that results will be of general interest, and tailored to specific Scotian Basin examples as we make progress during the overall project. Here, we report on model development and results from Phase 1 of the project.

The deliverables for Salt Tectonics Sub-Project 1 are as follows:

Q1, 2010 Modify Sopale software to include thermal aspects of modelling. Test models.

Below, we report on the methodology developed for thermo-mechanically coupled salt tectonic models.

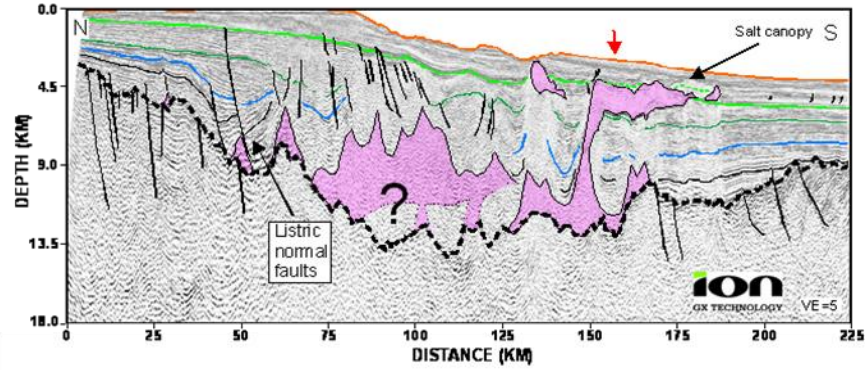
Q2, 2010 Modify Albertz et al. (in press) models for thermal effects.

We have used the new methods to adapt Albertz et al. (in press) style of models, termed Basin-Scale Models, which were purely mechanical to be thermo-mechanically coupled and report on a series of model experiments.

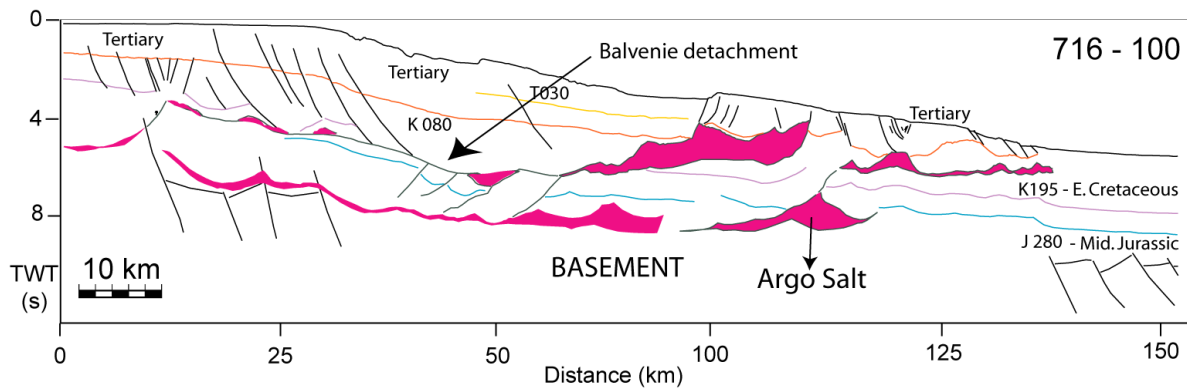
In addition, we have recognized that the Basin-Scale Models are limited by the close proximity of the base of the model to the autochthonous salt layer. This close proximity means that refraction of heat within the crust below the salt cannot be accurately calculated. To overcome this limitation we have developed a second style of model, termed Nested Upper-Mantle-Scale Models, in which the salt model is embedded in a larger, upper-mantle-scale model. This approach allows the refraction of heat below and in the vicinity of the salt to be accurately calculated. We describe the design of the Nested Upper-Mantle-Scale Model and report on a series of experiments.

Additional Research Goals, Not Specified as Deliverables

As noted above, three salt tectonic structural styles were modelled by Albertz et al. (in press). An interim goal of the present research is to investigate the Structural Style B (SSB) part of the Scotian Basin in more detail. Owing to limitations in data availability and interpretation Albertz et al. (in press) and Albertz and Beaumont (in press) only considered the first-order properties of the SSB region, as shown in Figure (B.1a), and including the salt canopy. More recent interpretations (Kris Kendell, pers comm., Figure B.1b) have pointed to second canopy system which has evolved from the Balvanie detachment. We have chosen to target the mechanisms by which canopies develop as a next step in the salt tectonic modelling. This component of the research is in progress and will continue in Phase 2. We do, however, provide a brief progress report (Section 5 below).



(a) from Albertz et al., (in press)



(b) Line interpretation (Courtesy: Kris Kendell, CNSOPB)

Figure B.1. (a) Seismic section showing the characteristic structures in the structural style B region of Scotian Basin (Albertz et al., in press). (b) Line interpretation of a seismic section (time section) showing the Balvenie detachment that is within the limits of the autochthonous salt basin and at a structurally higher level.

2. Model Design and Material Properties

In this section we describe both the Basin-scale and the Nested upper-mantle-scale models. The models are plane strain, vertical cross section, two dimensional Arbitrary Lagrangian Eulerian (ALE) finite element models and the calculations are made using the software Sopale and Nested Sopale, respectively. Both Sopale (Simplified Optimized Arbitrary Lagrangian Eulerian) and Sopale Nested, use velocity-based approach designed for large deformation Stokes or creeping flows (Fullsack, 1995; Willett, 1999). The model solves the equilibrium force balance equations for incompressible flows (sediment compaction is calculated separately) in two dimensions.

2.1 Model Geometry

Both model geometries represent a compromise in which the dynamics of salt tectonics under prograding and aggrading sediment loads is calculated in a kinematic framework that provides a first-order representation of the rifted continental margin setting of the evolving salt basin. The

main purpose of this kinematic framework is to include an initial geometry of the margin and the salt basin, corresponding to the time during the syn-rift when the salt (evaporite) has been deposited and then track the thermal subsidence of the margin and the flexural isostatic response of the system to sediment and water loading.

The kinematic part of the model therefore provides a geometry in which the salt tectonic system operates. However, the compromise is that no syn-rift tectonic development of the crust and evolution of the salt basin, owing to faulting during extension, is included. Instead, the salt basins have simple stylistic geometries. We have chosen this approach in order to focus on salt tectonics where the autochthonous salt basins have simple geometries. The fully coupled models in which both the lithospheric and salt tectonics are modelled will be addressed in Salt Tectonics Sub-Project 2.

2.1.1 Basin-scale Models

The basin-scale models described here are purposely designed to be simple and are based on the reference model used in Albertz et al. (in press). The goal is to demonstrate the thermal evolution of this type of model and its sensitivity to salt rheologies in which the effective viscosity depends on temperature.

The initial model geometry (Fig. B.2) represents a state near the end of syn-rift time in a basin that approximates a cross section of the Scotian basin, with a configuration in which the underlying crust has subsided and tilted tectonically, but prior to the onset of lithospheric cooling and thermal subsidence. We assume that the salt basin has a simple near-rectangular, cross-sectional geometry. In all the models presented in this report, the 2 km deep salt basin is embedded in the outer part of the margin above thin continental crust between $x = 170$ and 250 km. Sediment seaward of the salt basin comprises a uniform 2 km thick layer and can be interpreted as syn-rift sediment. That this sediment is deposited in part on oceanic crust is part of the kinematic compromise.

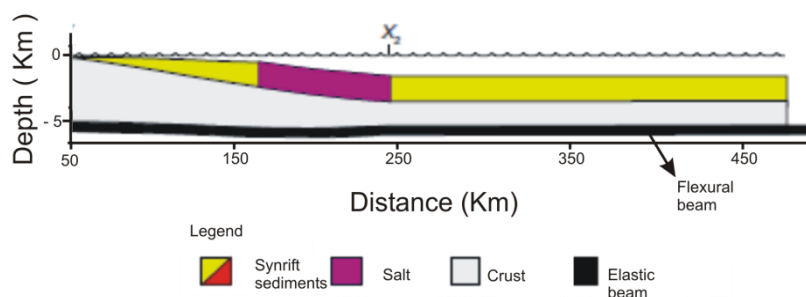


Figure B.2. Initial configuration of the basin scale models (models M1, MT2 and TMC1 to TMC 4) in this report.

The procedure in configuring the initial model geometry involves the following four steps:

- (1) Isostatic balance of the continental margin configuration at the lithospheric level.
- (2) Replacement of lithosphere below the base of the model by compensating buoyancy forces. This strategy allows the upper part of the model to reproduce the desired

geometry and isostatic response, while limiting the model to an uppermost crust/salt basin domain of interest, and thereby maximizing finite element resolution .

- (3) Initial thermal uplift and subsequent thermal subsidence of oceanic crust and margin.
- (4) Loading of the isostatically balanced model domain with salt, syn-rift sediment and water and recalculating the flexural isostatic balance. Water loading is present throughout the analysis and is represented as a boundary load applied normal to the upper surface of the model. Density of water used in the models is 1000 kg/m^3 and the top surface of water is at z (depth) = 0 (Fig. B.2). For more details on water loading, please refer to Gemmer et al. (2005).

The calculations and assumptions involved in each of the above four steps are discussed in detail in Appendix 1 of Albertz et al (in press).

<http://geodynamics.oceanography.dal.ca/index-salt.html>

<http://sopalepc.ocean.dal.ca/salt-ScotianBasin/2009TC002539-pip.pdf>

2.1.2 Nested Upper-Mantle-Scale Models

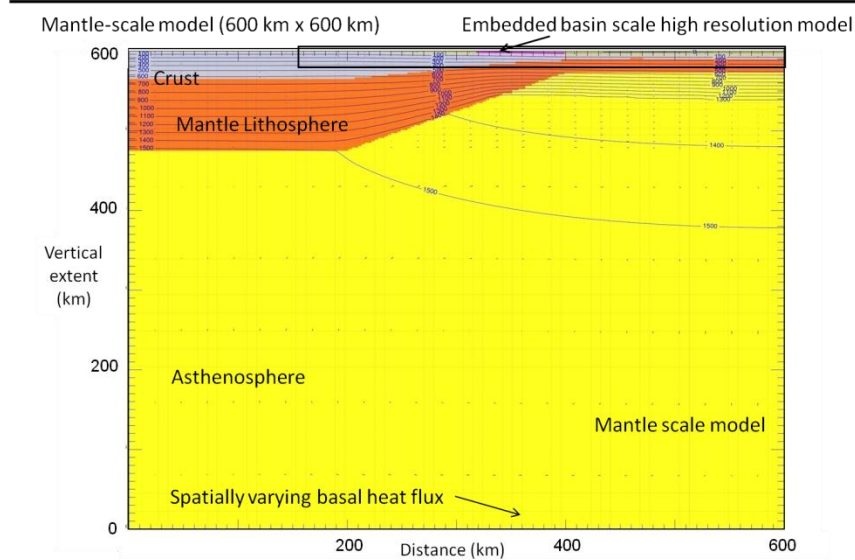
Nested upper-mantle scale models comprise a large-scale tectonic scale model (LS model) in which a high resolution basin scale model (small scale or SS model) is embedded (Fig. B.3). The LS model is $600 \text{ km} \times 600 \text{ km}$. Flow within the lithospheric mantle and asthenosphere in the LS model allows the model to adjust isostatically. The landward and the basal boundaries are fixed boundaries whereas the seaward edge has a vertical roller boundary condition. Water loading is present throughout the analysis and is represented as a boundary load applied normal to the upper surface of the model. Density of water used in the models is 1000 kg/m^3 and the top surface of water is at z (depth) = 0 (Fig. B.3b). For more details on water loading, please refer to Gemmer et al. (2005). A spatially varying heat flux is imposed at the base of the model for an initial finite element calculation of the thermal structure within the LS model. This provides an approximation to a hot syn-rift initial condition. Subsequently, during the model evolution, a constant vertical heat flux of 19.4 mW/m^2 is imposed at the base. Side boundaries are insulating with no lateral heat flux. The thermal boundary condition at the base is sufficiently deep such that constant basal heat flux boundary condition can be imposed at the bottom boundary. Thermal subsidence is not included in the models described here but will be included in future work. Initial finite element calculations within the LS model provide the boundary conditions for the higher resolution SS model in the area of interest (i.e., upper 25 km of the model).

2.2 Governing Equations

The models calculate the thermal-mechanical evolution of the system, under the assumptions of plane strain, incompressibility, and zero Reynolds number. Material deformation is governed by the equations of (1) conservation of volume (mass when incompressible) and (2) force balance:

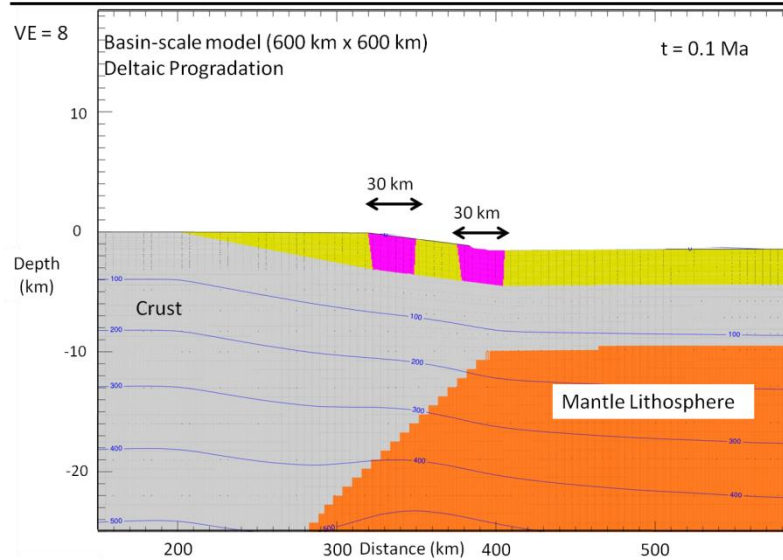
$$\frac{\partial v_j}{\partial x_j} = 0 \tag{1}$$

NEW APPROACH: NESTED MODELS
MANTLE SCALE + BASIN SCALE



(a) Upper-Mantle-Scale, LS model

NEW APPROACH: NESTED MODELS
MANTLE SCALE + BASIN SCALE WITH TWO SALT BASINS



(b) Basin-Scale, SS model

Figure B.3. Geometry of the Nested upper-mantle-scale models. (a) Geometry of the large scale (LS) model. A uniform McKenzie type extension (McKenzie, 1978) is assumed in the lithosphere. The landward and basal boundaries are fixed and the seaward side has a roller boundary condition. (b) Geometry of the high resolution SS model which extends from $x = 150$ km to $x = 600$ km in the LS model and is embedded in the top 25 km of the LS model. The geometry shown here is from the nested model NS1 discussed below.

$$\frac{\partial \sigma_{ij}}{\partial x_i} + \rho g = 0 \quad i,j=1,2 \quad (2)$$

where x_{ij} are spatial coordinates, v_{ij} are components of velocity, ρ is density, and g is (vertical) gravitational acceleration. Repeated indices imply summation. The associated stress tensor is:

$$\sigma_{ij} = -P\delta_{ij} + \sigma'_{ij} = -P\delta_{ij} + 2\eta_{\text{eff}} \dot{\epsilon}_{ij} \quad (3)$$

where P is pressure (mean stress), σ'_{ij} is the deviatoric stress tensor, η_{eff} is effective viscosity, δ_{ij} is the Kronecker delta (1 for $i=j$ and 0 otherwise), and the strain rate tensor is:

$$\dot{\epsilon}_{ij} = \frac{1}{2} \left(\frac{\partial v_i}{\partial x_j} + \frac{\partial v_j}{\partial x_i} \right) \quad (4)$$

The temperature field is calculated using the energy balance equation:

$$\rho c_p \left(\frac{\partial T_K}{\partial t} + v_i \frac{\partial T_K}{\partial x_i} \right) = k \frac{\partial}{\partial x_i} \frac{\partial T_K}{\partial x_i} + A \quad (5)$$

where c_p is specific heat, T_K is the absolute temperature, t is time, k is thermal conductivity, and A is volumetric radioactive heat production.

These equations are solved, subject to specified boundary conditions and imposed loads (sedimentation), using Arbitrary Lagrangian-Eulerian (ALE) finite element techniques (Fullsack, 1995). Mechanical and thermal calculations (in all models except model M1) are carried out on an Eulerian grid that stretches vertically to conform to the upper model surface. Materials are tracked on a Lagrangian mesh and additional Lagrangian tracer particles, which are advected with the model velocity field.

In the Basin-scale models, TMC 1 to TMC 4 below, the thermal field is coupled to the mechanical field through the temperature-dependent density and the viscous rheology (pressure – solution creep and dislocation creep) of model materials. The initial temperature field is laterally uniform and the system is assumed to be in thermal steady state in the initial configuration. The model has a constant heat flux across the base ($q = 50 \text{ mW/m}^2$) and is insulated ($q = 0$) along the sides (i.e., no heat flux). The Eulerian grid has 800 elements in the horizontal direction and 88 elements in the vertical direction.

In Nested upper-mantle-scale models NS1 to NS4, a constant heat flux of 19.4 mW/m^2 is imposed along the base. The LS model has 200 elements in the horizontal direction and 100 elements in the vertical direction. The embedded SS model (within the upper 25 km of the LS model) has 750 elements in the horizontal direction and 112 elements in the vertical direction. Of the 112 elements in the SS, 72 elements are initially included within the 2 km thick salt basin.

2.3 Material properties

In all the models in this report, the continental crust and oceanic crust are assigned a constant cohesion of 50 MPa and an internal angle of friction of 30°. Properties of other materials as follows.

2.3.1. Basin scale models

We present two sets of models where the salt is modeled either as linear viscous material (models M1 and MT 2) or as deforming by grain boundary diffusion creep (models TMC 1, TMC 3 and TMC 4) and/or dislocation creep (models TMC 2, TMC 3 and TMC 4). Where salt is modeled as a linear viscous material, it evolves according to the following flow law:

$$\sigma = 2 \eta \dot{\epsilon} \quad (6)$$

where σ is the deviatoric stress tensor, η is the viscosity (10^{18} Pa s) and $\dot{\epsilon}$ is the strain rate.

For salt deforming by grain boundary diffusion creep (pressure solution creep), the rheology is governed by the following equation (Spiers et al., 1990):

$$\dot{\epsilon} = 7.05 \times 10^{-19} \exp(-24500 / RT) \sigma_d / (Td^3) \quad (7)$$

where $\dot{\epsilon}$ is the second invariant of the strain rate tensor, σ_d is the second invariant of the deviatoric stress tensor, T is the absolute temperature, R is the universal gas constant and d is the grain size of salt. Note that the flow stress for this creep mechanism is inversely related to the third power of the grain size of salt. Sensitivity to grain size is discussed in models TMC3 and TMC 4 below.

For salt deforming by dislocation creep, the rheology is governed by the following equation (Carter et al., 1993):

$$\dot{\epsilon} = 1.80 \times 10^{-24} \exp(-51600 / RT) (\sigma_d)^n \quad (8)$$

where $\dot{\epsilon}$ is the second invariant of the strain rate tensor, σ_d is the second invariant of the deviatoric stress tensor, T is the absolute temperature, R is the universal gas constant and the n is the stress exponent in the power law equation. In models TMC 2 to TMC 4, n is taken as 3.4.

Sediments and the upper crust are modeled as frictional-plastic materials. We use Terzaghi's (1943) effective stress principle to account for the effect of pore fluid pressure on the Drucker-Prager yield criterion (Drucker and Prager, 1952) in the frictional-plastic sediment matrix. In terms of the scalar invariants, the yield stress, σ_y is given by:

$$\sigma_y = J^{1/2}_{2D} = (P - P_f) \sin \phi + C \cos \phi \quad (9)$$

where $J^{1/2}_{2D}$ is the square root of the second invariant of the deviatoric stress, P is the mean stress, P_f is the pore fluid pressure, ϕ is the internal angle of friction of the sediment matrix, and C is the cohesion. P_f is assumed to be hydrostatic unless stated otherwise.

In all the models: (1) the prograding sediments are assigned a constant cohesion of 0.1 MPa and a ϕ of 30° and (2) the syn-rift sediments are assigned a cohesion of 0.1 MPa in model M1. They are assigned cohesion of 50 MPa in models MT2 and TMC 1 to TMC 4. ϕ is equal to 30° in all the models. Compaction of syn-rift or prograding sediments is not incorporated in these models.

2.3.2. Nested upper-mantle scale models

In the nested models (NS1 to NS5), the asthenosphere and lithospheric mantle are modeled as linear viscous materials which evolve according to the following flow law:

$$\sigma = 2 \eta \dot{\epsilon} \quad (10)$$

The viscosities for the asthenosphere are 10^{21} Pas (models NS1 and NS2) and 10^{23} Pas (models NS3, NS4 and NS5) and the viscosity used for the lithospheric mantle is 10^{24} Pas (models NS1 to NS5).

Continental crust, oceanic crust, syn-rift sediments and prograding sediments are modeled as frictional-plastic materials as in section 2.3.1, with the following properties:

(1) the prograding sediments are assigned a constant cohesion of 0.1 MPa and a ϕ of 30° in models NS1 and NS2. In models NS3 – NS5, they are assigned a ϕ of 15° and (2) the syn-rift sediments are assigned a cohesion of 0.1 MPa and a ϕ of 30°.

2.3.3 Sediment compaction - Nested upper-mantle scale models

Syn-rift and sediments in the nested upper-mantle scale models undergo compaction in which the density increases with increasing depth according to the exponential density-depth relation of Athy (1930). The density increases rapidly at shallow depths, then progressively more slowly, asymptotically reaching the grain density (2640 kg/m^3) as shown in Figure B.4. For more detail on the compaction method, please refer to Appendix 2, Albertz et al (in press).

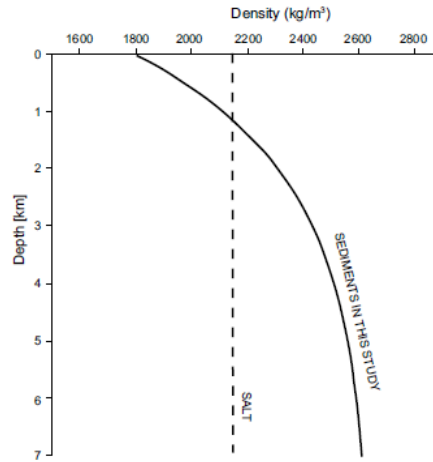


Figure B.4. Density versus Depth curve for the syn-rift and sediments. Density of salt, which is constant at 2150 kg/m^3 , is also shown.

2.4 Sedimentation

In the basin-scale models, a half Gaussian function is used to define a progradational profile for the sediments. This profile is translated seaward from the left end of the model at a constant horizontal velocity of 0.15 cm/a. Aggradation is defined by a laterally uniform bathymetric level for the upper surface of sedimentation. In the basin scale models discussed below, this surface moves vertically at velocity 67 m/Ma. The surface position and velocity can have different values for different time intervals. The space between the existing surface of the sediment and desired bathymetry is iteratively filled with sediment and the associated isostatic adjustment calculated. In places where the existing sediments are higher than the aggradation profile sediment is not removed. Aggradation can be combined with progradation in different regions of the model and under these circumstances the higher profile takes precedence. Note that this method of aggradation specifies the way in which the surface position of the aggrading sediments evolves in the same way as the progradation method. For a detailed description of the sedimentation models, please refer to Appendix 1 of Albertz et al (in press).

In the nested upper-mantle-scale models the same general types of progradation and aggradation sedimentation models are available. Specifically, in NS1 to NS5, sedimentation occurs in two phases. An initial phase of aggradation (velocity = 25 m/Ma) is followed by a progradation (0.075 cm/a) phase. The sedimentation profiles have the additional feature that they are sinusoidally perturbed. That is, sinusoidal modulations are superimposed on the sedimentation profiles. These modulations are spatially restricted to the lateral limits of the autochthonous salt basin. The sinusoids have amplitude of 20 m and a wavelength of 20 km and the sinusoid wave train tapers off linearly, outward from the edges of the salt basin, over a distance of 20 km. The sinusoidal modulation will create superimposed small amplitude lows and highs in the new sedimentation profile, designed as a simplified first order representation of bathymetric unevenness observed in nature.

2.5 Thermal properties

Except model M1, all the other models are thermo-mechanically coupled and are used to investigate the thermal effects associated with presence and mobility of salt in the system. Thermal properties of the sediments and salt used in these models are shown in Table 1 below. Values for syn-rift and prograding sediments (shale values) and salt are based on thermal model A of Mackenzie et al (1985) for the Nova Scotia margin.

Thermal Properties	Crust (used in models)	Syn-rift sediments (used in models)	Prograding sediments (used in models)	Salt (used in models)
Thermal Conductivity K (W/(m K))	2.25	1.255 (MT 2, and TMC 1 – TMC 4)	1.255 (MT 2, TMC 1 – TMC 4)	5.858 (All)
Density for thermal calculation (kg/m ³)	2860	2300 (MT 2, and TMC 1 – TMC 4)	2300 (MT 2 and TMC 1 – TMC 4)	2150
Specific heat J/(kg K)	750 (All)	837 (MT 2 and TMC 1 – TMC 4)	837 (MT 2 and TMC 1 – TMC 4)	750 (All)
Frictional heating coefficient	0 (All)	0 (All)	0 (All)	0 (All)
Radioactive Heat generation (μ W/m ³)	0 (All)	1.04 (MT and TMC 1 – TMC 4)	1.04 (MT 2 and TMC 1 – TMC 4)	0 (All)

Table 1. Thermal properties used in the **basin-scale** models discussed in the report. Basal heat flux in all the models (except model M1) is 50 mW/m².

Thermal Properties	Crust	Syn-rift sediments	Prograding sediments	Salt	Lithospheric Mantle	Asthenosphere
Thermal Conductivity K (W/(m K))	2.25	1.255	1.255	5.858	2.25	2.25 (T < 1603 K) 48.5 (T > 1623K)
Density for thermal calculation (kg/m ³)	2860	2300	2300	2150	3000	3000
Specific heat J/(kg K)	750	750	837	750	750	750
Frictional heating coefficient	0	0	0	0	0	0
Radioactive Heat generation (μ W/m ³)	2	1.04	1.04	0	0	0

Table 2. Thermal properties used in the nested upper-mantle-scale models (NS 1 to NS 5).

3. Basin-Scale Models

3.1 Model M1 – Purely mechanical model with a constant salt viscosity (10^{18} Pa s)

Model M1 investigates the evolution of the salt basin that is subjected to differential loading due to sedimentary progradation. The salt is initially 2 km thick. This model is identical to the reference model “R” of Albertz et al. (in press) except that compaction of sediments is not incorporated. Salt is modeled a linear viscous material with a constant viscosity of 10^{18} Pa s.

At 5 Ma (Fig. B.5a), the salt in the original basin thickens and shortens due to a combination of gravitational gliding and differential loading from the prograding sediments. The salt spills over the seaward edge of the salt basin and the relief of the salt glacier is about 0.6 km. At 30 Ma (Fig. B.5b), a significant amount of salt is expelled from of the autochthonous salt basin and the salt sheet advances in the seaward direction. The salt sheet is driven by the gravitational spreading and progradation of the overburden which results in large scale normal faulting within the sediments. The flanks of the autochthonous salt basin subside flexurally owing to the increasing load from the influx of sediments. This flexure, combined with the aggrading sediments, results in an increasing climb angle for the salt sheet. As more sediments are deposited on the seaward side of the salt sheet, it climbs up section by ‘tank tread’ advance. By 50 Ma (Fig B.5c), the sedimentary overburden on the landward side of the salt sheet becomes stable and normal faulting ceases. The sediments subjacent to the allochthonous salt sheet are deposited as sub-horizontal layers. Note that the system is ‘open ended’ as salt is extruded on the seaward side of the autochthonous basin. Therefore, unlike the landward end, these sediments seaward of the advancing salt sheet do not preserve any record of attendant deformation (shortening). The deformation observed in different regions of this model is controlled by the differential loading i.e., sedimentary progradation rate, shape of the prograding profile and the rate of advancement of the salt sheet. Models such as these provide insights into various controlling factors concerning the geometric evolution of salt systems.

3.2 Thermal and Mechanical Basin-Scale Models

Another important aspect of passive margin salt systems, which is not addressed in model M1, is an understanding of the thermal histories of salt systems and related sediments, and how they change with evolving geometry of the salt bodies. Higher thermal conductivity of salt relative to adjacent sediments significantly alters the heat transfer in the vicinity of salt bodies. These modifications may have a significant impact on the hydrocarbon maturation and generation in salt systems. In order to analyze how the temperature within salt systems is affected by salt mobility, we present below, both models in which the mechanical and thermal components are decoupled (model MT 2) and thermo-mechanically coupled models (models TMC 1 to TMC 4).

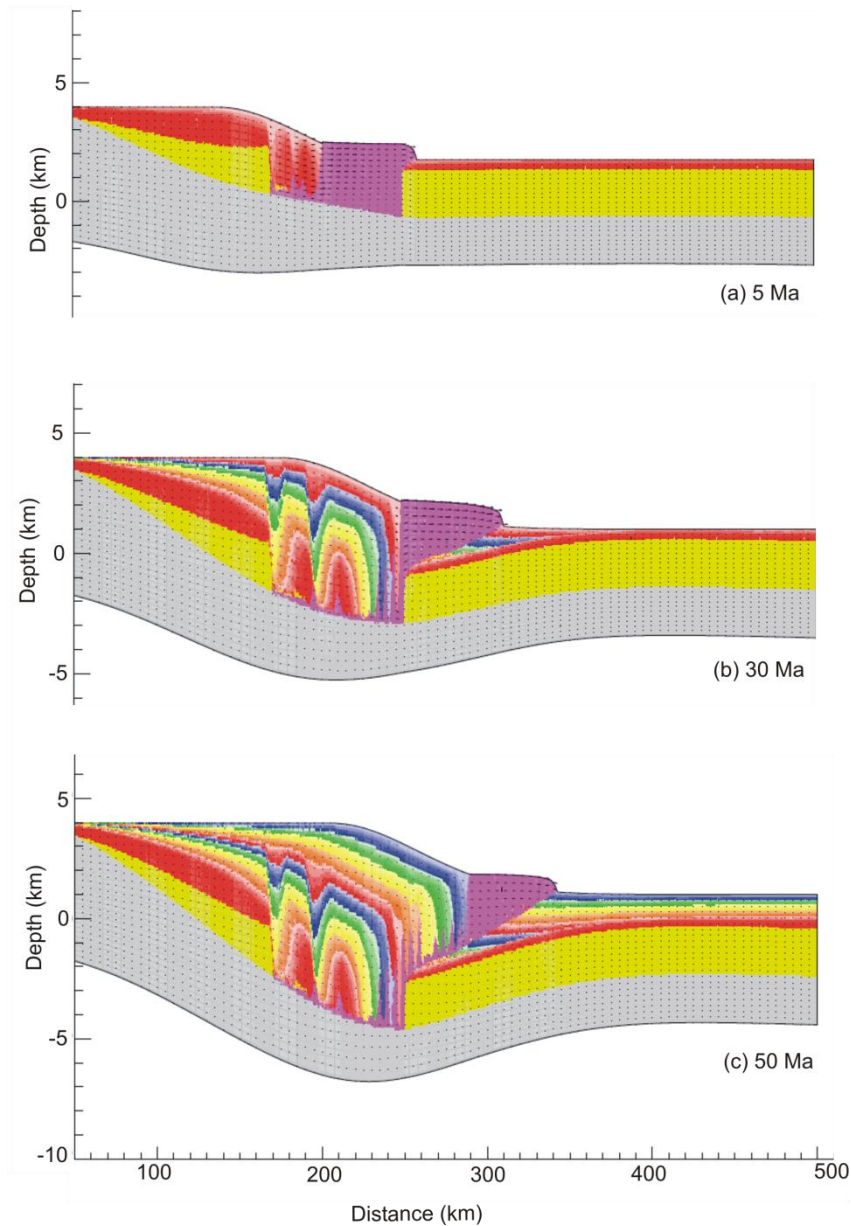


Figure B.5. Results from Model M1. Initial sedimentation results in thickening and shortening of the salt and extrusion of salt over the seaward edge of the autochthonous salt basin. From 30 – 50 Ma, the salt sheet advances in the seaward direction and the landward sedimentary overburden fails by normal faulting. There is a minor increase in climb angle of allochthonous salt with time. As the system is ‘open ended’ there is no record of deformation in the seaward sediments subjacent to the allochthonous salt sheet. Note the large vertical exaggeration, approximately 16.6.

3.2.1 Model MT2 – Thermal-Mechanical models with Constant Salt Viscosity (10^{18} Pas) (Rock types have individual thermal properties – Thermal conductivity of salt 5.858 W/mK)

The presence of salt structures in passive margin settings impacts the structural and stratigraphic evolution of the basin. This influence is due to the unique mechanical behaviour of salt which deforms by creep under geological strain rates. While the structural and stratigraphic features associated with salt mobility may significantly influence the movement of hydrocarbons, the unique high thermal conductivity of salt perturbs the thermal structure in the surrounding rocks in a complex manner which in turn affects the hydrocarbon maturation and generation. Earlier analytical models (e.g., Petersen and Lerche, 1996) for thermal structure around salt bodies are limited by simplified assumptions on the geometry of the salt structures. These models often assume prescribed geometric evolution of the salt structures. However, observations from analogue models (e.g., Koyi, 1996) and numerical models (e.g., Gemmer et al. 2004, Albertz et al., in press) have shown that the geometry of allochthonous salt sheets in passive margin settings evolves in a complex manner as a function of the salt viscosity, rate of sediment progradation and aggradation, and initial shape of the salt basin.

In order to understand the thermal evolution of rocks adjacent to complexly evolving salt structures, we have modified the finite element models of Albertz et al. (in press) to incorporate the calculation of the thermal evolution. These calculations include basic thermal properties of the salt, crust and sediments. Owing to the high conductivity of salt, salt structures often result in positive and negative thermal anomalies above and beneath the salt body. Based on the evolving shape of the salt body, these perturbations may evolve in a complex manner. We refer to these anomalies as the ‘thermal image’ of the salt and we investigate how they move in relation to the salt.

Model MT 2 demonstrates this thermal image effect. The syn-rift and depositing sediments are assigned thermal values that are based on modeling studies of subsidence history of the Nova Scotian margin (Mackenzie et al., 1985) and are shown in Table 1. The basal heat flux is 50 mW/m^2 and is uniform in space and time.

At 5 Ma (Fig. B.6a), salt is shortened and thickened in the autochthonous salt basin, isotherms beneath the salt are significantly depressed and the temperature beneath the 3 km thick salt body reaches a value of only 25°C . This is due to the high thermal conductivity of salt relative to adjacent units. Within the sedimentary fill in the autochthonous basin on the landward side of the salt, the temperatures reach values of up to 100°C .

At 30 Ma (Fig. B.6b), a significant amount of salt has been expelled from the autochthonous salt basin. A thin vertical stock connects the allochthonous salt sheet with the remaining salt in the basin. Temperatures in the autochthonous basin reach values of up to 200°C . On the seaward side of the salt sheet which is up to 3 km thick, the subjacent sediments reach temperatures of only up to 25°C and the isotherms are gently dipping in the landward direction. On the landward side of the salt sheet, temperatures decrease significantly towards the salt sheet and the isotherms are steeply dipping in the seaward direction. Thermal patterns within the underlying crust, when

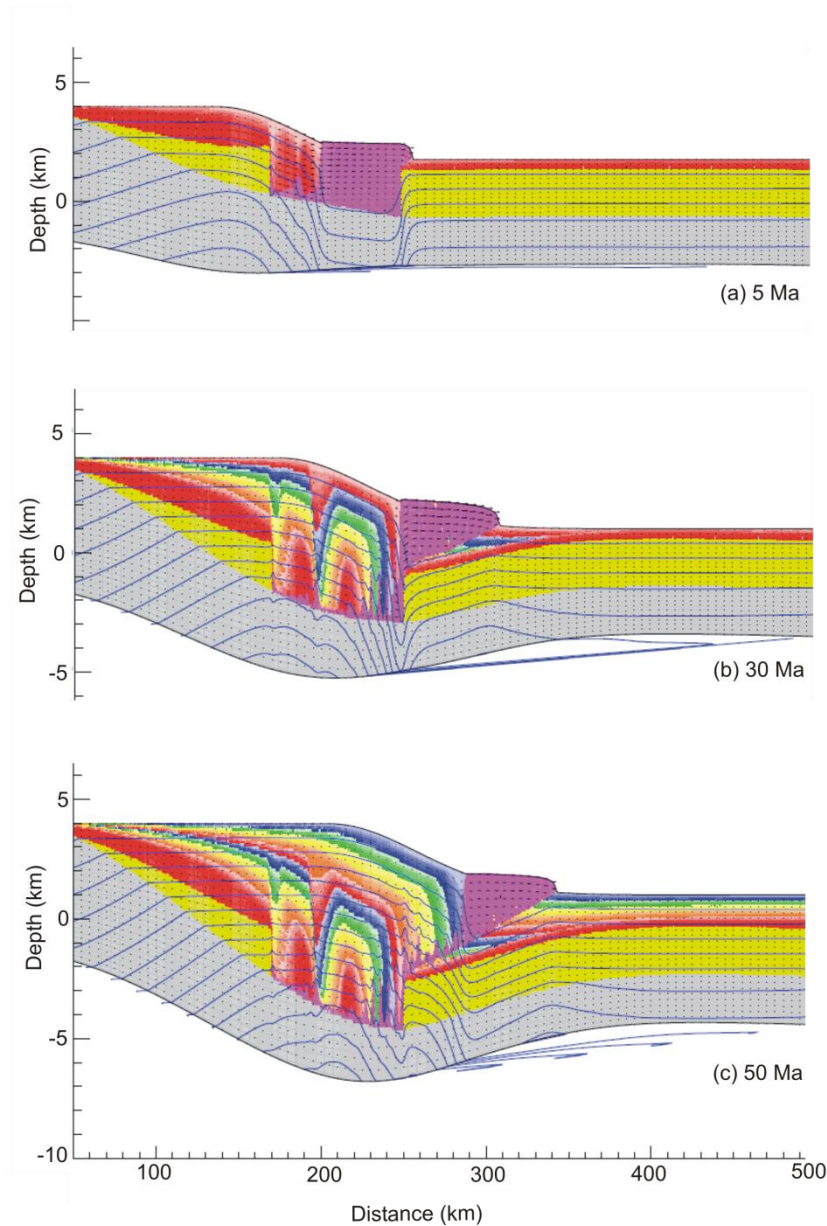


Figure B.6. Results from model MT 2. The continental crust is assigned typical thermal properties of upper crust whereas the syn-rift (yellow) sediments, prograding sediments and salt are assigned different thermal properties obtained from Mackenzie et al. (1985). The thermal conductivity of salt is 5.858 W/(mK). Isotherms (blue) are also shown. Seabed temperature is 0°C and isotherms are shown increasing at 25° C intervals below the seabed. VE = 16.6.

proximal to the salt body are also significantly perturbed. Thus, we see that the thermal image of the salt, which depresses temperatures below it, migrates laterally at approximately the same rate as the salt.

At 50 Ma (Fig. B.6c), the salt sheet advances farther by tank tread advance and climbs over the sediments deposited on the seaward side of the salt sheet. The slope of the isotherms beneath the

salt sheet reflects the geometry of the salt – sediment contact. As the climb angle increases, the salt sheet thickens thereby enhancing its thermal image, and the isotherms dip more steeply in the landward direction.

Owing to the low thermal conductivity of sediments infilling the autochthonous salt basin, the isotherms are elevated beneath the basin. These elevated temperatures are maintained after the evacuation of the salt by continued infilling of the prograding sediments which results in a thick sedimentary basin. As salt climbs up section and flows seaward by tank tread advance over the sediments, it provides a conduit for heat flow from subjacent units. This effect is most pronounced when the thickness of the allochthonous salt sheet is of the same order of magnitude as the underlying units. Where the thickness of salt is much lower (e.g., in the evacuated basin or above the seaward edge of the autochthonous salt basin) (Figs. B.6b, c), the temperatures tend to be higher as the heat is conducted out less efficiently.

In summary, as the prograding sediments gradually expel the salt from the autochthonous salt basin, the influence of salt on the thermal patterns in the basin becomes increasingly focused towards the seaward edge of the basin; the thermal image of the salt has migrated. With increasing sedimentation, the temperatures within the basin increase nearly as fast as the salt is replaced by low thermal conductivity sediment. As the salt sheet advances over the sediments deposited on the seaward side, the isotherms are depressed beneath the salt sheet and this thermal image moves with the salt sheet. It can be seen that the model allows us to dynamically track the evolution of temperature at any point in the salt system, so that the temperature-time history of parcels of material, the Lagrangian tracking particles can be calculated. These histories can be used in thermal maturation studies and the results have potential implications for hydrocarbon production. Kerogen maturation in source rocks is strongly dependent on their temperature history and is a key component to the assessment of the hydrocarbon potential of sedimentary basins. Typical thermal windows range from (60° -160° C) for oil to (160° -220° C) for gas and depend on the type of kerogen. From this illustrative model result we see that these windows will be depressed during the salt translation above strata and will subsequently be elevated as the salt is evacuated. The dynamic models presented in this report allow us to quantify these transient thermal patterns in passive margin salt systems. This approach provides increased conceptual insight by comparison with thermal maturation models that incorporate salt tectonics in a cumbersome stepwise geometrical manner.

3.3 Thermal and Mechanical Basin-Scale Models – Temperature dependent non-linear creep in salt

Model MT 2 gives us useful insights into the first-order evolution of transient thermal patterns in mobile passive margin salt tectonics systems and allows us to understand the coupled advective-conductive thermal evolution of salt systems adjacent to complex salt structures. However, in nature, salt (in this case, specifically halite) deforms predominantly by temperature-dependent viscous deformation. In order to understand how the effective viscosity may vary with temperature and its impact on the salt tectonics, we present below equivalent thermo-mechanically coupled models in which salt is modeled as a non-linear viscous material in which the viscosity also depends on temperature.

3.3.1 Model TMC 1 - Thermo-Mechanical Coupled model – Salt deforms by Grain Boundary Diffusion Creep

Experimental studies have shown that deformation in halite at low strain rates most likely occurs by two creep mechanisms – Grain boundary diffusion creep which is dominant in wet halite (> 45 ppm water) or by Dislocation creep (in dry halite), or by a combination of the two. Because both of these creep mechanisms are thermally activated, the effective viscosity within the salt body is strongly dependent on the ambient temperature of deformation. That is, depending on the structural position within the salt system, the effective viscosity of the salt may be low (at higher temperatures or deeper levels) or high (at lower temperatures or near surface levels). Therefore the constant viscosity models, such as model MT2, likely do not accurately capture the rheological response of natural salt to stress at geological strain rates. The temperature effect becomes particularly important in large, basin scale salt bodies (kilometre scale) where temperature differences and, therefore the salt mobility variations, may be large in different parts of the basin. The predominant creep mechanism is controlled by the grain size, strain rate and the water content within salt, together with other environmental factors. In order to illustrate how the rheological behaviour of halite will affect the overall geometric and thermal evolution of salt systems, we first describe model TMC1 in which salt deforms by pressure-solution creep and then compare it with models in which salt deforms by dislocation creep, and a combination of pressure-solution creep and dislocation creep.

Model TMC1 is assigned the same material properties for the frictional plastic materials as in model MT2. Salt is modeled as material deforming by grain boundary diffusion or pressure solution creep. The material parameters chosen for salt are based on experimental studies of Spiers et al (1990) and are described in section 2. The model has the same thermal properties as model MT2.

At 5 Ma (Fig. B.7a), the salt sheet shortens and thickens in response to the differential load due to the prograding sediments and salt begins spilling over the seaward edge of the autochthonous salt basin. However, owing to the low temperature at the near surface levels, the effective viscosities are higher than those of the constant viscosity model MT2. This results in less shortening and thickening of the salt sheet and a relatively low relief on the salt glacier.

With increasing sedimentation (30 Ma, Fig. B.7b), a significant amount of salt is squeezed out of the autochthonous salt basin. The higher effective viscosities within the salt sheet at low temperatures at the near surface levels impede the rate of advancement of the salt glacier at the surface. The structural relief on the salt glacier relative to the top surface of the seaward sedimentary layers is greater than in the case of model MT 2. At 30 Ma, the lateral extent of the salt glacier is ~ 30 km which is significantly less than the ~ 60 km extent in the constant viscosity model. Owing to the slow advance rate relative to the progradation rate, the salt sheet is forced to climb more steeply up section which results in shortening and thickening of the sheet. Consequently for the same duration of sedimentation, the sediments in the footwall of the salt canopy- sediment contact are significantly thicker. Owing to high effective viscosity of salt at the surface the whole system is less mobile as it evolves by gravitational spreading. Extensional growth faulting in the sediments deposited landward of the allochthonous salt sheet is therefore significantly reduced. In contrast, the salt glacier in model MT2 flowed more easily owing to

lower viscosity of salt (10^{18} Pa s). This facilitated gravitational spreading of the landward sediments which failed by extension earlier than in model TMC1.

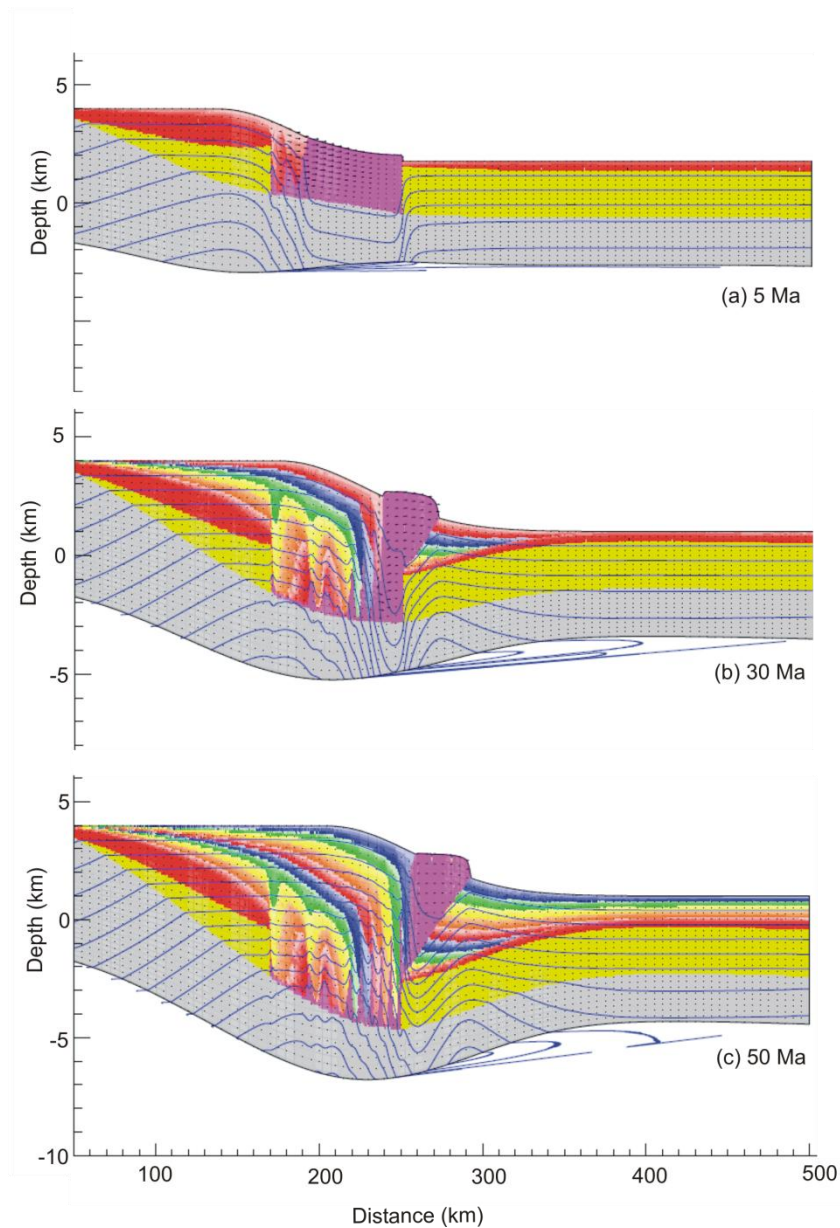


Figure B.7. Results from thermo-mechanically coupled model TMC 1 in which salt is modeled as a viscous material deforming by pressure solution creep (Spiers et al., 1990). The shortening and thickening of salt in the initial increments of sedimentation and the subsequent lateral transport are lower than in models with constant viscosity for salt (Models MT 1 – MT2). Isotherms (blue) are also shown. Seabed temperature is 0°C and isotherms are shown at 25°C increasing intervals below the seabed. $\text{VE} = 16.6$.

3.3.2 Model TMC 2 - Thermo-Mechanical Coupled Model – Salt deforms by Dislocation Creep

In order to understand the geometrical and thermal evolution of salt deforming predominantly by dislocation creep, we analyzed models in which salt is modeled as a non-linear viscous material deforming according to the halite power law creep of Carter et al. (1993). The material properties of crust, synrift and prograding sediments are same as in the models discussed above (TMC2 and TMC 1).

At 5 Ma (Fig. B.8a), differential loading due to prograding sediment and the gravitational gliding due to tilt of the autochthonous salt basin result in the shortening and thickening within salt. The relief of the salt glacier over the seaward edge of the basin is slightly less than in the case of salt deforming by pressure solution creep. As dislocation creep is predominantly a high temperature mechanism, it is most active where the temperatures within salt reach high values. That is, at the base of the salt sheet and within the salt remaining in the autochthonous salt basin. Owing to low temperatures at near surface conditions, the effective viscosity of salt deforming by dislocation creep, is significantly higher than at deeper levels. As a consequence, the lateral transport within the salt glacier is less than in the earlier models.

At 30 Ma, salt evacuation from the autochthonous basin is not as efficient as in the case of model TMC 1. Even though the salt extrudes as a glacier, the mobility of salt higher up within the sheet is significantly lower. This impedes efficient expulsion of salt from the autochthonous basin. This influence is more prominent at 30 Ma (B.8b) when the differential load on the salt in the autochthonous salt basin is higher. For the depth range within model TMC 2, the effective viscosities at the base of the salt sheet are significantly larger than in the case of salt deforming by pressure solution creep. Therefore deformation within autochthonous salt is lower than in the case of model TMC 1. As a consequence, the salt wall at the seaward edge of the autochthonous salt basin is wider than in model TMC 1. In addition, for the same model duration, the salt sheet advances farther seaward by ~ 35 km in constant viscosity models MT1 and MT 2, and by 15 km when salt deforms predominantly by pressure solution creep in model TMC 1.

With increasing sedimentation, at 50 Ma, salt rises diapirically with minimal lateral transport outboard of the seaward edge of the autochthonous salt basin. The salt glacier is farther inboard than in earlier models and its top surface is higher by more than 1 km relative to model TMC 1. A continuous salt diapir extends from the top free surface to the bottom of the autochthonous salt basin. This continuity and the higher effective viscosity of salt deforming by dislocation creep, result in the salt diapir acting as a more competent buttress for the prograding sediments landward of the diapir than in the case of earlier models. As a result extension due to gravitational spreading and faulting within these sediments is less than in earlier models.

At ~ 50 Ma (B.8c), the seaward advancement of the salt glacier is significantly less (up to $x = 280$ km) than in the case of models with constant salt viscosity ($x = 340$ km) and also in case of models with pressure solution creep ($x = 290$ km). The slow rate of advance results in increased

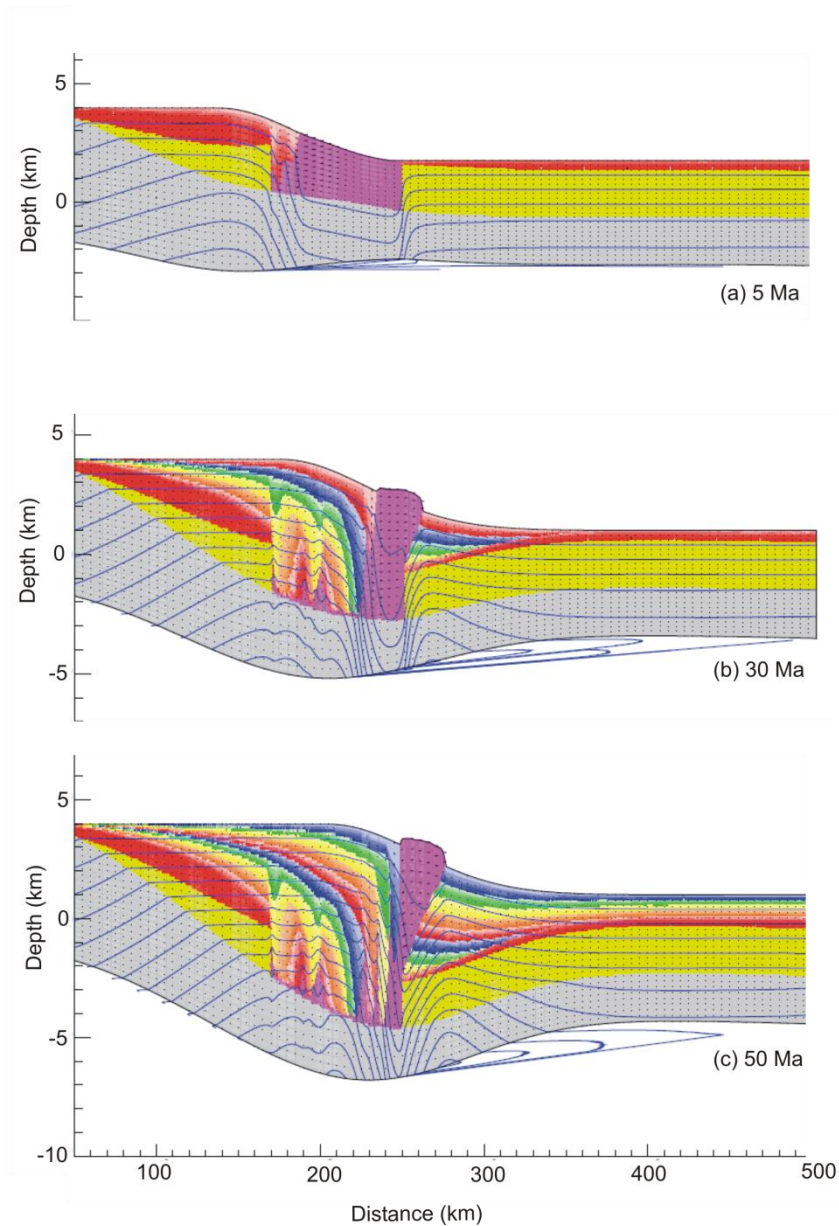


Figure B.8. Results from thermo-mechanically coupled model TMC 2 in which salt is modeled as a non-linear viscous material deforming by dislocation creep (Carter et al 1993). The shortening and thickening of salt in the initial increments of sedimentation and the subsequent lateral transport is lower than in models with 10^{18} Pa s, constant viscosity salt (Models MT 1 – MT 2) and also in model TMC 1. Component of vertical diapiric rise of salt is higher than lateral transport when compared to model TMC 1. Isotherms (blue) are also shown. Seabed temperature is 0° C and isotherms are shown at 25° C increasing intervals below the seabed. VE = 16.6.

thickness of the sediments deposited seaward of the salt glacier than for models MT 2 and TMC 1. These sediments, adjacent to and in front of the allochthonous salt body dip in the seaward

direction. For the same duration of sedimentation, in purely mechanical models (e.g., MT 2), they dip in the landward direction at 50 Ma.

3.3.3 Models TMC 3 and TMC 4 - Thermo-Mechanical Coupled Models – Pressure Solution and Dislocation Creep in Serial Combination

Field observations and experimental studies have shown that salt can deform both by dislocation creep and pressure solution creep. For a large range of grain sizes, microstructural studies document characteristics of both pressure solution creep and dislocation creep in natural rock samples. In order to investigate the influence of both the above creep mechanisms operating simultaneously and the influence of grain size on the evolution of the system, we present the following two end-member models. In model TMC 3, the grain size is held constant at 0.01 m and in model TMC 4 it is held constant at 0.175 m.

(a) Model TMC 3 –Grain size of salt – 0.01 m

For a chosen grain size of 0.01 m, model TMC 3 (Fig. B.9) evolves in a similar way to model TMC 1 (Fig. B.7). This is because, for the given grain size, the flow stress for pressure solution creep will be significantly lower than that for dislocation creep. At 5 Ma (Fig. B.9a), the salt layer thickens and shortens and is evacuated efficiently from the landward side of the autochthonous basin. Minor amounts of remaining salt within the basin rise diapirically as triangular bodies.

Owing to the higher temperatures at the base of the autochthonous basin at 30 Ma, both dislocation creep and pressure solution contribute towards the deformation in salt. As a result, salt evacuation from the basin is more efficient than in model TMC 1. As both the creep mechanisms operate simultaneously, the effective viscosity at a given point in the salt sheet will be less than that in either models TMC 1 or TMC 2. Therefore the lateral transport as a salt glacier is greater in this model. The toe of the salt glacier advances up to $x = 280$ km as compared to up to $x = 270$ km in model TMC 1. This faster advance of the salt glacier (relative to sedimentary progradation rate) also results in a relatively thin sedimentary package that is deposited seaward of the allochthonous salt sheet. At 30 Ma (Fig. B.9b), the relief of the rising salt sheet above the sea floor, is comparable to that in models TMC1 and TMC 2. However the lateral extent of the salt glacier is 100% greater than in either of these models.

At 50 Ma (Fig. B.9c), the salt sheet advances to $x = 310$ km. The trailing side of the allochthonous salt sheet undergoes segmentation as the prograding sediments advance over the rear of the salt sheet. The differential load from the prograding sediments and overall low effective viscosities result in further seaward advancement of the salt glacier. As a result, sediments deposited seaward of the salt sheet dip slightly either in the seaward direction or landward direction. Note that this is in contrast to the nearly sub-horizontal sedimentary layers in models MT 1 and MT 2 and the relatively steeply dipping sedimentary layers in models TMC 1 and TMC 2.

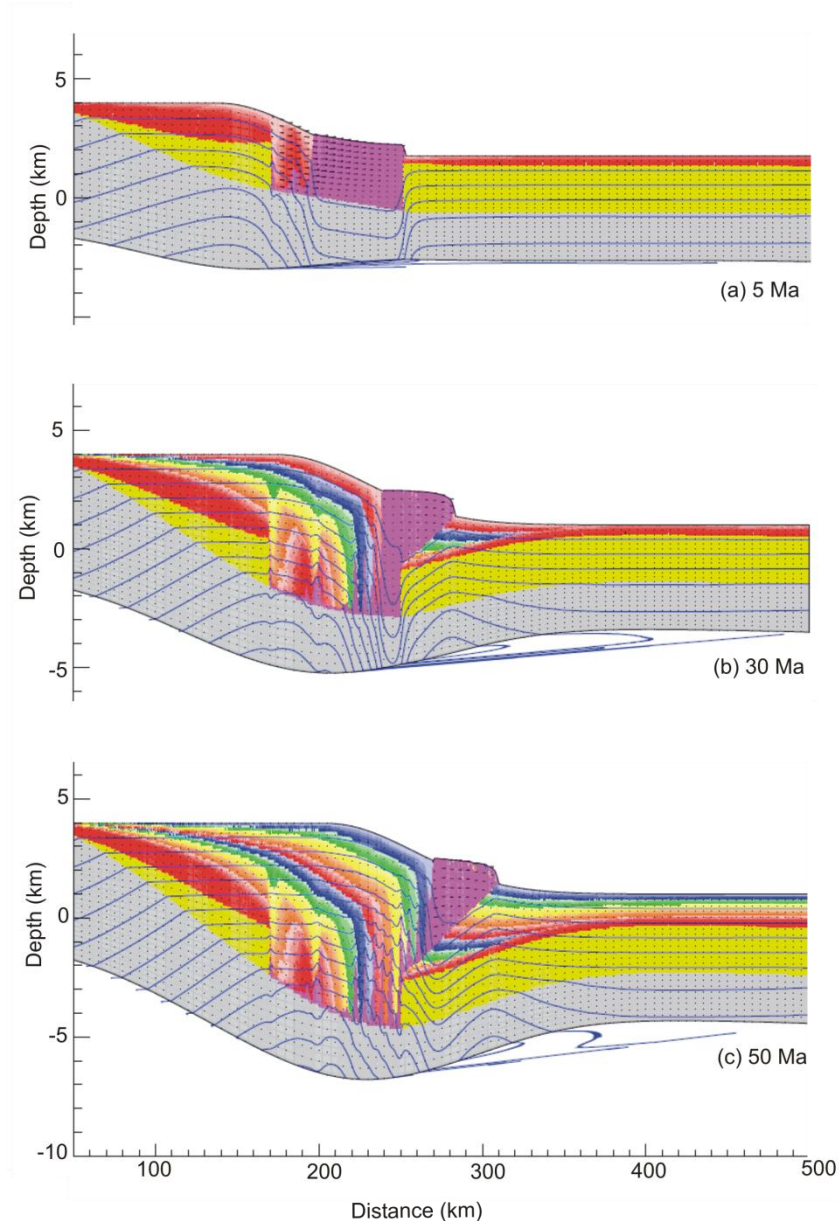


Figure B.9. Results from model TMC 3. Salt deforms by a combination of pressure solution and dislocation creep. The grain size for pressure solution creep is 0.01 m. The overall behaviour of the model is similar to model TMC 1 as the flow stress for pressure solution creep is significantly lower than that for dislocation creep. Isotherms (blue) are also shown. Seabed temperature is 0° C and isotherms are shown at 25° C increasing intervals below the seabed. VE = 16.6.

(b) Model TMC 4 – Salt Grain size in Pressure Solution Creep – 0.175 m

In the previous model, the grain size is held constant at 0.01 m. At this grain size, we have shown that pressure solution creep predominates over dislocation creep. In order to understand the evolution of salt sheets when the relative contributions of pressure solution creep and

dislocation creep are similar, we present a model (Fig. B.10) in which the grain size of salt is increased to 0.175 m. This is an unrealistically high value for grain size in natural salt and the model is intended to illustrate behaviour when both creep mechanisms contribute equally to the deformation. All other model input parameters are exactly the same as in model TMC 3.

With increased grain size, the effective viscosity of the salt due to pressure solution creep increases. Therefore the overall viscosity of salt in this model is higher than in model TMC 3. As a consequence, at 5 Ma (Fig. B.10a), the shortening and thickening within the salt in the autochthonous salt basin is significantly lower than in model TMC 3. The relief of the salt glacier over the seaward edge of the autochthonous salt basin is minimal to non-existent. This is in contrast to nearly 0.6 km relief observed in model TMC 3. With increasing sedimentation, the seaward advancement of the salt sheet is less than in the case of model TMC 3.

At 30 Ma (Fig. B.10b) the toe of the salt glacier advances by about 30 km from the seaward edge of the autochthonous salt basin as opposed to 60 km when the grain size was 0.01 m (model TMC 3). At 50 Ma (Fig. B.10c), the salt sheet maintains connectivity with the salt in the autochthonous salt basin as observed in model TMC 2. With increasing sedimentation, the salt diapir connecting the salt glacier with the salt in the autochthonous basin is segmented by the prograding sedimentary overburden. However, this occurs after 70 Ma in model TMC 4 (not shown here) as opposed to 50 Ma in model TMC 2. The slow climb rate of salt in the current model allows a very thick basin to develop on the seaward side of the allochthonous salt sheet. The climb angle is consistently higher throughout the evolution in models TMC 2 (Fig. B.8) and TMC 4 (Fig. B.10), when compared to that in models TMC 1 (Fig. B.7) and TMC 3 (Fig. B.9).

The models described above clearly show that in thermo-mechanical coupled models the evolution of the geometry of the salt sheet and of seaward sedimentary layers (dip direction) and the deformation within the landward sedimentary overburden are strongly dependent on the dominant creep mechanism. Given all other parameters are equal, salt sheets in natural settings in which salt deforms predominantly by pressure solution creep tend to be more mobile than in the case of deformation by dislocation creep. When both the creep mechanisms operate (1) the lateral transport of salt in open ended salt systems may be high for fine grained salt, and (2) the lateral transport may be significantly lower for coarse grained salt.

These results provide a first assessment of the effect of the simplifying assumption of uniform 10^{18} Pa s salt by comparison with salt deforming by mechanism observed naturally. An important conclusion is that the style of the salt tectonics remains the same in these illustrative models even though the salt rheology varies. Although this may also be true for cases where the salt bodies are large and thick, the difference in behaviour of vertically or laterally thinner bodies will be much more pronounced. One implication is that it is important to have information on the grain size of halite and the way this grain size varies during deformation.

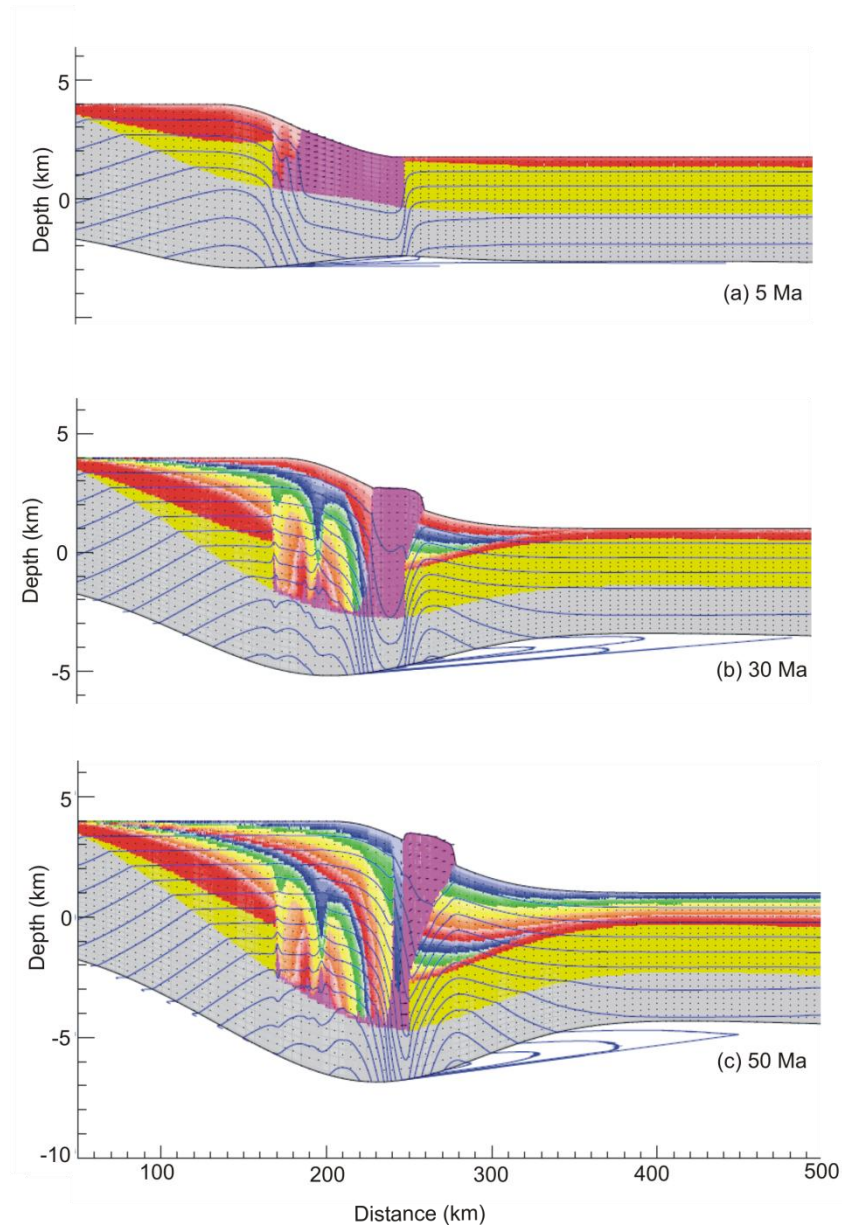


Figure B.10. Results from model TMC 4. Salt deforms by a combination of pressure solution and dislocation creep. The grain size for pressure solution creep is 0.175 m. The overall behavior of the model is similar to model TMC 2. Isotherms (blue) are also shown. Seabed temperature is 0° C and isotherms are shown at 25° C increasing intervals below the seabed. VE = 16.6.

3.4 Assessment of the Basin-Scale Thermal-Mechanical Models

The simple thermo-mechanical numerical models presented above clearly demonstrate that the thermal patterns in a salt tectonic system will evolve with time. These Basin-Scale Models have

a constant basal heat flux boundary condition of 50 mW/m^2 , which is applied close to the bottom of the salt layer. While this basal boundary condition is acceptable for a first approximation of the thermal effects of the salt and is much better than a constant basal temperature, it is clear that the thermal image of the salt penetrates much deeper than the base of this type of model (Figs B5-B10, Fig. B11). Such deep-penetrating thermal anomalies imply that heat is refracted at depth and that the heat flux is not solely vertical as assumed in the basal boundary condition. The implication is that the Basin-Scale Models are potentially inaccurate and that they are likely to be most inaccurate beneath laterally extensive autochthonous salt basins which produce the deepest penetrating thermal images and significant refraction and channelling of heat through the salt.

The solution to this problem is to have a ‘constant heat flux boundary’ that is deep enough so that it is not affected by the thermal focusing of heat beneath a salt body (Petersen and Lerche, 1996). In order to address this issue, we have adopted a new approach in modeling salt systems, which we refer to as the ‘Nested Upper-Mantle-Scale Model’.

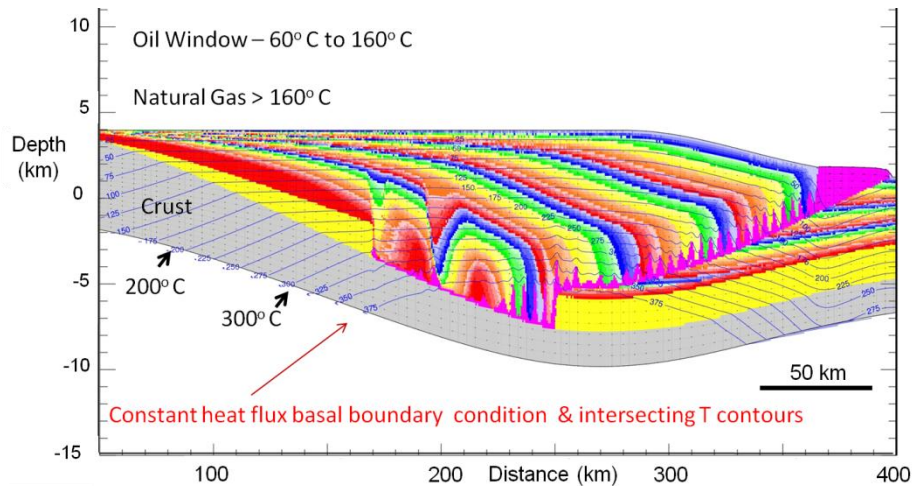


Figure B.11. Results from model MT 2. The continental crust is assigned typical thermal properties of upper crust whereas the syn-rift (yellow) sediments, prograding sediments and salt are assigned different thermal properties obtained from Mackenzie et al. (1985) (Table 1). The thermal conductivity of salt is 5.858 W/(mK) . Isotherms (blue) are also shown. Seabed temperature is 0° C and isotherms are shown at 25° C increasing intervals below the seabed. $VE = 8$.

4. Nested Upper-Mantle Scale Models

4.1 Model NS1 – Interaction between two salt basins and impact on the lithospheric thermal structure

The nested upper-mantle scale models, as described in section 2.1.2, consist of a large (600 km × 600 km) mantle- scale model (referred to as the Large-Scale or LS model), in which a high resolution basin scale model (here 600 km × 25 km – referred to as the Small-Scale or SS model) is embedded in the top 25 km. This nested modeling approach allows us to investigate the basin scale problem at a high enough resolution to calculate deformation in salt accurately and, at the same time, to have the constant basal heat flux boundary condition deep enough so that it is consistent with the thermal refraction that occurs near the salt basin. All the models below use this nested modeling approach. We investigate the thermal and structural evolution of salt basins subject to different styles of sedimentation. Only the results from the SS model, within the larger nested upper-mantle scale models, will be discussed below.

Model NS1 (Fig. B.12) investigates the evolution of and interaction between two salt basins, separated by a block of syn-rift sediments, when subjected to prograding deltaic-type sedimentation. The salt basins are approximately 3 km thick and the landward and the seaward edges of the salt basins have dips of 45° and 30° respectively. Salt is modeled as linear viscous material (10^{18} Pa s). The initial geometry is designed to represent the configuration of the margin late in the syn-rift period when salt has already been deposited and the outer part of the margin has continued to subside tectonically. The model does not include post-rift thermal subsidence of the lithosphere.

At 5 Ma (Fig. B.12b, B.13a), the salt in the tilted autochthonous basins gravitationally settles and flows towards the seaward side so that the top of the salt basin is flat. As a result, salt in the landward basin forms an incipient glacier. More importantly, the presence of salt in these basins results in depressed isotherms immediately beneath the salt basins. The temperatures are relatively higher beneath the intervening syn-rift block compared to the surrounding temperatures. The low temperatures are a consequence of the high thermal conductivity of salt. The thermal perturbation near the salt basins extends to a depth of at least 25 km, an important feature that could not be reproduced in the basin-scale models discussed above (models M1, MT2 and TMC 1 – TMC 4). Note that the result presented here is from the embedded high resolution SS model. The constant heat flux boundary condition is imposed at the bottom of the LS model (600 km) and is therefore consistent with the principles discussed above.

At 25 Ma (Fig. B.13b), owing to the differential pressure exerted by the prograding sediments, salt in the landward basin begins to shorten and thicken and form a glacier on top of the syn-rift block between the salt basins. Thickening of the salt sheet results in narrowing the thermal focusing beneath the salt stock. The expulsion of the salt from the landward basin and deposition of lower thermal conductivity sediments results in increased temperatures within the landward basin.

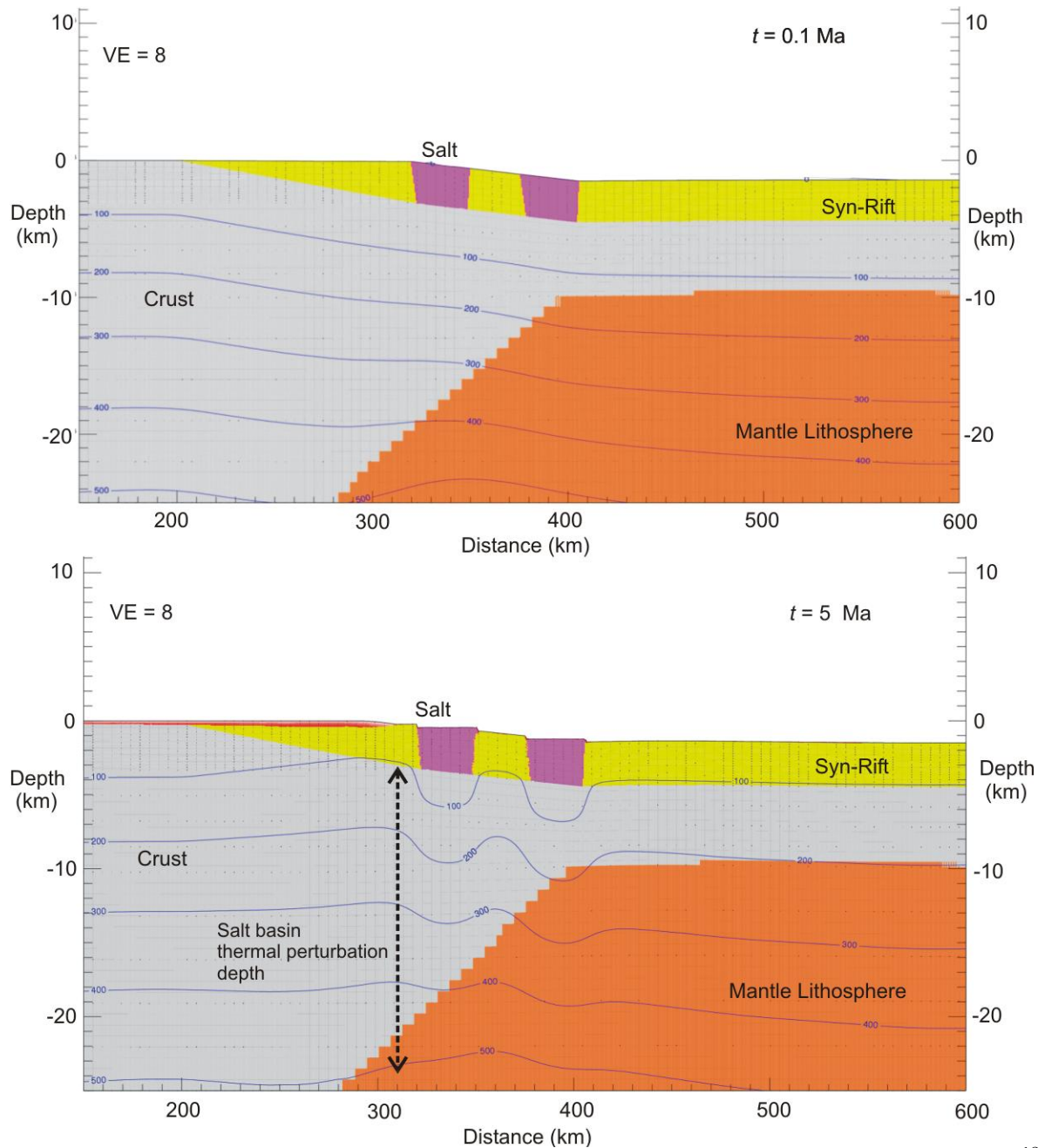


Figure B.12. Evolution of nested model NS1. Salt deforms as a linear viscous material (10^{18} Pas). Isotherms (blue) are also shown. Seabed temperature is 0°C and isotherms are shown at 100°C increasing intervals below the seabed. (a) Model Geometry (b) Salt flows towards the seaward edge of the basins owing to the seaward tilt of the basin floor. Note that the thermal perturbation due to two salt basins extends to a significant depth into the lithosphere.

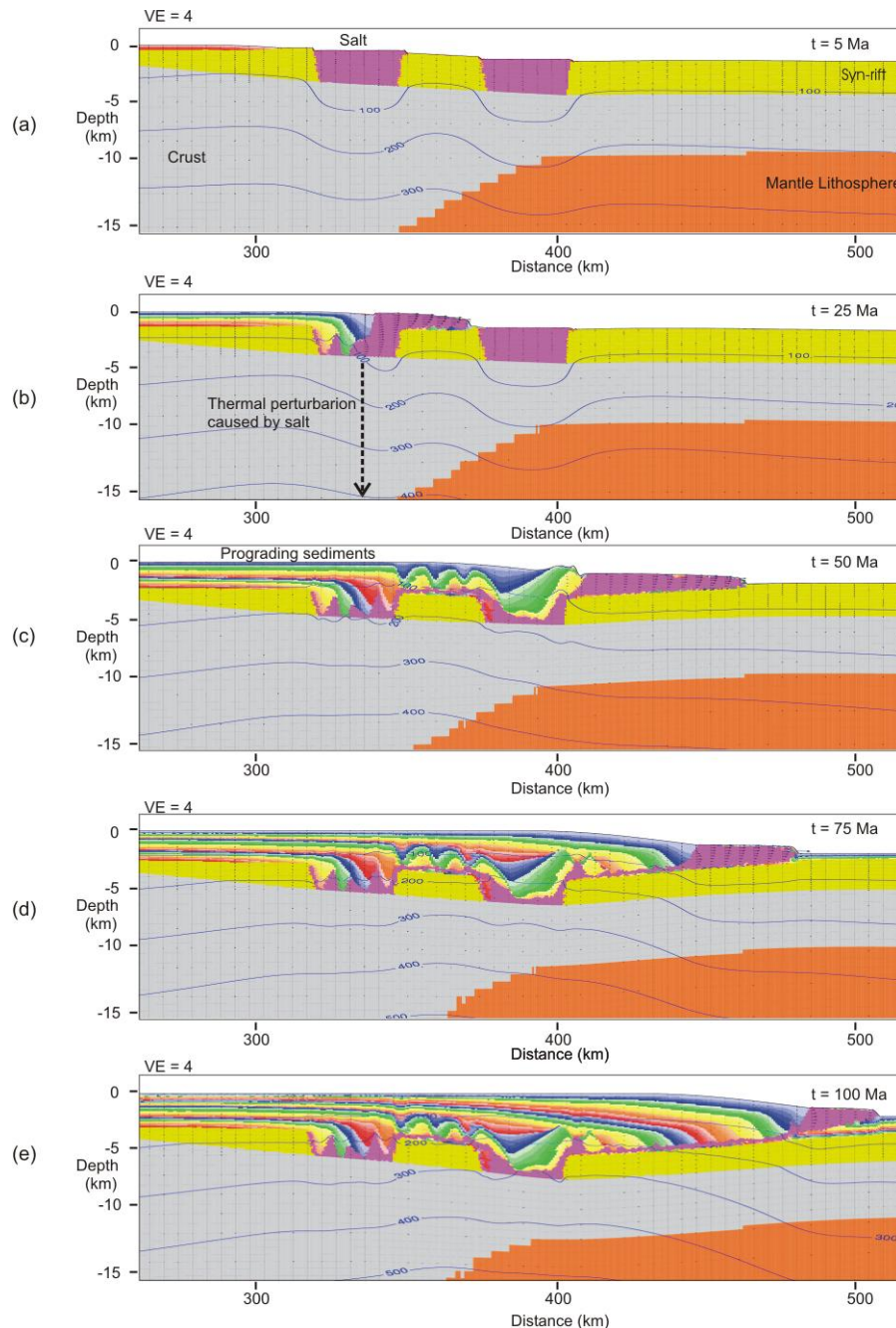


Figure B.13. Evolution of nested model NS1. Salt deforms as a linear viscous material (10^{18} Pas). Isotherms (blue) are also shown. Seabed temperature is 0°C and isotherms are shown at 100°C increasing intervals below the seabed. The thermal perturbation beneath the autochthonous salt basins decreases as salt is replaced by low thermal conductivity sediment. The thermal perturbation beneath the salt sheet moves with it at the same rate.

Continued progradation (50 Ma, Fig. B.13c) expels most of the salt from the landward basin. The salt from the landward basin and the prograding sediments together exert a differential pressure on the seaward basin. This results in expulsion of a significant amount of salt from the seaward basin which advances as a glacier on top of the syn-rift sediments. Remaining salt within the

autochthonous basins forms a continuous detachment surface that extends from the landward edge to the salt glacier. This continuous thin salt sheet acts as a detachment for normal faulting within the sediments deposited on the syn-rift block and in the seaward basin. Temperature within the autochthonous basins increase and thermal perturbation decreases owing to the evacuation of salt from the basins and deposition of less conductive sediments. By 50 Ma, the thermal perturbation is more pronounced beneath the seaward basin and is minimal beneath the landward basin. By 100 Ma (Fig. B13e) the salt sheet moves by tank-tread advance over the sediments deposited seaward of its snout. The thermal image within the basin moves with the advancement of the salt sheet. Temperature beneath the salt sheet is significantly lower compared to that at the same depth above the autochthonous salt basins.

This model shows that interactions between narrow autochthonous salt basins exert significant control on the thermal and structural evolution of the system. The results indicate that the thermal perturbations due to autochthonous and allochthonous salt bodies can extend to significant depths and affect the thermal structure of the lithosphere. Dynamic nested models that take into account the thermal refraction around salt bodies, such as model NS1, can therefore be used to better quantify the heat flow history within salt basins and represent an improvement over the basin-scale models discussed earlier.

4.2 Model NS2 – Single wide salt basin on the highly thinned continental crust

Model NS2 investigates the evolution of a single wide salt basin which is located farther outboard than the basins in model NS1 in a region that can be interpreted to be above thinned continental crust or oceanic crust (Fig. B.14a). The salt basin is rectangular, 120 km wide and 2 km thick. Salt is modeled as a linear viscous material (10^{18} Pas). The initial configuration is designed in the same way as model NS1.

Sedimentation occurs in two distinct phases. An initial phase of sedimentary aggradation (25 m/Ma for 10 Ma) is followed by sedimentary progradation (progradation velocity 0.15 cm/yr). During both the phases, sinusoidal perturbations are superimposed on the sedimentation profiles above the autochthonous salt basin. The sinusoidal perturbations can be envisaged as a first-order representation of bathymetric unevenness, lateral density variations and/or channel-levee systems observed in nature.

At 5 Ma (Fig. B.14b), aggradation results in sediments deposited on the seaward side of the salt basin. More importantly, sediment deposited on the autochthonous salt basin results in the formation of minibasins, some of which are grounded by 5 Ma. The differential pressure caused by the sinusoidal perturbations on the aggrading sediments results in the formation of these salt diapirs and minibasins. With increasing sedimentation (10 Ma, Fig. B.15b), the diapirs and the intervening minibasins are fully developed.

The thermal image of the salt body extends deep into the mantle lithosphere. Note that the thermal effects of salt being replaced by the aggrading sediments results in locally higher temperatures beneath the grounded minibasins. However, owing to the thermal focusing of heat by salt, the minibasins remain significantly cooler than the sediments outside the salt basin. To

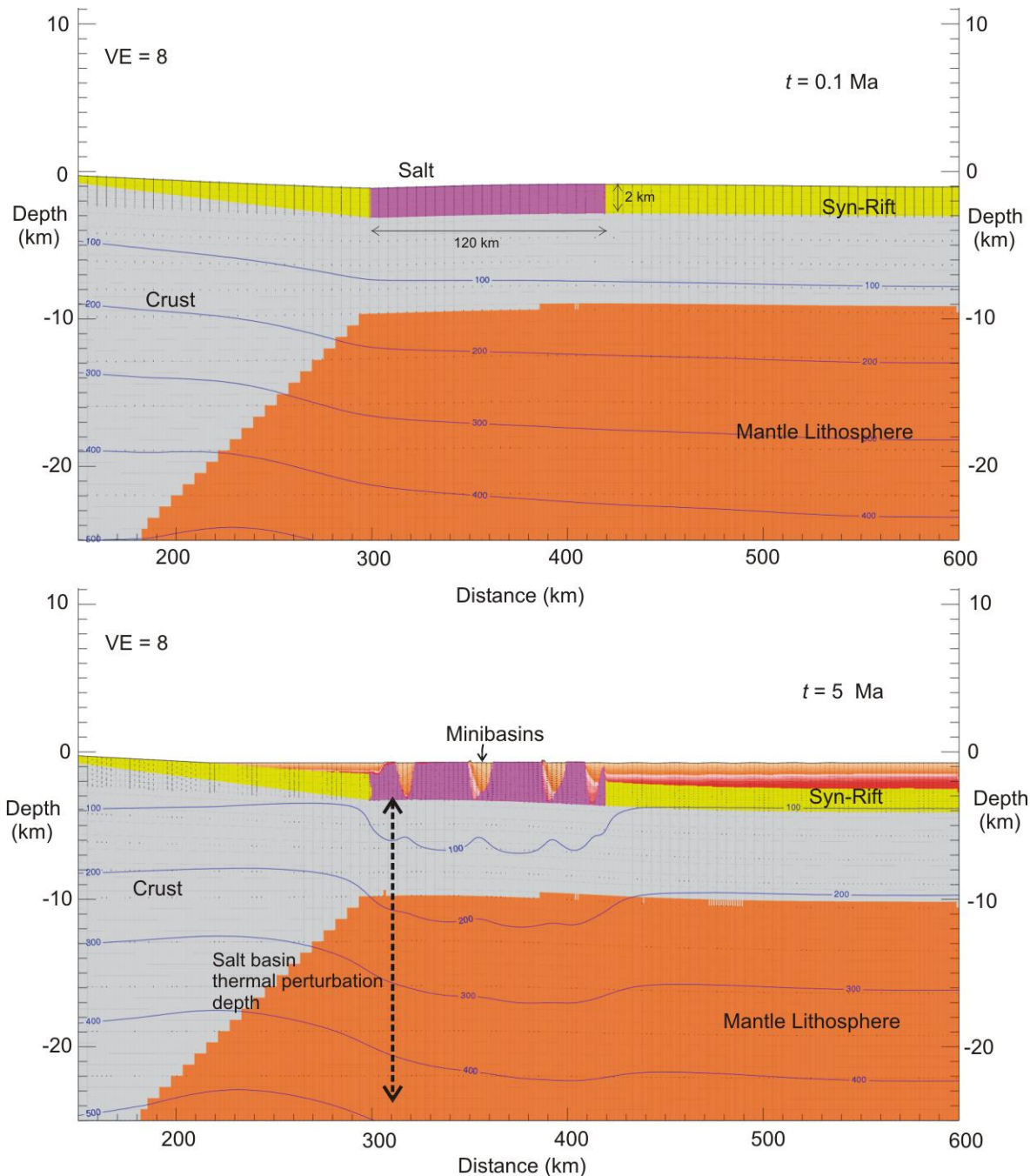


Figure B.14. Evolution of the SS region of nested model NS2. Salt deforms as a linear viscous material (10^{18} Pas). Isotherms (blue) are also shown. Seabed temperature is 0°C and isotherms are shown at 100°C increasing intervals below the seabed. (a) Model geometry (b) Initial phase of sedimentation with sinusoidal perturbation superimposed on a flat aggradational profile results in the formation of minibasins and salt diapirs. Sediments compact as explained in section 2.3.3. Note that the thermal perturbation due to the 120 km wide salt basin penetrates to a significant depth into the lithosphere.

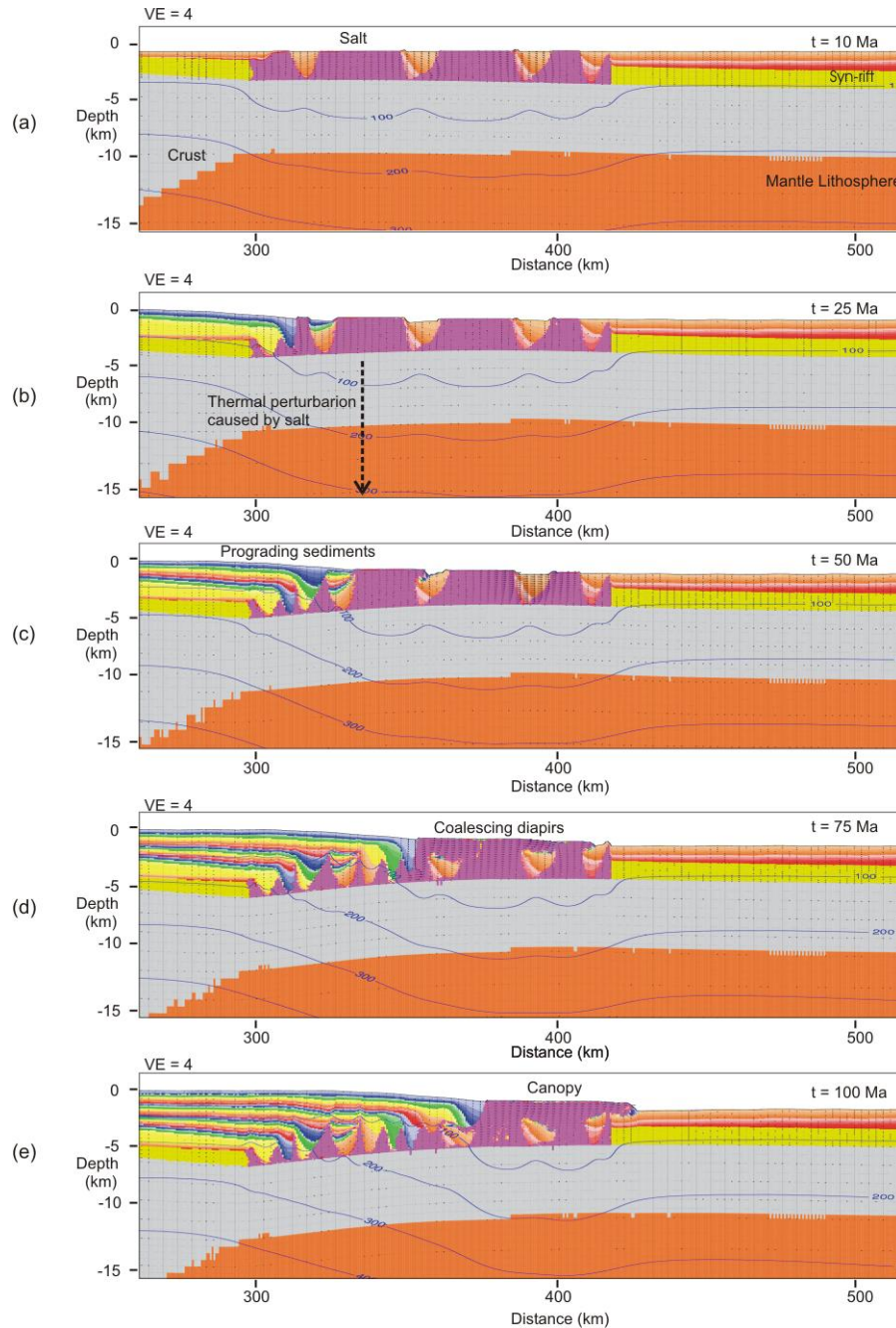


Figure B.15. Evolution of a subregion of the SS part of nested model NS2. Salt deforms as a linear viscous material. Isotherms (blue) are also shown. Seabed temperature is 0° C and isotherms are shown at 100° C increasing intervals below the seabed. Bulbs of the salt diapirs that form during the aggradation phase coalesce and form a canopy at a structurally higher level than the autochthonous basin. Minibasins are cold early in their history when surrounded by salt. Their temperatures increase when prograding sediments are deposited above them, but they remain cold beneath the salt canopy.

a first approximation the thermal gradients in the minibasins are almost as low as those in the adjacent salt despite the significantly lower thermal conductivity of the sediment.

Between 25 and 50Ma, prograding sediments exert differential pressure on the salt diapirs which respond by segmentation at deeper levels and by developing a seaward inclination at shallower depths (Fig. B.15b, c). With progressive sedimentation, the remaining salt in the landward side of the autochthonous basin is overlain by sediments. This results in progressively increasing temperatures with increasing sedimentation within these minibasins (Fig. B.15d, e). In contrast, minibasins that are more seaward are surrounded by salt (Fig. B.15d, e) and are therefore cooler.

With further progradation, by 75Ma the tops of the salt diapirs coalesce and form a salt canopy which is at a structurally higher level than the autochthonous basin but within its limits. Landward minibasins which are buried by the prograding sediments reach significantly higher temperatures, than the seaward minibasins which are surrounded by the salt. At 100 Ma (Fig. B.15e), the salt canopy translates farther seaward and results in the formation of a salt glacier. Correspondingly, the thermal image beneath the salt body is significantly narrower and is most prominent beneath the seaward edge of the autochthonous salt basin.

The dynamical model presented here suggests that uneven bathymetry can result in the formation of salt diapirs and intervening minibasins provided that the locations of the uneven sedimentation persist for sufficiently long, approximately 3- 5Ma in this particular case. Subsequent progradation can result in the formation of inclined and squeezed diapirs which can coalesce and form salt canopies that act as a detachment at structurally higher levels. Note that results from model MT2 (Fig. B.6) discussed above, suggest an alternative mechanism in which salt canopies form by expulsion rollover caused by prograding sediments. These mechanisms and potential implications for structures such as the Balvenie detachment (Fig. B.1) are discussed in more detail in the next section.

5. Insights into the formation of salt canopies from numerical models

Structural style B (SSB) (Albertz et al., in press) region in the Scotian margin comprises a salt tectonic system marked by landward listric normal faults and salt rollers linked to seaward contractional structures, including an allochthonous salt canopy system (Fig. B.16a) as well as small scale thrust faults. Albertz et al. (in press) have shown that the seaward salt canopies in this region of the Scotian basin may have formed as salt was expelled from the autochthonous salt basin by a progradational Cretaceous deltaic sedimentation regime.

Recently available seismic data (e.g., Dip Line 716- 100, Fig. B.1b, B.16a) have allowed better delineation of the salt structures in this part of the Scotian margin. In addition to the canopy system located adjacent to the interpreted seaward edge of the salt basin (shown in Fig. B.1a), they reveal (Kris Kendell, pers. comm.) canopies that formed at a structurally higher level than the autochthonous basin but within its interpreted lateral limits. The Tertiary sedimentary overburden in the SSB region of the Scotian margin is interpreted to have been detached above

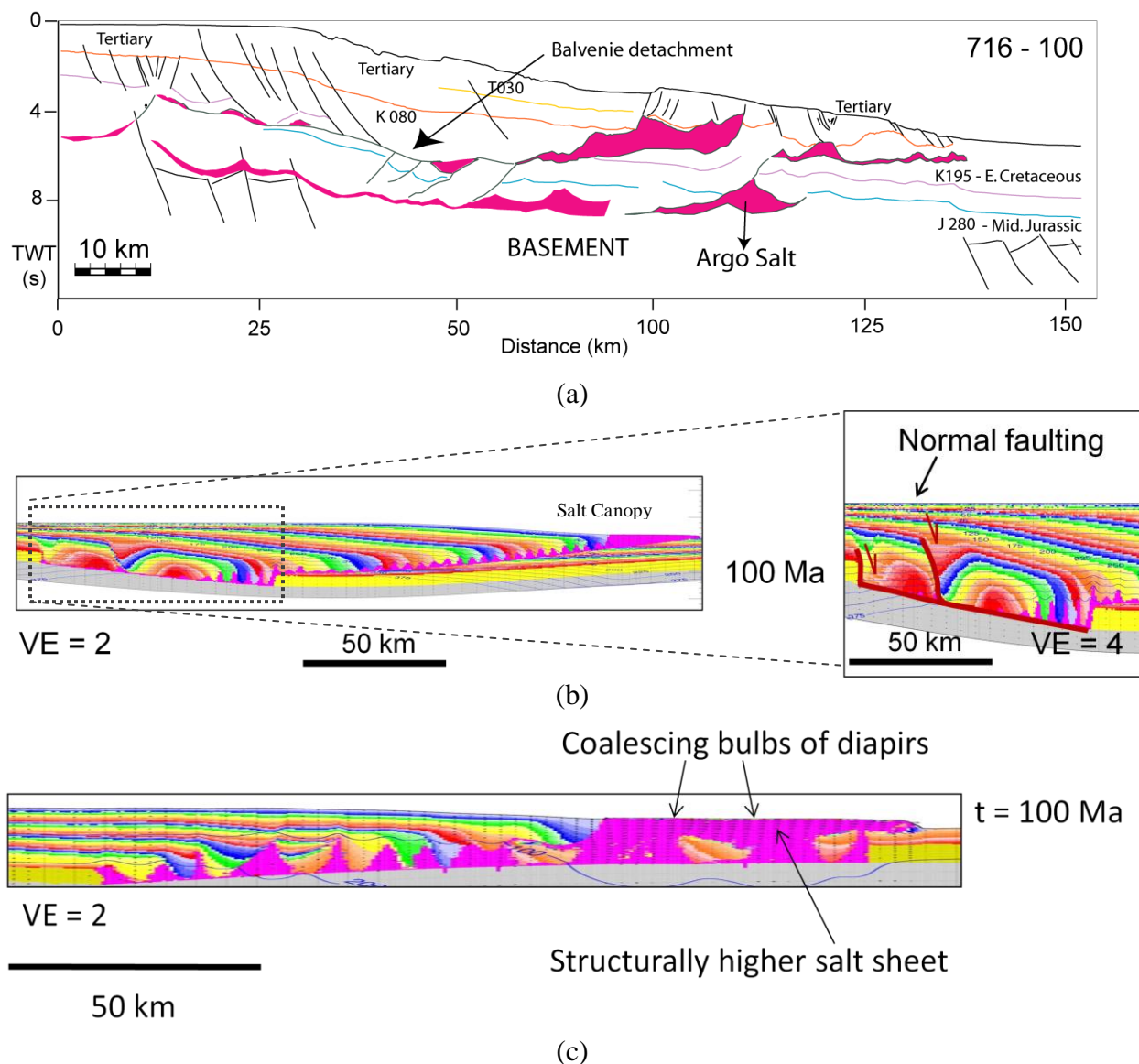


Figure B.16. (a) Line interpretation of seismic line 716 – 100 offshore Nova Scotia (courtesy: Kris Kendell, CNSOPB) (b) Results from model MT2 at $t = 100$ Ma showing the expulsion rollover and the emplacement of a salt sheet at a structurally higher level than the autochthonous salt basin (c) Results from model NS2 at $t = 100$ Ma showing the formation of a salt canopy, at a structurally higher level than the autochthonous salt basin, by coalescence of the bulbs of squeezed diapirs.

such a canopy. This detachment surface is referred to as the Balvenie detachment surface in Figure B.16a. Seismic and well studies (e.g., Fletcher et al., 1995) and physical modeling (e.g., Jackson et al., 1994) indicate that such canopies can form by extrusive glacier-like flow along (or close to) the paleoseabed rather than intruding as a sill. Preliminary results from our models offer insights into potential mechanisms by which such canopies, possibly including the Balvenie

detachment and the canopy on the interpreted seaward edge of the autochthonous salt basin, may have formed. We present results from two models discussed above, that offer insights into how glacier like extrusion can result in the formation of salt sheets that are structurally higher than the autochthonous salt basin.

Basin-scale model MT2 offers a possible mechanism in which the differential pressure caused by prograding sediments, expels the salt from the autochthonous salt basin. Salt withdrawal results in down-building of the overburden. Lateral salt expulsion results in the formation of a salt glacier that advances seaward by tank-tread advance on top of the sediments being deposited on the seaward side of the salt sheet. In this case, expulsion rollover in the autochthonous basin results in the formation of the salt sheet (nappe) at a structurally higher level (Fig. B.16b).

Results from nested upper-mantle scale model NS2 (Fig. B.15 and Fig. B.16c), offer another possible mechanism by which canopies may form. In this model, an initial phase of aggradation in which, the aggradation profile is sinusoidally perturbed, results in the formation of salt diapirs and intervening minibasins. Subsequently, differential loading from prograding sediments, causes these diapirs to tilt in the seaward direction. With continued progradation, the bulbs of diapirs on the seaward side of the basin are squeezed and coalesce to form an incipient salt canopy at a structurally higher level than the autochthonous salt basin.

While the overall structural patterns in our models differ from the example shown in figure B.16a, the preliminary results suggest that, mechanisms of expulsion rollover and coalescence of bulbs of salt diapirs, as observed in our models, can lead to the formation of structures such as the Balvenie detachment. Future research will develop these models, investigate additional mechanisms for canopy formation, and specialise the models in regard to Structural Style B of the Scotian margin.

6. Future Salt Tectonic Model Development

The nested upper-mantle scale models discussed above (Models NS1 and NS2) have shown clearly that salt bodies exert significant control on the thermal structure of the lithosphere and sediments adjacent to them. In these models we have investigated the control of salt basin geometry and location (with respect to the transition between the continental and oceanic crust) on the salt tectonic system. These salt basins are simplified representations of cross sections of those within the Scotian Basin system. The initial model geometry (Fig. B.2) was designed to represent a state near the end of syn-rift time, with a configuration in which the underlying crust has subsided and tilted tectonically, but prior to the onset of lithospheric cooling and thermal subsidence.

In nature, however, autochthonous salt basins normally form by deposition of evaporites in shallow water environments such as coastal sabkhas. The Argo Formation in the Scotian Basin is therefore interpreted to have been deposited close to sea-level, sometime during the syn-rift. If we are to gain more insight into the syn-rift evolution of the model salt basins there is a need to include their shallow marine deposition and subsequent syn-rift tectonic, and possibly thermal subsidence in the models.

Below, we present some preliminary results from models which incorporate a finite syn-rift timescale with tectonic subsidence, during which time the salt in the autochthonous basin flows owing to tectonic tilting and subsidence of the crust. Only the results from the SS model, within the larger nested upper-mantle scale models, will be discussed below.

Model NS3 (Fig. B.17a) investigates the evolution of a system in which a salt basin with tapered ends (taper slope $\sim 2.4^\circ$) is bounded on both sides by syn-rift clastics. The top of the salt basin is horizontal and at sea-level. Initially, the continental margin and the oceanic crust, but not the continent, subside over a finite, 10Ma, syn-rift timescale (Fig. B.17b). This results in an overall seaward tilting of the crust and the salt basin. Aggradation during the initial subsidence phase, results in the formation of minibasins within the autochthonous salt basin by the same mechanism as in model NS2. Sediments are deposited on top of the subsiding oceanic crust and the right end of the model attains an equilibrium water depth of ~ 1.3 km. Note that, even though the diapirs in the autochthonous salt basin are taller than the original thickness of the salt basin (2 km), the tops of these diapirs are beneath sea-level. A prograding deltaic type sedimentation begins to interact with the salt diapirs at 40 Ma (Fig. B.17e). Model NS3 therefore represents a situation in which the salt basin evolved relatively early in syn-rift time and subsequently underwent syn-rift subsidence and tilting.

Model NS 4 (Fig. B.18a) investigates the evolution of a similar system (i.e., top of salt basin is horizontal and at sea-level at $t = 0$) as above, but the tapered autochthonous salt basin is bounded on the seaward side by a triangular buttress. This buttress is assigned mechanical and thermal properties that are intermediate between those of the syn-rift sediments and the continental crust (section 2.3 and Table 2) and for the purposes of this model can be interpreted as either syn-rift sediments, crust, or volcanics.

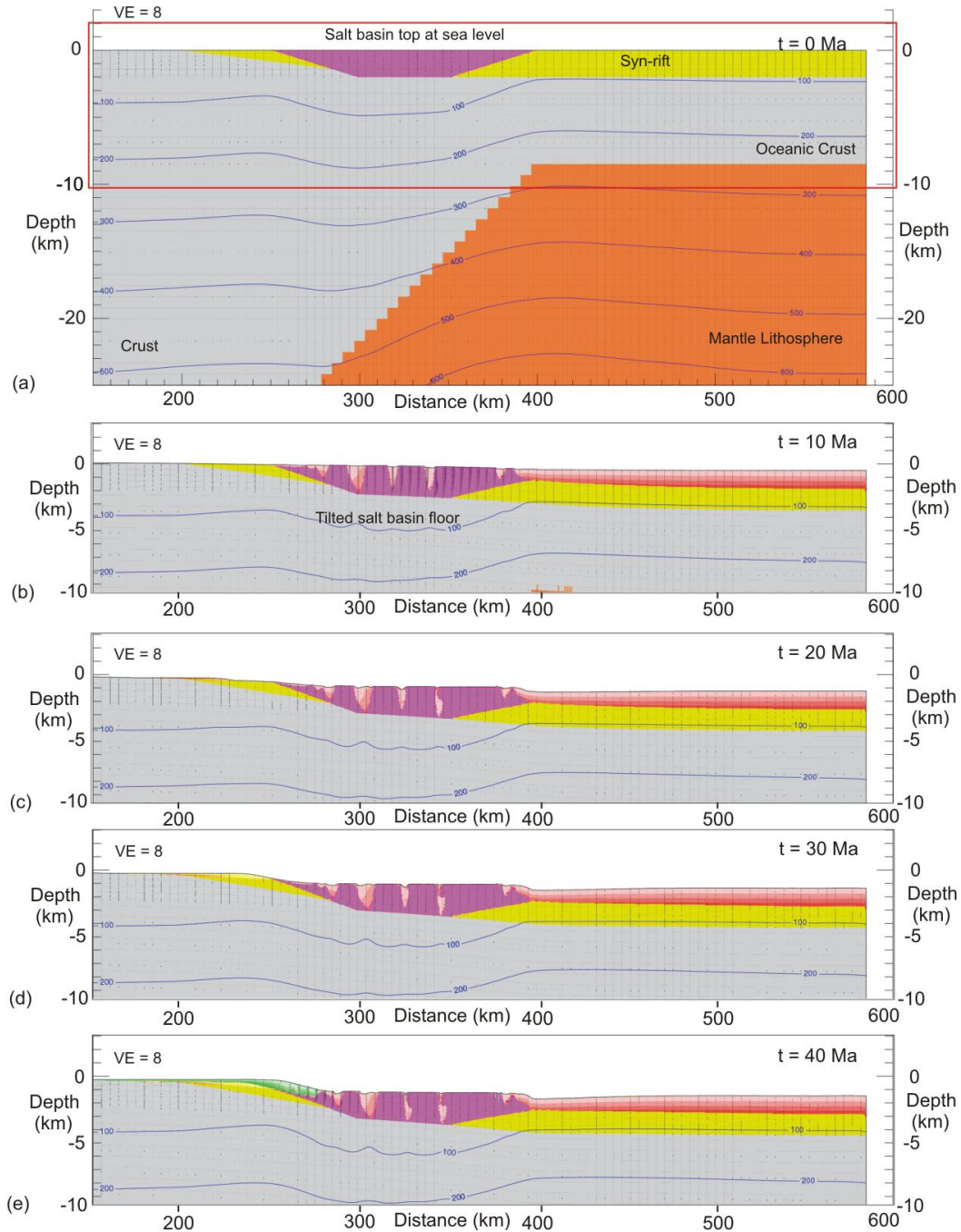


Figure B.17. Results from nested upper-mantle scale model NS3 showing the effect of a finite, 10Ma, syn-rift time scale with tectonic subsidence and synchronous sedimentation on an initially tapered salt basin. Seabed temperature is 0° C and isotherms are shown at 100° C increasing intervals below the seabed. Red box in (a) shows the regions of the model shown in (b) – (e).

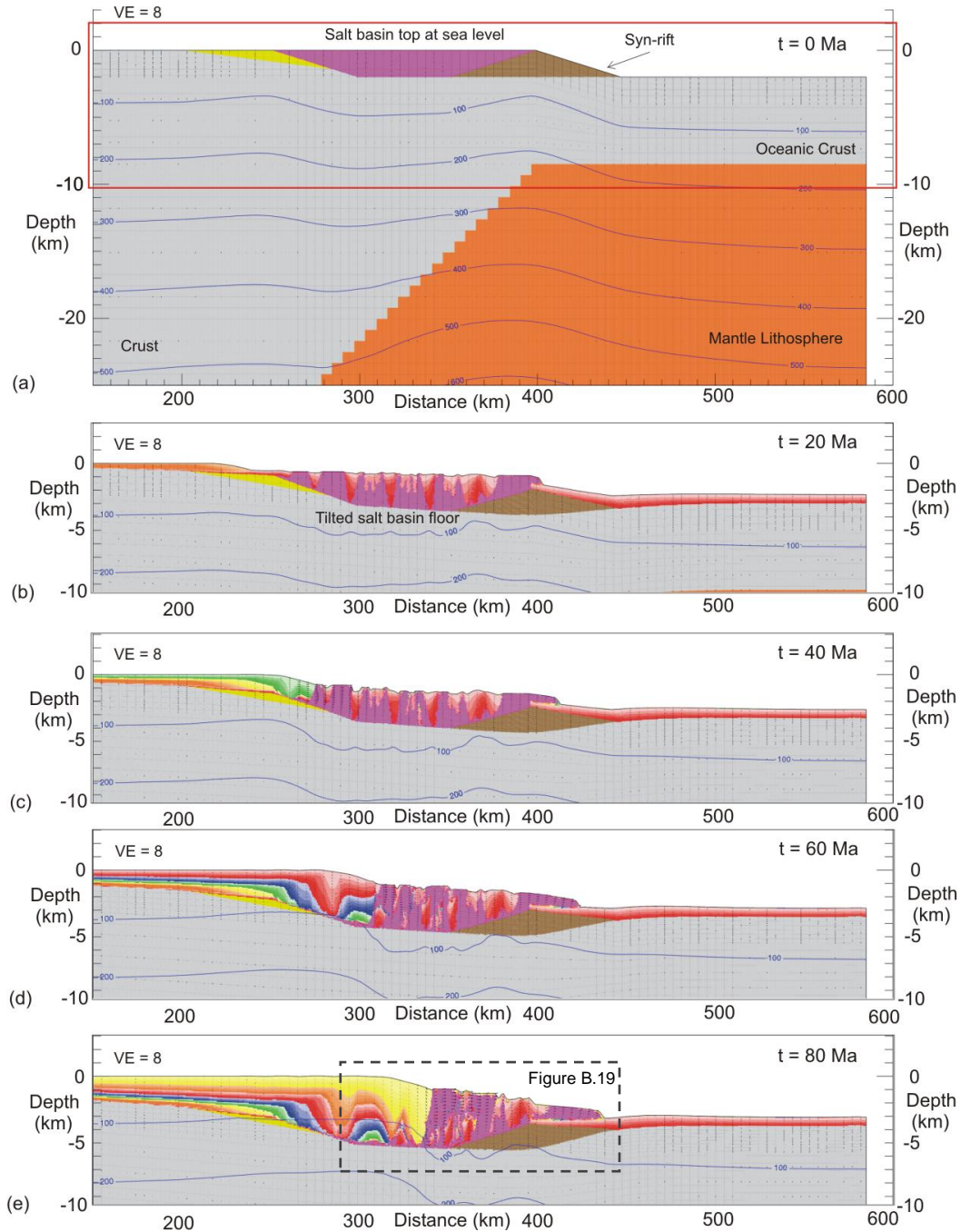


Figure B.18. Results from nested upper-mantle scale model NS4 showing the effect of finite, 10Ma, syn-rift time scale with tectonic subsidence, and synchronous and subsequent sedimentation on an initially tapered salt basin which is bounded on the seaward side by a triangular buttress. Seabed temperature is 0°C and isotherms are shown at 100°C increasing intervals below the seabed. Red box in (a) shows the regions of the model shown in (b) – (e).

The continental and oceanic crusts subside and tectonically tilt over a 10 Ma syn-rift subsidence time. Local flexural response of the crust beneath the buttress can also be observed. The model is designed such that the initial phase of subsidence is also accompanied by sediment aggradation. This is followed by a phase of prograding deltaic type sedimentation. By 20 Ma (Fig. B.18b), minibasins form in the autochthonous salt basin and a thin sedimentary cover is deposited on top of the syn-rift unit, at a water depth of ~ 2.2 km. The floor of the salt basin, which was initially horizontal, develops an overall seaward dip due to the syn-rift subsidence of the margin and oceanic regions. Salt near the seaward end of the autochthonous salt basin rises forming diapirs over the triangular buttress and flows as a glacier over the thin sedimentary cover on the seaward side of the buttress.

By 40 Ma, prograding sediments exert a differential load on the salt basin which expels the salt towards the seaward end of the basin. The accommodation space created by the expulsion of salt is filled by the prograding sediment. By 80 Ma (Fig. B.18e), normal faulting within the basin fill and continued progradation result in the development of squeezed salt diapirs that are inclined in a seaward direction. The bulbs of the squeezed inclined diapirs coalesce to form an incipient canopy (Fig. B.19). Sediments above the landward side of the salt sheet and over the diapirs on the seaward end of the autochthonous salt basin undergo normal faulting, as the salt glacier advances farther seaward and the toe of the glacier reaches $x = 426$ km.

Model NS5 (Fig. B.20) is similar to model NS5 except that the salt basin has a rectangular geometry and the triangular buttress has a vertical edge on the landward side. The 10 Ma initial phase of syn-rift subsidence results in a seaward tilt to the base of the autochthonous salt basin. By 10 Ma (Fig. B.20b), sedimentary aggradation results in the formation of minibasins within the salt basin and salt diapirs form above the triangular buttress and eventually advance as a salt glacier. A subsequent phase of progradation over the salt basin results in expelling salt towards the seaward side of the basin. Remnant salt on the landward side of the basin acts as a detachment over which the sedimentary overburden detaches and undergoes normal faulting above the landward edge of the basin. The toe of the salt glacier advances to $x = 413$ km by 40 Ma (Fig. B.20e). Note that this is similar to the advance of the glacier in model NS4 (Fig. B.19c at $x = 408$ km).

The models discussed above, which incorporate a finite syn-rift timescale with tectonic subsidence, allow us to investigate more natural settings which take into account the shallow depositional environments in which salt basins form and the effects of syn-rift subsidence and tilting on the flow of the salt. These models have the potential to show how gravitational gliding, in addition to gravitational spreading, develops in salt tectonic systems.

Future model developments will involve:

- (1) Building upon the basin-scale thermo-mechanically coupled models presented above and the incorporation of non-linear, temperature-dependent creep of salt into nested models,
- (2) Incorporating thermal subsidence into the nested upper-mantle scale models,
- (3) Incorporating temperature-dependent thermal conductivity for salt and the sediments, and
- (4) Continued work on our latest set of models (such as NS3 – NS5) with finite syn-rift timescale, including design of generic models and those representing cases from the Scotian Basin.

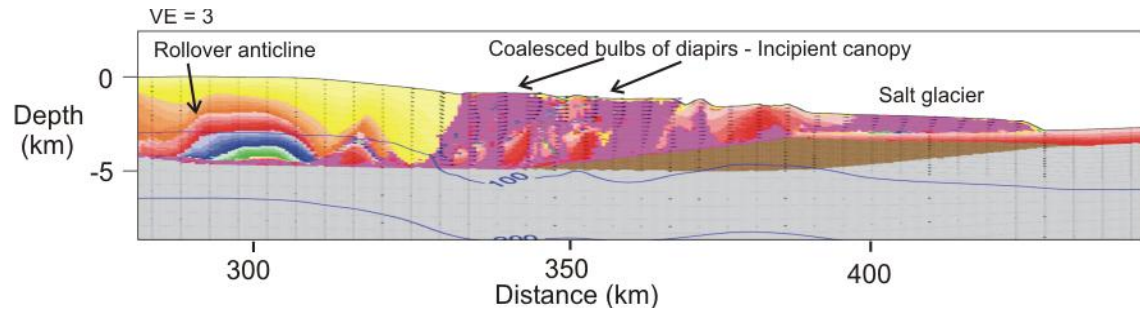


Figure B.19. Close-up view of result from model NS4 at $VE = 3$ which shows development of an incipient canopy by coalescence of bulbs of diapirs. The area shown here is highlighted in figure B.18e.

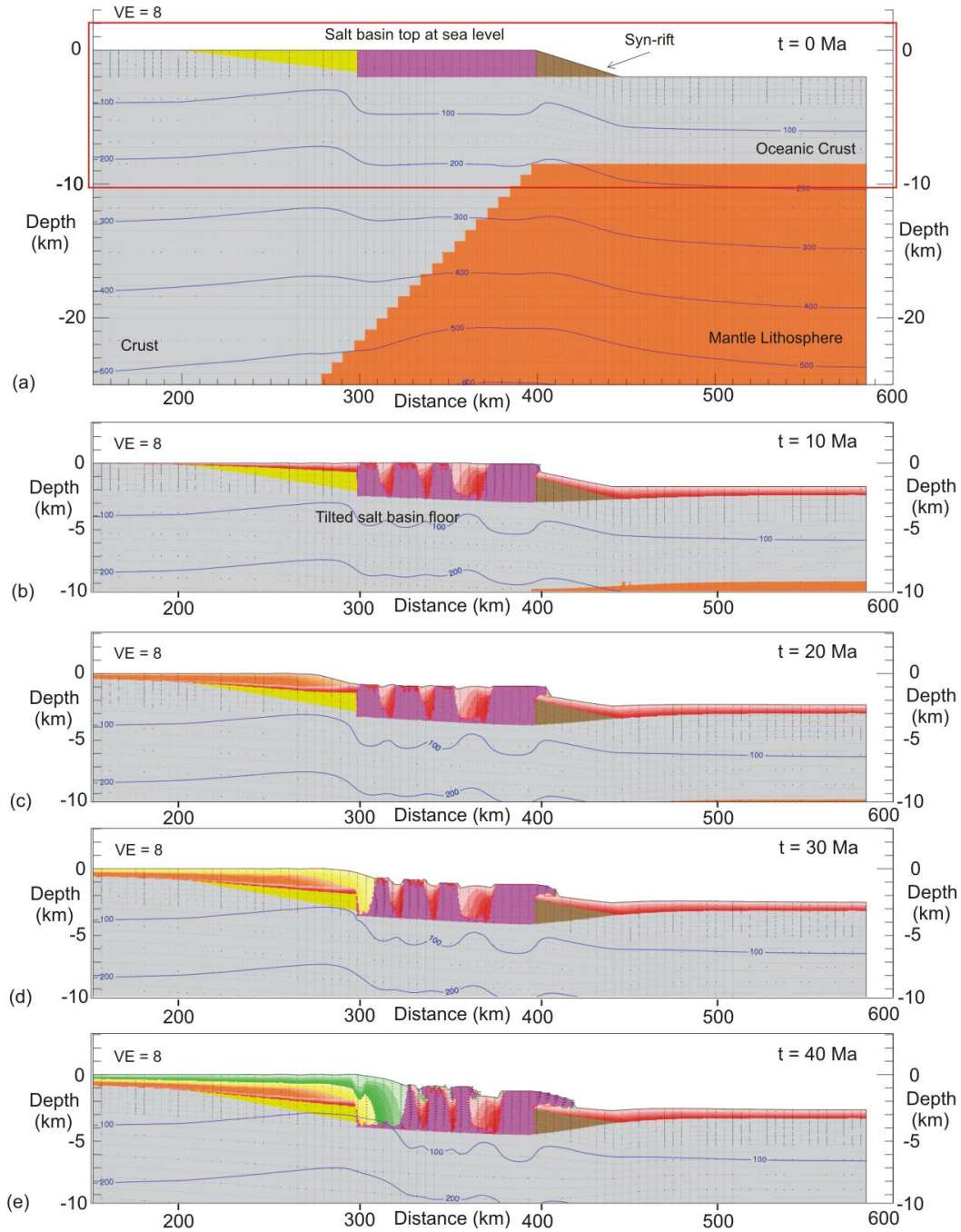


Figure B.20. Results from nested upper-mantle scale model NS5 showing the effect of finite, 10Ma, syn-rift time scale with tectonic subsidence, synchronous and subsequent sedimentation on an initially rectangular salt basin which is bounded on the seaward side by a triangular buttress. Seabed temperature is 0°C and isotherms are shown at 100°C increasing intervals below the seabed. Red box in (a) shows the regions of the model shown in (b) – (e).

7. Coupled Continental Rifting and Salt Tectonics

We have proposed to investigate aspects of salt tectonics affected by rifting. Specifically, the following deliverables are stated in the proposal:

Q2, 2010. Demonstrate ability to compute salt tectonics driven by basal tectonics (i.e., using nested modelling approach).

Q3-Q4, 2010. Investigate generic models showing how syn-rift lithospheric tectonics may interact with and drive syn- and post-rift salt tectonics

In order to investigate the feedback mechanisms between continental rifting and salt tectonics, we require a model with sufficient size and resolution to capture rifting-related upper-mantle-scale tectonics and basin-scale salt tectonics. Of particular interest is the formation of syn-rift evaporite basins and the development of these basins during syn- and post-rift clastic sedimentation.

The nested modeling approach described elsewhere in Appendix 1 is suitable for this problem. The upper-mantle-scale model is 1200 km wide and 600 km deep and driven by velocity boundary conditions at the side. This larger-scale model captures thermo-mechanical evolution of the extending lithosphere and associated asthenosphere flow. However, the crust and sediments in the upper-mantle scale model, with a resolution of 3km horizontally, 1.25 km vertically, are not resolved well enough to investigate details of salt tectonics. Thus, a smaller basin-scale model is used to capture the evolution of the crust and sediments at a higher resolution (750 m horizontally and 312 m vertically). The two models are dynamically linked but are separate finite-element calculations.

The following model, Model RS, demonstrates the feasibility of using the nested model approach to investigate syn-rift salt tectonics driven by lithospheric extension and sediment loading. Post-rift sedimentation can also be investigated, but is not included in Model RS.

7.1. Model RS: preliminary model of tectonic extension and salt tectonics

The starting design of Model RS (Fig. B.21) is similar to Model 2 in Appendix 1A (Figs. A9 and A11). In this model, rifting progresses in a similar manner as in Model 2, except that as accommodation space is created owing to syn-rift tectonic subsidence, salt is deposited at base level and fills all available accommodation space. In Model RS, salt has the same thermo-mechanical properties as Model MT2 in Appendix 1B (viscosity, $\eta = 10^{18}$ Pa.s, density, $\rho = 2150 \text{ kg/m}^3$, and thermal conductivity, $K = 5.85 \text{ W/mK}$).

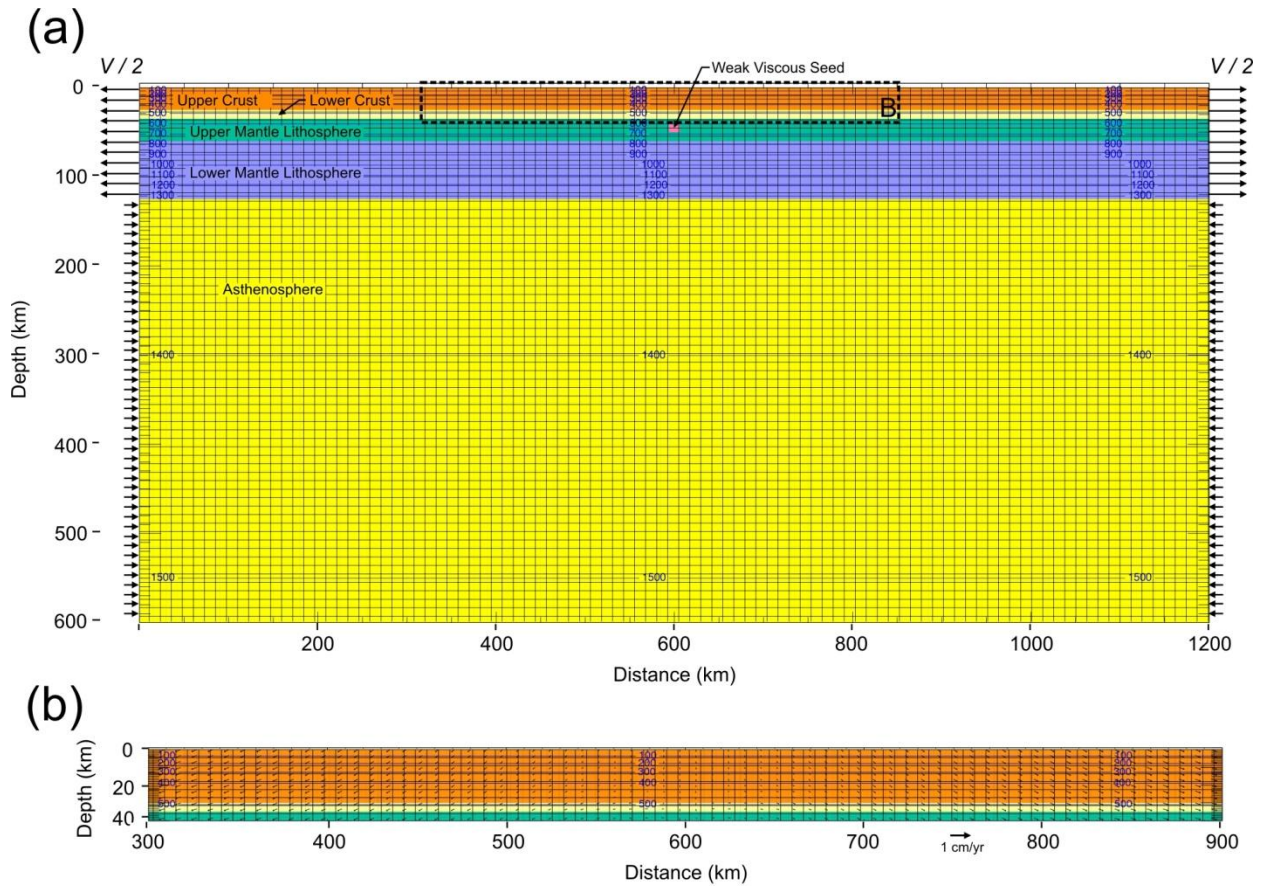


Figure B.21. a) Large scale model setup showing upper crust (orange), lower crust (sand colour), upper mantle lithosphere (green), lower mantle lithosphere (light blue), and the asthenosphere (yellow). The crust and lithosphere are subjected to velocities at the side boundaries as shown by the arrows. The upper crust has a wet quartz rheology ($f = 0.04$), the lower crust has a dry Maryland diabase rheology ($f = 0.02$), the mantle lithosphere (upper and lower) has a wet olivine rheology ($f = 2$) and the sub-lithospheric mantle has a wet olivine rheology ($f = 1$). The reference density of the crust is 2860 kg/m³, 3250 kg/m³ for the mantle lithosphere, and 3300 kg/m³ for the asthenosphere. b) Small scale embedded model setup. Position of embedded domain in the large scale model is shown in (a). The resolution of the embedded small scale model is 4 times greater than the large scale model.

After 5 Ma of extension, a 90 km wide basin has formed, which, when filled with salt, is ~3 km deep (Fig. B.22b). By 10 Ma, continued extension and salt deposition has created a salt-filled basin 165 km wide and ~6 km deep (Fig. B.22c). After 10 Ma, no more salt is deposited. Instead, a clastic sediment delta starts to prograde across the model, from left to right, starting at 10 Ma. Owing to the low viscosity of the salt layer, it flows efficiently in response to continued extension and maintains a near-flat surface. After 15 Ma evolution, the salt layer has increased in width to ~210 km, but decreased in thickness to ~5 km. This broad skim of salt overlies both developing conjugate margins, and the nascent ridge centre (Fig. B.22d). At this stage there is very little impact from the prograding delta, so the change from 10 Ma to 15 Ma is caused purely by salt readjustment in response to extension.

After 20 Ma evolution, the salt basin width has continued to increase, while prograding clastic sediments have started to fill shelf basins on the left margin (Fig. B.22e). The salt is squeezed out from landward flanks and base of the fault-bounded basins (i.e., distance = 500 km). Continued extension and progradation (Fig. B.22f and B.23) causes the salt basin to increase in width to ~280 km, but the thickness is reduced to ~2 km (maximum). It is also notable that once the crust has rifted, salt drapes the exhumed mantle lithosphere owing to continued flow toward to rift centre from both conjugate margins.

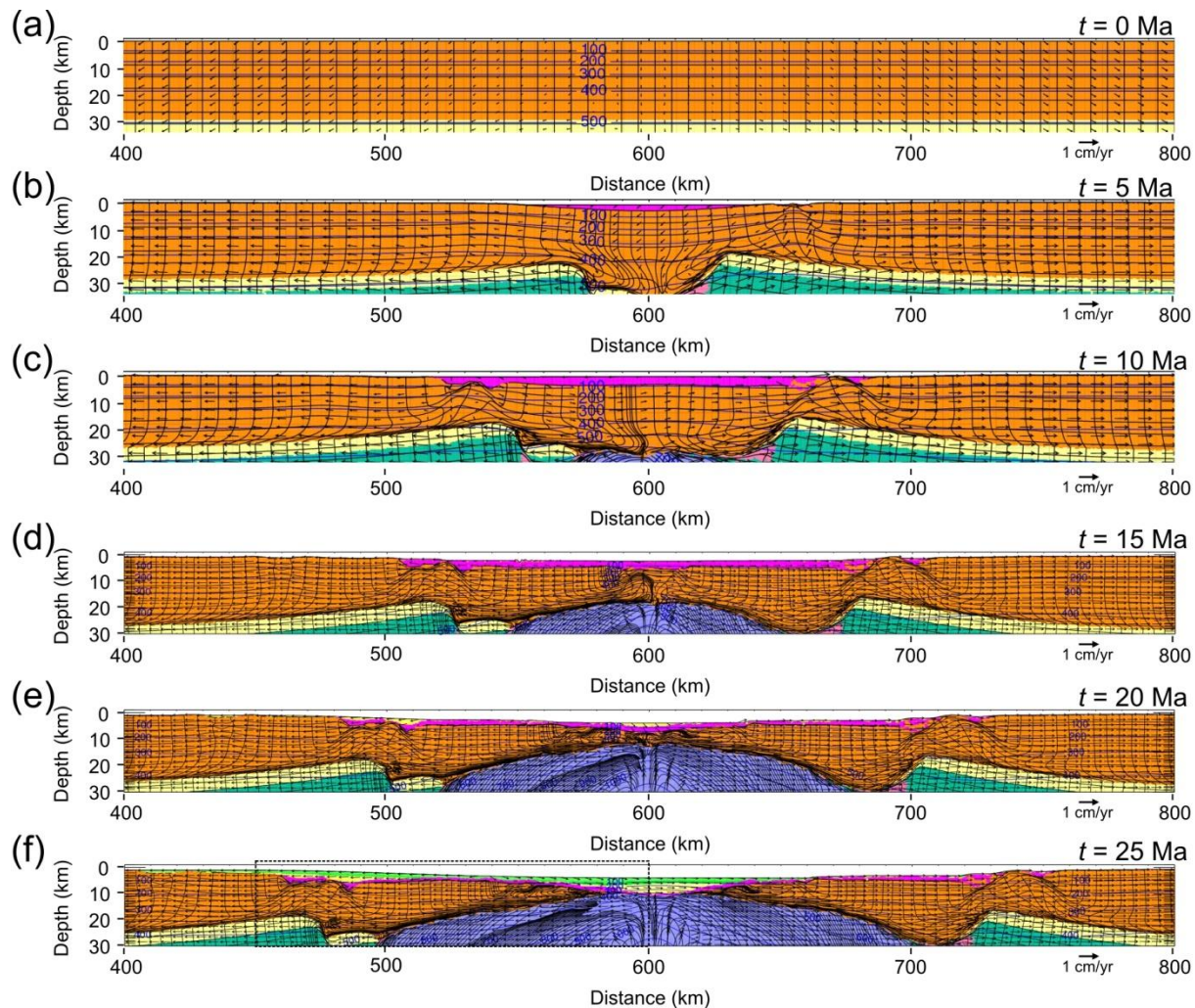


Figure B.22. Evolution of a Model RS, a dynamic model of salt deposition and subsequent clastic sedimentation during tectonic extension associated with rifting. Salt, shown in magenta, is deposited at base level and fills all available accommodation space until $t = 10$ Ma, after which a clastic sediment delta (yellow/green) progrades across the salt from the left side of the model. Dashed box shows position of Figure B.23.

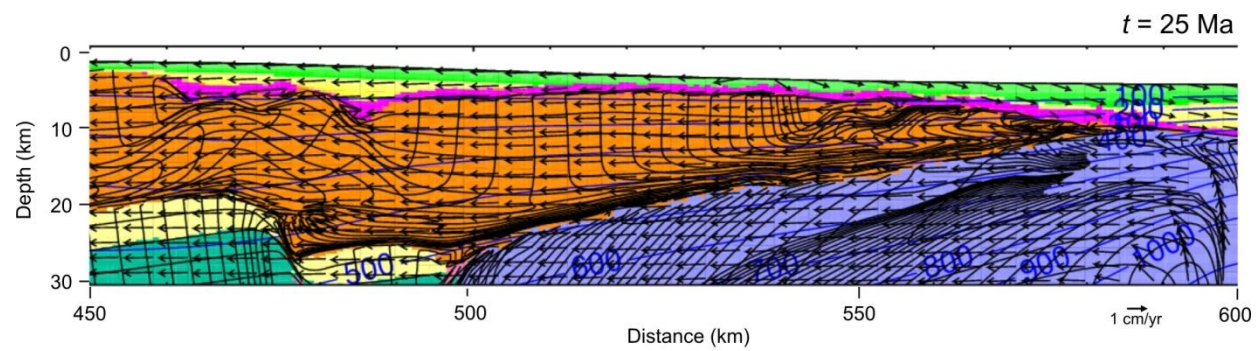


Figure B.23. Expanded view of region annotated in Figure B.22f showing salt and sediment in more detail.

8. References

- Albertz, M., C. Beaumont, J.W. Shimeld, S.J. Ings, and S. Gradmann (2010), [An investigation of salt tectonic structural styles in the Scotian Basin, offshore Atlantic Canada: Paper 1, Comparison of observations with geometrically simple numerical models](#), Tectonics (in press).
- Albertz, M., and C. Beaumont (2010), [An investigation of salt tectonic structural styles in the Scotian Basin, offshore Atlantic Canada: Paper 2, Comparison of observations with geometrically complex numerical models](#), Tectonics (in press).
- Athy, L. F., 1930, Density, porosity, and compaction of sedimentary rocks, AAPG Bulletin, v. 14, pp. 1–22.
- Carter, N.L., Handin, J., Russell, J.E. and Horseman, S.T., 1993, Rheology of rocksalt, Journal of Structural Geology, 15(9/10): 1257-1271.
- Drucker D.C., and Prager, W., 1952, Soil mechanics and plastic analysis of limit design, Quart. Applied Mathematics 10, 157-165.
- Fletcher, R.C., Hudec, M.R., and Watson, I.A., 1995, Salt glacier and composite salt-sediment models for the emplacement and early burial of allochthonous salt sheets, *in* Jackson, M.P.A., et al., Salt tectonics: A global perspective: American Association of Petroleum Geologists Memoir 65, p. 77–108.
- Fullsack, P., 1995, An arbitrary Lagrangian-Eulerian formulation for creeping flows and its application in tectonic models, Geophysical Journal International, v. 120, p. 1-23.
- Gemmer, L., Ings, S.J., Medvedev, S., and Beaumont, C. 2004, Salt tectonics driven by differential sediment loading: Stability analysis and finite element experiments, Basin Research, 16, 199-219.
- Gemmer, L., Beaumont, C., and Ings, S.J., 2005, Dynamic Modelling of Passive Margin Salt Tectonics – Effects of Water Loading, Sediment Properties and Sedimentation Patterns. Basin Research, v. 17, pp. 383-402.
- Jackson, M. P. A., Vendeville, B. C., and Elia, D. D. S., 1994, Structural dynamics of salt systems, Ann. Rev. Earth and Planet. Sci., 22, pp. 93–117.
- Koyi, H., 1996, Salt flow by aggrading and prograding overburdens (*in* Salt tectonics) Geological Society Special Publications, 100 243-258.
- MacKenzie, A. S., Beaumont C., Boutilier R., and Rullkötter, J., 1985, The aromatization and isomerization of hydrocarbons and the thermal and subsidence history of the Nova Scotia margin, Phil. Trans. Roy. Soc. London, Ser. A, 315, 203-232.

- McKenzie, D. 1978. Some remarks on the development of sedimentary basins. *Earth and Planetary Science Letters*: 40, 25–32.
- Petersen, K., and Lerche, I., 1996, Temperature dependence of thermal anomalies near evolving salt structures; importance for reducing exploration risk (*in* Salt tectonics), *Geological Society Special Publications*, 100, 275-290.
- Spiers, C.J., Schutjens, P.M.T.M., Brzesowsky, R.H., Peach, C.J., Liezenberg, J.L. and Zwart, H.J., 1990, Experimental determination of constitutive parameters governing creep in rocksalt by pressure solution, *J. Geol. Soc. Spec. Publ.* 54, pp. 215–227.
- Terzaghi, K., 1943, *Theoretical soil mechanics*, John Wiley and Sons, New York.
- Willett, S. D., 1999, Orogeny and orography, the effects of erosion on the structure of mountain belts, *Journal of Geophysical Research, B, Solid Earth and Planets*, v.104, pp. 28957–28982.